1979

Kinetic models for irreversible processes on a lattice

Nicholas Owen Wolf
Iowa State University

Kinetic models for irreversible processes on a lattice

by

Nicholas Owen Wolf

A Dissertation Submitted to the
Graduate Faculty in Partial Fulfillment of
The Requirements for the Degree of
DOCTOR OF PHILOSOPHY

Department: Chemistry
Major: Physical Chemistry

Approved:

Signature was redacted for privacy.

In Charge of Major Work

Signature was redacted for privacy.

For the Major Department

Signature was redacted for privacy.

For the Graduate College

Iowa State University
Ames, Iowa

1979

TABLE OF CONTENTS

	Page
CHAPTER 1. INTRODUCTION	1
An Overview of Lattice Kinetics	1
Literature Survey - Models	14
Literature Survey - Applications	31
CHAPTER 2. NON-COOPERATIVE, IRREVERSIBLE MODELS	40
The Infinite Lattice of Equivalent Sites	40
The Infinite Lattice with a Continuous Distribution of Sites	57
The Semi-Infinite Lattice	65
The Finite Lattice	71
CHAPTER 3. COOPERATIVE MODELS ON AN INFINITE LATTICE	77
Cooperative Events with a 0th n.n. Blocking Potential	78
Cooperative Events with a 1st n.n. Blocking Potential	98
Cooperative Events with an rth n.n. Blocking Potential	106
Cooperative Models - Expansion Solutions	113
CHAPTER 4. A COOPERATIVE MODEL ON A SEMI-INFINITE LATTICE	124
A Semi-Infinite Lattice Model - Iterative Solutions	126
A Semi-Infinite Lattice Model - Transform Solutions	129

CHAPTER 5. THE STICKING COEFFICIENT 141

The Exact Sticking Coefficient on an Infinite Lattice 142

Sticking Coefficient Density Expansions on the Infinite Lattice 157

Nucleation Effects on the Sticking Coefficient 166

CHAPTER 6. OTHER APPLICATIONS 177

Surface Chemistry Applications 177

Applications to Other Lattice Systems 190

Model Refinements 196

CHAPTER 7. THE ACTIVATED CHEMISORPTION OF METHANE ON W(110): AN EXPERIMENTAL STUDY 201

Introduction 201

Experimental Methods 205

Results and Discussion 211

LITERATURE CITED 214

ACKNOWLEDGEMENTS 218

CHAPTER 1. INTRODUCTION

Modeling the kinetics of atomic or molecular processes has long been of interest to chemists and physicists alike. In particular, models describing molecular or atomic events, such as chemical or physical changes in state which occur at discrete sites on a regular periodic lattice, have been studied since the early part of this century. Most of the model studies reported in the literature have been devoted to the equilibrium statistical mechanics investigations. These studies span a wide range of disciplines including polymer chemistry, surface chemistry, the lattice theory of solutions and many others. However, there has also been considerable interest in describing the nonequilibrium or kinetic behavior of lattice systems. Kinetic lattice models have been applied to a diverse selection of problems of current interest in the physical and biological sciences such as the catalytic activity of metal or metal oxide surfaces (1), the characteristics of spin-lattice systems (2), and the structure and conformation of polymer molecules (3).

An Overview of Lattice Kinetics

We open our discussion of kinetic lattice models with an overview of the physical concepts and the mathematical formalism used in the description of kinetic lattice processes.

One of the first kinetic models of a lattice process was reported in 1918 by I. Langmuir (4) in connection with his study of the rate of heat loss from a hot tungsten filament in an ambient atmosphere of hydrogen gas. In the model Langmuir considers, molecules from the gas are assumed to collide randomly with the lattice with the possibility that they can be adsorbed onto vacant sites at a rate determined by the rate constant, k, and the gas pressure, P. Adsorbed molecules can be desorbed from the surface at a rate determined by the rate constant, k'. In this model each adsorbed molecule is assumed to occupy a single site, with only one molecule being allowed per site, and there is no interaction between adsorbed molecules. Thus, neighboring adsorption events are assumed to have no effect on the probability of adsorption at a site, and the geometry of the lattice is unimportant. The kinetic equation for this model can be written as

$$\frac{d\theta}{dt} = kP(1-\theta) - k'\theta, \tag{1.1}$$

where θ is the covering fraction (i.e., the fraction of sites occupied). This equation has the solution

$$\theta = \frac{kP}{kP+k'}\left[1 - e^{-(kP+k')t}\right], \tag{1.2}$$

which reduces to the equilibrium distribution

$$\theta = \frac{HP}{1+HP} \quad , \; H = k/k', \tag{1.3}$$

as $t\to\infty$. The quantity H is a function of temperature, but not pressure. Equation 1.3 is the well-known Langmuir isotherm. Even though this model is simple, it affords insight into the nature of the adsorption problem and thus it has become a cornerstone in the development of theories of adsorption and other lattice processes.

The Langmuir model is an example of a model which we term reversible and noninteracting. By reversible we mean that both adsorption and desorption occur. Using a terminology more suited to general applications, we say that both a transition and its reverse can occur at a site in a reversible model. By noninteracting we mean that an event occurring at a site has no influence on what happens at other sites.

Now suppose that the rate constant k' is small so that desorption is an unimportant process on the time scale of interest. Then Eqns. 1.1 and 1.2 reduce to

$$\frac{d\theta}{dt} = kP(1-\theta), \tag{1.4}$$

and

$$\theta = 1 - e^{-kPt}. \tag{1.5}$$

Clearly, no equilibrium can be established now and the lattice saturates at $\theta=1$ as $t\to\infty$. A model such as this, where the reverse transition does not occur (and therefore no equilibrium is established and the forward process continues until saturation), we refer to as an irreversible

model. Most of the models discussed in this thesis are of this kind.

Let us further extend our considerations to include cases where the condition of one site can influence what happens at a neighboring site. We term models describing such cases as interacting. It is convenient at this stage to make the somewhat artificial distinction between an interaction which prohibits an event at a neighboring site, which we call a blocking interaction, and an interaction which influences the rate of transition at a neighboring site, but does not prohibit transitions, which we call a cooperative interaction. A simple but important example of a blocking interaction is found in the irreversible chemisorption of homonuclear diatomic molecules. In this case, it is convenient to discuss the adsorption process by considering two different lattices. The first is the so-called "atomic" lattice. Each atom of an adsorbed diatomic molecule occupies a single site on this lattice. If we assume that the mechanism of the adsorption is such that the two atoms from a single molecule must occupy adjacent sites, then the point between these two sites can be thought of as a lattice site on a conjugate lattice which we call the "molecular" lattice. Sites on the molecular lattice are occupied by adsorbed molecules. Although it might appear that the atomic lattice is the more physical of the two, in

a sense the molecular lattice is more useful from a theoretical point of view. This is because each adsorption event takes place on a single molecular lattice site whereas the same event involves two sites on the atomic lattice. Since two adjacent molecular sites have a common atomic site, and each atomic site can only be singly occupied, adsorption on one molecular site precludes adsorption on a neighboring molecular site. This is what we mean by a blocking potential. In the case at hand, an adsorption event blocks an event only on the first nearest neighbor molecular sites, and hence we refer to this event as having a 1st n.n. blocking potential. By obvious extension we can also have 2nd n.n., 3rd n.n., and etc. blocking potentials. Unlike the Langmuir case, the geometry of the lattice is important when an adsorption event at one site can influence the probability of adsorption at another site. The lattices we consider in most of our discussions are linear.

Since the chemisorption problem discussed above is assumed to be irreversible, adsorption continues until the lattice saturates (i.e., until there are no two adjacent atomic sites or, in other words, until there is no molecular site on which adsorption can occur). However, because of the random nature of the process, there will be isolated, vacant sites remaining at saturation. In fact, on an infinite linear lattice the fraction of sites remaining

vacant is e^{-2}. We refer to this result often in this thesis and explicitly derive it in Chapter 2.

The specific model discussed above is called the dimer problem and is of central importance throughout this thesis. Although we have introduced the dimer problem in the context of irreversible chemisorption, it arises in other physical contexts. For example, in a classic paper, Flory (5) utilizes the dimer model to investigate the condensation of adjacent substituent ketone groups on the polymer poly-(methyl-vinyl)ketone. Equation 1.6 illustrates the reaction.

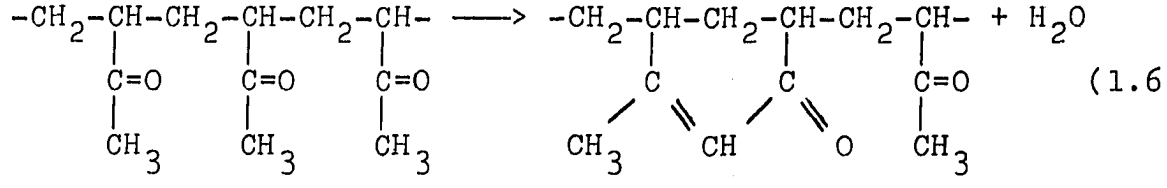

(1.6)

The random reaction of pairs of adjacent ketone groups along the chain leaves a distribution of isolated, unreacted ketone groups, in analogy to the dimer adsorption problem. Flory finds the distribution of unreacted groups on a chain of length N at saturation by solving a sequence of finite difference equations. Of course, in the limit as $N \to \infty$, the fraction of unreacted groups approaches the previously cited result of e^{-2}. In the terminology previously introduced, the carbon atoms of the polymer backbone to which the ketone groups are attached are the "atomic" sites and the intervening carbons are the "molecular" sites. Clearly, this

language is not particularly appropriate here, and hence we introduce the more general terms of "event lattice" for "molecular lattice", and "space-filling lattice" for "atomic lattice". The rationale for the use of the term "space-filling" will become clear when we discuss the theoretical relationship between the two lattices in Chapter 2.

As mentioned above, we also want to consider cooperative interactions (i.e., interactions which influence, but do not prohibit events on neighboring sites). We use a similar notation to describe such interactions. For example, we might have a 1st n.n. blocking potential with 2nd and 3rd n.n. cooperative interactions. Figure 1.1 illustrates this situation. For cooperative interactions, we must also specify to what extent an event favors or disfavors the occurrence of a second event at a neighboring site.

Throughout our discussion we will have reason to refer to distributions on both types of lattices previously discussed. In general, we will use the generic symbol "f" to refer to event lattice distributions and "P" to refer to space-filling lattice distributions. The two types of distributions are obviously related as is discussed in detail in Chapter 2. The densities on the lattices (i.e., the singlet distribution functions) are given the special symbols "η" for the event density and "θ" for the space-filling density. For the case of monatomic adsorption (i.e., the Langmuir

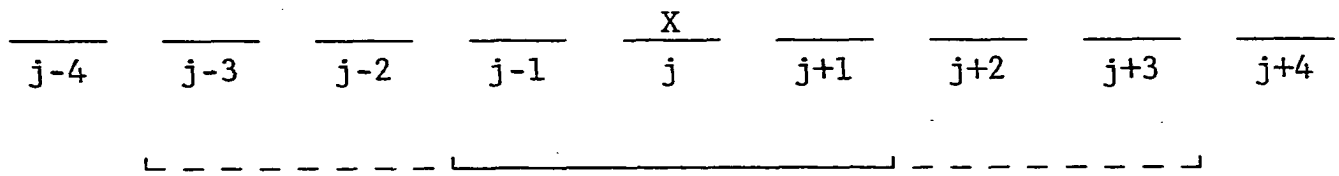

Figure 1.1. The interaction scheme for an event, X, on site j with a 1st n.n. blocking potential and 2nd and 3rd n.n. cooperative interactions. The solid line indicates the range of the blocking potential and the dashed line indicates the range of the cooperative interactions

case) the event and space-filling lattices are obviously the same, and $\eta=\theta$. However, for the dimer problem, $\eta=2\theta$ because each event site has associated with it two space-filling sites. Thus, we see that the relationship between η and θ depends on the particular problem.

Having given a simple example of a kinetic lattice model to introduce most of the major concepts of a lattice process we can now briefly discuss the general mathematical formalism through which most lattice processes can be described. We first consider a lattice system of arbitrary geometry in which the various lattice sites can exist in one of a number of different conditions and arbitrary transitions of a site from one condition to another is allowed. We refer to such transitions as events. We assume that the condition of the sites in the neighborhood of a given site can promote, inhibit, or prohibit the occurrence of events at that site. A general description of the time evolution of the distribution of events over the entire lattice is given by a master equation (6,7) of the form

$$\frac{dF(\underline{A})}{dt} = \sum_{\underline{B}} \{W(\underline{B}\rightarrow\underline{A})F(\underline{B}) - W(\underline{A}\rightarrow\underline{B})F(\underline{A})\}. \qquad (1.7)$$

Here, $\underline{A}$ and $\underline{B}$ are macroscopic (as opposed to quantum) states of the entire lattice, where the lattice state is designated by specifying the condition of each of the lattice sites, $F(\underline{A})$ and $F(\underline{B})$ are the distribution functions for states $\underline{A}$

and $\underline{B}$, and $W(\underline{A}\rightarrow\underline{B})$ is the time independent probability for the transition from state $\underline{A}$ to state $\underline{B}$. The first term on the right side of this equation describes the increase in the probability $F(\underline{A})$ due to the transition of one or more sites of state $\underline{B}$ to give rise to state $\underline{A}$, summed over all contributing states $\underline{B}$. The second term similarly describes the loss of $F(\underline{A})$ due to site transitions of state $\underline{A}$ to another state $\underline{B}$. The solution of this equation gives a complete description of the time evolution of the distribution function for the general lattice state $\underline{A}$. The kinetic equation for the Langmuir model, Eqn. 1.1, is an example of a simple master equation.

The solution of the master equation (Eqn. 1.7) generally provides more information than is useful in a particular problem; one is typically more interested in the kinetics of distributions of much smaller configurations of conditions such as the distributions of conditions for a single site. We can obtain the kinetic equations for the distribution of conditions on a particular set of n sites, designated by {n}, irrespective of the condition of all other sites of the lattice, by formally summing Eqn. 1.7 over all macroscopic states in which the desired configuration of conditions appear. The resulting kinetic equation has the general form

$$\frac{df_{\{n\}}^{(n)}(\underline{x})}{dt} = \Gamma_{\{n\}}(\underline{x}) - \Lambda_{\{n\}}(\underline{x}); \qquad (1.8)$$

where $f^{(n)}_{\{n\}}(\underline{x})$ is the n site distribution function for the configuration of conditions on {n}; $\underline{x}$ is an n-dimensional vector whose ith component, x_i, denotes the condition of the ith site of {n}; and $\Gamma_{\{n\}}(\underline{x})$ and $\Lambda_{\{n\}}(\underline{x})$ are terms that respectively describe the gain and loss of $f^{(n)}_{\{n\}}(\underline{x})$. Explicit forms of this equation for the kinetics on a linear lattice will be derived from slightly different considerations in Chapters 2 and 3.

In most cases Eqn. 1.8 does not constitute a master equation because the transition probabilities contained in the gain and loss terms are conditioned on the local distribution of conditions and couple $f^{(n)}_{\{n\}}(\underline{x})$ with distributions of larger configurations of conditions. The distributions on the {n} sites therefore generally do not evolve as a closed set and do not satisfy a master equation. Instead, Eqn. 1.8 represents an infinite hierarchy of coupled differential equations that are analogous to the BBGKY hierarchy of equations that are fundamental to the kinetic theory of fluids (8). If we consider the particular case where we have only a single, irreversible event, a lattice site can be in one of two conditions; an initial condition which we shall refer to as a vacancy and denote by 0, and a final condition brought about by the event which we denote by 1. If initially all sites are in the same condition, then a site being in another condition is equivalent to an

event occurring. Hence we can also meaningfully refer to a distribution of final conditions as a distribution of events. In this case, Eqn. 1.8 takes on a simple form in either of two special cases. When $\underline{x}$ describes a configuration composed only of events (i.e., $\underline{x} = \underline{1}$, where $\underline{1}$ is the occupation vector with a one in every component) there can be no loss in $f^{(n)}_{\{n\}}(\underline{x})$ and only the gain term survives. In the opposite case where $\underline{x}$ describes a configuration of vacant sites (i.e., $\underline{x} = \underline{0}$) there is no gain in $f^{(n)}_{\{n\}}(\underline{x})$ and only the loss term survives. The latter situation is the one we consider throughout most of this thesis.

The objective of the work presented in this thesis is to develop and investigate models that describe the cooperative kinetic behavior of interacting events on linear lattices through a kinetic equations approach. We also consider the application of these models to specific problems of current interest as well as the general applicability of the models to a wide range of other lattice problems.

The study begins in Chapter 2 with a review of the basic model used to describe the kinetics of noninteracting events on an infinite, semi-infinite, and finite linear lattice. The methods of solution of the kinetic equation for these models is presented in detail. In Chapters 3 and 4, we then extend these models to describe the kinetics of cooperative events and discuss the general solubility of

the associated kinetic equations in terms of the range of the cooperative interaction. In order to test the validity of the models, we calculate the sticking coefficient for monatomic and homonuclear diatomic molecules and compare the covering fraction and temperature dependence with published experimental data in Chapter 5. In Chapter 6, we present specific examples of the application of these models to other problems of surface chemistry and catalysis. The general applicability of the models to the kinetic description of a broad range of other lattice based processes is discussed in detail. Finally, in Chapter 7, we present a brief description of an attempt to experimentally study the photoinduced chemisorption of methane onto the hexagonal (110) face of a tungsten crystal. As opposed to the statistical emphasis of the major portion of this thesis, this experimental study is intended to investigate the mechanistic aspects of the chemisorption processes.

In the next two sections we review a major portion of the literature concerning the development of kinetic lattice models and their application to various problems of physical interest. We include such an extensive review in this thesis, first of all, because the body of literature concerning these kinetic models is not large, but more importantly, because lattice models have a wide application, and for this reason, are scattered throughout the literature

of several scientific disciplines. This dispersion in the literature has led to the repetitious solution of the same basic lattice problem in several different contexts. For example, the dimer problem has been solved as a polymer problem, a statistical space-filling problem, and an adsorption problem, without it being apparent that the authors are aware of each others work. It is our goal to review the various published articles concerning kinetic lattice problems and present them in one place for comparison and reference purposes. Except for occasional references to these two sections, the remainder of this thesis is self-contained and the reader who is not particularly interested in a literature review can go on to Chapter 2.

Literature Survey - Models

The literature from the years following the 1939 work of Flory contains a number of models describing the kinetics of various irreversible lattice processes. Most of the models are similar to those discussed in the first section and we will therefore discuss the results of the various authors in terms of these models. We primarily limit ourselves to a discussion of linear lattices since these are the most widely used.

Space-filling problems in which the event exhibits a 1st n.n. blocking potential comprise a large portion of the

literature on kinetic lattice models. McQuistan and Lichtman (9) have studied the distribution of events with a 1st n.n. blocking potential on a linear lattice of N sites. They derive difference relations, similar to those derived by Flory, for the quantities $\bar{P}^{(n)}_{\{n\}}(\underline{0}) = \frac{1}{N-n+1} \sum_{i=1}^{N-n+2} P_i^{(n)}(\underline{0})$, which is the average distribution of n-fold sequences of vacant lattice sites. Solutions to the recursion relations give $\bar{P}^{(n)}_{\{n\}}(\underline{0})$ as a complicated double sum. In the limit of an infinite lattice, all sites become equivalent and the time dependence of the fraction of single, vacant sites, $P^{(1)}_{\{j\}}(0)[t]$ is given by

$$P^{(1)}_{\{j\}}(\underline{0})[t] = 1 - \theta(t) = \exp[-2\{1-\exp(-\sigma t\}], \quad (1.9)$$

where σ is the rate of occupation of pairs of vacant sites on the lattice. In the limit as $t \to \infty$, this result approaches $P^{(1)}_{\{j\}}(\underline{0}) = e^{-2}$, which is the result cited in the first section. A somewhat more general treatment of this space-filling problem was given by Cohen and Reiss (10). The average kinetic distribution of dimers on a linear lattice of N sites and on rings of N sites were obtained from kinetic equations describing the time evolution of $\bar{P}^{(n)}_{\{n\}}(\underline{0})[t]$. Solutions on the linear lattice are given by

$$\bar{P}^{(n)}_{\{n\}}(\underline{0})[t] = \exp[-(n-1)\sigma t] \sum_{S=0}^{N-n} \left(1 - \frac{S}{N-n+1}\right) \frac{(2e^{-\sigma t}-2)^S}{S!} \quad (1.10)$$

On the infinite chain, this equation is written

$$P^{(n)}_{\{n\}}(\underline{0})[t] = \exp\{-(n-1)\sigma t\}\exp\{-2(1-\exp(-\sigma t))\}, \qquad (1.11)$$

which reduces to Eqn. 1.9 for n=1. Equation 1.11 can now be written in the form

$$P^{(n)}_{\{n\}}(\underline{0})[t] = P^{(1)}_{\{j\}}(\underline{0})[t]q^{n-1}(t),$$

where j is the leftmost site of {n}, and $q(t) = \exp(-\sigma t)$. This very important result represents an exact truncation of the hierarchy of kinetic equations and will be discussed at length in Chapter 2. We shall see then that q(t) can be interpreted as a conditional probability.

The N-membered ring problem is virtually the same as that for a linear lattice of N-2 members. This is easily understood since after the occupation of the first pair of sites on an empty ring of N sites, the distributions on the remaining N-2 sites evolve exactly as would the distribution on a linear array of N-2 sites.

Cohen and Reiss also solve the kinetic equations on the finite lattice by generating function or transform techniques. For large N, $\bar{P}^{(1)}_{\{j\}}(\underline{0})[t=\infty]$ is shown to go as $\bar{P}^{(1)}_{\{j\}}(\underline{0})[\infty] \approx \frac{N+2}{N} e^{-2}$, and the variance in $\bar{P}^{(1)}_{\{j\}}(\underline{0})$ to go as $\sigma^2(\infty) \approx 4(N+2)e^{-4}$. The generating function approach has been used independently by Page (11) to establish the same results.

Vette et al. (12) derive the kinetics of irreversible, non-cooperative dimer events on a lattice of general dimensionality from the master equation approach. In particular, a master equation describing the kinetics of the dissociative chemisorption of dimers, including atomic skating, dimer desorption, and dimer adsorption processes is presented. If it is assumed that the rates of desorption and skating are negligible as compared to the rate of adsorption, the master equation reduces to the kinetic equations describing the dimer space-filling problem. The hierarchy of equations is truncated and exactly solved on the linear lattice with the results

$$P^{(n)}_{\{n\}}(\underline{0}) = (1-\theta)[1 + \tfrac{1}{2} \ln (1-\theta)]^{n-1} \qquad (1.12)$$

and

$$\theta(t) = 1 - \exp\{-2(1 - \exp(-\sigma t))\}, \qquad (1.13)$$

where σ is once again the rate of adsorption onto empty sites. The hierarchy of equations cannot be truncated exactly for lattices of higher dimension and must therefore be solved in approximation. To this end, several levels of approximation are introduced by the authors that serve to truncate the hierarchy and allow the solution of the equations. The approximations are based on the number of lattice sites on which the various probabilities in the kinetic equations are conditioned and in essence are the non-equilibrium analogue to the Bethe approximation for a

lattice gas (13). A first shell approximation, the lowest level of approximation, is made when all conditional probabilities having the same configuration of events on sites one lattice vector away from the site of interest are set equal, regardless of the condition of conditioning sites farther away than one lattice vector. This is illustrated in Figure 1.2. In this manner, only probabilities conditioned on the first shell sites appear in the kinetic equations, thereby truncating the hierarchy and allowing solutions to be found. The first shell approximation leads to an exact result for this noncooperative model for the linear lattice. The next higher level approximation, the second shell approximation, equates all conditional probabilities have the same configuration of events on sites lying within a radius of two lattice vectors from the site of interest. It is evident that extending this sequence to larger shells gives an increasingly higher level of approximation. Vette et al. report the saturation covering fraction at several levels of approximation for square, hexagonal, and triangular lattices. It is noted that the formalism applies equally well to irreversible desorption from a completely full lattice. We later use this fact as a basis for comparison of adsorption and desorption processes.

A slightly different approach to the space-filling problems on lattices of general dimensionality was discussed

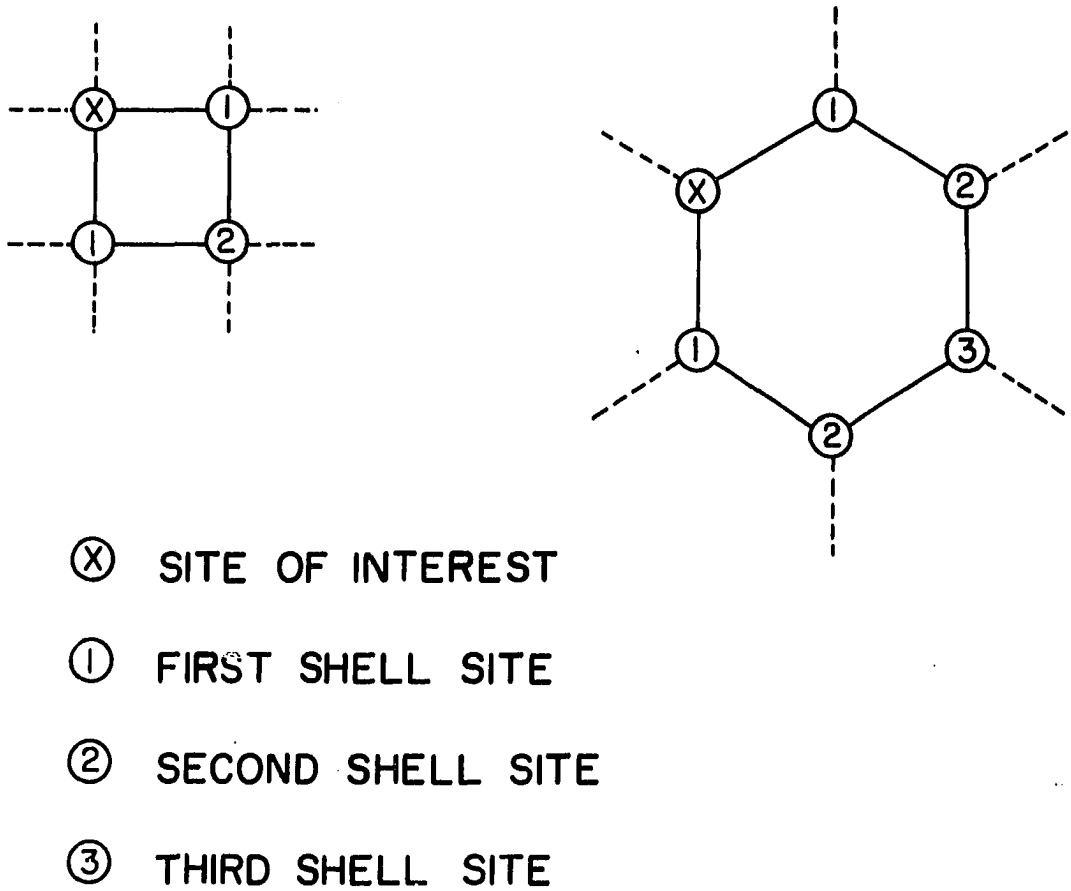

Figure 1.2. First, second, and third shell sites on a square and hexagonal lattice.

by Widom (14). The model is explicitly developed to describe the distribution of a hard sphere lattice gas with nearest neighbor exclusion on one and two dimensional lattices. The event for this model is, of course, the occupation of a lattice site by a sphere with a spherically symmetric 1st n.n. blocking potential. On the linear lattice this model is the same as the dimer space-filling models. In this one-dimensional case, the kinetic equations are solved as density expansions and compared to expansions of equilibrium distributions of similar events. The two expansions were found to differ beginning with the third virial coefficient. Widom's results are consistent with the results of Hoffman, whose work is examined later in this section. Widom calculated the saturation covering fraction for the kinetic distributions on a discrete lattice and on a line with the reported results of $\theta_{sat} = 0.826$, and 0.7476, respectively. The result on the line agrees with that of Rényi (15), and is correct. Widom later corrected his discrete lattice value of θ_{sat} to the standard result (16), $\theta_{sat} = 1 - e^{-2}$.

The two dimensional version of Widom's model differs from the dimer model in that the blocking potential is radially symmetric on the plane. For example, on a hexagonal lattice the occupation of one site protects the three nearest neighbor sites from occupation. As with the dimer model in two dimensions, the kinetic equations for this model are not

exactly soluble. Widom therefore calculates the saturation density on a hexagonal lattice to be 0.76±0.02 by Monte Carlo techniques.

Several models have been developed to examine the effect of longer range blocking potentials on the kinetic distributions of the space-filling problems. Boucher (17), for example, models the kinetics of an event with a 2nd n.n. blocking potential within the framework of side group reactions on a polymer chain (similar to the Flory model). He derives the kinetic equations for the reaction of three adjacent pendant groups on a polymer chain of length N and solves the equations using a combination of recursion relations and generating function techniques for $N\bar{P}^{(1)}_{\{j\}}(\underline{0})[t]$ and $(N-1)\bar{P}^{(2)}_{\{j,j+1\}}(\underline{0})[t]$, the average number of single and double isolated vacancies at time t. In the limit as N, $t\to\infty$, a total fraction of sites equal to e^{-2} remain unreacted in singlets or pairs. Of this amount, the fraction of pairs of unreacted sites is $2e^{-3} \simeq 0.0996$. Mackenzie (18) describes a further extension of the model on a lattice of length N to which events with a general rth n.n. blocking potential and also utilizes generating function or transform techniques in its solution. His results show that in the limit as $t\to\infty$, for large N, the average distribution of isolated vacancies is given by

$$\bar{P}^{(1)}_{\{j\}}(\underline{0}) \sim (N+r+1)\ A_1(r+1) \qquad (1.14)$$

and the dispersion of this quantity is given by

$$\sigma^2 \sim (r+1)(N+r+1)A_2(r+1) \qquad (1.15)$$

where $A_1(r)$ and $A_2(r)$ are quadratures that are parametrized on r, the range of the blocking potential. For the case where r=1, the integrals can be evaluated explicitly in closed form to give $A_1(2) = e^{-2}$ and $A_2(2) = 2e^{-4}$, and Eqns. 1.14 and 1.15 reduce to the results cited previously for the work of Cohen and Reiss, and Page.

If, in the above model, the limit as $N\to\infty$ is taken such that the ratio N/r is held constant, we obtain a description of the distribution of unit intervals on the infinite line. In this limiting case, Mackenzie finds that the distribution of vacant intervals of length x at lattice saturation is given by

$$P_0(x) = \frac{2}{P_0(0)} \int_0^\infty dv e^{-vx} \exp\{-2\int_0^v dt(\frac{1-e^{-t}}{t})\}, \qquad (1.16)$$

where x lies in the range $0 \leq x < 1$. This space-filling problem on the infinite line was first treated by a direct analysis of the distributions on the line by Rényi, and has come to be known as the parking problem. Analyses and generalizations of this problem are given by Domb (19) and Ney (20).

Kinetic models describing the distribution of cooperative, irreversible events can generally be considered as direct extensions of the space-filling models where the

transition probabilities are now dependent on the cooperative interactions of the local distribution of events on the site with the site of interest. The kinetic equations for these models are similar to those of the space-filling models; however, in general they are more difficult to solve because of the increased coupling between distributions. In many cases it is still possible to truncate and solve the hierarchy exactly on the linear lattice. This is in contrast with the kinetic equations for reversible events that can be solved exactly in only a very few cases (cf. Langmuir model).

We can begin our review of the comparatively few cooperative, irreversible models presented to date by considering the work of Schwarz (21) who describes the kinetics of an event with a 0th n.n. blocking potential with 1st n.n. cooperative interactions on a linear lattice of length N. As is the case for all problems on the finite or semi-infinite lattice, the kinetic equations derived by Schwarz are dependent on the position of the configuration of events on the lattice and the distributions are therefore characterized by the additional parameter "i" that locates the site on which the leftmost member of the configuration of events occurs. To truncate this site dependent hierarchy of equations, a relation referred to as the triplet closure rule is presented that allows the distribution of any configuration of events to be written entirely in terms of

triplets and pairs of events. This rule can be written in the form

$$P_i^{(n)}(\underline{x}) = \frac{P_i^{(3)}(x_i,x_{i+1},x_{i+2})P_{i+1}^{(3)}(x_{i+1},x_{i+2},x_{i+3})}{P_{i+1}^{(2)}(x_{i+1},x_{i+2})P_{i+2}^{(2)}(x_{i+2},x_{i+3})} \times \frac{P_{i+2}^{(3)}(x_{i+2},x_{i+3},x_{i+4})P_{i+3}^{(3)}(x_{i+3},x_{i+4},x_{i+5})}{P_{i+3}^{(2)}(x_{i+3},x_{i+4})} \cdots, \tag{1.17}$$

where $P_i^{(k)}(x_i,x_{i+1},\ldots,x_{i+k-1})$ is the distribution of events on sites $i,i+1,\ldots,i+k-1$. It is shown in Chapter 3 that the triplet closure rule is exact in only one case, but provides a convenient approximation with which to truncate a kinetic hierarchy, especially in the limit of low event density or small cooperative interaction. Using the triplet closure rule, Schwarz truncates the kinetic hierarchy and obtains four coupled differential equations that are still parameterized on i. He also presents the equations for the problem on the infinite linear lattice. None of the equations are solved in his paper.

E. A. Boucher (22,23) extends the cooperative model to describe events with a general rth n.n. blocking potential and r+1st n.n. cooperative interaction on the finite lattice of length N. Generating function techniques are used to solve the site dependent kinetic equations for $P_i^{(n)}(\underline{0})$, θ, and $\dot{\theta}$, where $\dot{\theta}$ is the rate of occupation of a site. His

results are presented as complicated quadratures. Numerical values of the saturation values of $P^{(n)}_{\{n\}}(\underline{0})$ are tabulated as a function of r. Gonzalez et al. (24) attack a similar problem on the infinite linear lattice by assuming that the solutions to the kinetic equations have the form

$$P^{(n)}_{\{n\}}(\underline{0})\ [t] = F(t)\ \exp\{-2t(n-2r+k)\}$$

where F(t) is an unknown function of t, and k is that portion of the rate constant reflecting the r+1st n.n. cooperative interactions. The equations are then solved for F(t) in terms of a quadrature. In the case where r=0, results found for the limit where $N\to\infty$ agree with those of Boucher. The continuous limit for noninteracting events is shown to agree with the results of Rényi.

An approach based on the grand ensemble formalism is used by Hoffman (25) to formulate a cooperative irreversible kinetic model of general application. As presented, the events of this model have 1st n.n. blocking potentials and mth n.n. cooperative interactions. The $f^{(n)}_{\{n\}}(\underline{x})$, the distribution of events on a specified set of {n} sites without regard to the condition of the rest of the lattice, are expanded in a series of the form

$$f^{(n)}_{\{n\}}(\underline{x}) = \sum_{m=0} \frac{1}{m!} \left\langle \Phi^{(n+m)}_{\{n+m\}} \right\rangle^{n+m}_{n+1}, \qquad (1.18)$$

where $\Phi^{(n+m)}_{\{n+m\}}$ is the probability that only the set $\{n\}\cup\{m\}$ sites are occupied, the set $\{m\}$ are sites on the lattice other than $\{n\}$, and $\langle\ \rangle^{n+m}_{n+1}$ indicates an average over all possible positions of the set $\{m\}$. The kinetic equations governing the $\Phi^{(j)}_{\{j\}}$ are basically master equations (cf. the discussion following Eqn. 1.7) since $\Phi^{(j)}_{\{j\}}$ is a distribution function for the whole lattice, and are given in the form

$$\frac{d\Phi^{(n)}_{\{n\}}}{dt} = \sum_{j\varepsilon\{n\}} \sigma_{j,\{n\}-j}\ \Phi^{(n-1)}_{\{n\}-j} - \langle\sigma_{n+1,\{n\}}\rangle_{n+1}\ \Phi^{(n)}_{\{n\}}, \quad (1.19)$$

where $\sigma_{k,\{n\}}$ is the rate at which event k occurs on a lattice occupied by the set of $\{n\}$ events. The kinetic equations for the model are obtained from the time derivative of equation 1.18 and the appropriate substitution equation 1.19. After extensive manipulation, these equations are expressed as expansions in $n-1,\ell$ a generalized Ursell function (8). These equations are then solved as expansions in η, the time dependent event density. The coefficients of these expansions are written as sums of cluster diagrams representing the interaction of events on a lattice of general dimensionality. It is the cluster diagrams that contain all of the information relating to geometries and cooperative effects in various systems. A general procedure for the generation of contributing cluster diagrams in the

coefficient of the jth power of η is presented, where for practical reasons $j = 1,2,3,4$. The model has great versatility as presented. It is also easily extended to include a general rth n.n. blocking potential by including constraints on the evaluation of the cluster diagrams. There are, however, drawbacks to this model. Even though the density expansions are exact solutions of the kinetic equations, the evaluation of cluster diagrams for higher terms often becomes impractical, limiting the expansions to as little as three or four terms. This, of course, limits the accuracy, especially at high event densities. Numerical results are presented that compare the four term density expansion for the pair distribution ($f^{(2)}_{\{j,j+1\}}(\underline{x})$) of random events on the linear lattice to exact solution obtained previously (17) and to four term density expansions of equilibrium pair distributions.

Yet another approach is used by Gō (26) to describe the irreversible cooperative kinetics of a general chemical system. Based on the path-integral model of Kikuchi (27), this model describes the time evolution of an ensemble of chemical systems in terms of the most probable path taken by a system. A path is the sequence of possible transitions from one state of the system to another. The most probable path is the one most likely to be taken by an ensemble member as it evolves in time. In the case of a lattice

system, the most probable path will describe the evolution in time of the irreversible distribution of events over the entire lattice. A brief description of the Gō model is as follows: it is assumed that an ensemble of systems is in contact with a heat reservoir that induces transitions between states of the system. The time evolution, or path, of a system is specified by the transition probability between two states, θ_{ij}, a set of state parameters, $\{p_i(t)\}$, which describe the probability that the system is in state i at time t, and a set of path parameters, $\{P_{ij}(t,t+\Delta t)\}$, which reflect the conditional probability that a system that is in state i at time t will be in state j at time $t+\Delta t$. The logarithm of the expression describing a path probability is maximized with respect to the path parameters, subject to the constraints of the conservation of probability. The resulting equations give the most probable path in terms of the path and state parameters, transition probabilities, and Boltzmann-like weight factors written in terms of the free energy of the state. The kinetic equations for the irreversible chemical changes of state are obtained from the time derivative of these equations and have the form

$$\frac{dp_j}{dt} = \sum_i \theta_{ij}\{p_j \exp[-\beta(f_i-f_j)/2] - p_i \exp[-\beta(f_j-f_i)/2)\}, \tag{1.20}$$

where f_i is the free energy of state i, and β is the statistical temperature. Equation 1.20 represents the

hierarchy of equations that must be truncated and solved according to the conditions of the situation under consideration.

The criterion of reversibility of events in a kinetic lattice model is necessary to examine the relaxation of a distribution of conditions to an equilibrium configuration. However, as we noted earlier, the kinetic equations that describe the evolution of these distributions are more difficult to solve than those for a single, irreversible event, and have been exactly solved in only a very small number of instances. One important example of a cooperative, reversible model that has been solved exactly was presented in 1967 by R. J. Glauber (2). The system he considered was a linear lattice of N atoms, for which each atom had a magnetic spin of $\sigma = \pm 1/2$. The master equation for this system is

$$\frac{dP(\sigma,t)}{dt} = \sum_j \omega_j(-\sigma_j|\underline{\sigma}^{(j)})P(\underline{\sigma}^{(j)},t) - \sum_j \omega_j(\sigma_j|\underline{\sigma})P(\underline{\sigma},t) \qquad (1.21)$$

where σ_j is the spin of the jth site, $\omega_j(x_j|\underline{\sigma})$ is the transition probability from spin x of site j as a function of the particular lattice state $\underline{\sigma}$. Here $\underline{\sigma}$ is the spin occupation vector for the entire lattice, and $\underline{\sigma}^{(j)}$ differs from $\underline{\sigma}$ in that the spin of site j is reversed. Equation 1.21 was used by Glauber to derive the following kinetic

equations for the average spin on site j, $\langle \sigma_j(t) \rangle$, and the two spin correlation function, $\langle \sigma_j(t)\sigma_k(t) \rangle$, for sites j and k:

$$\frac{d}{dt} \langle \sigma_j(t) \rangle = -2\langle \sigma_j(t)\omega_j[\sigma_j(t)] \rangle \tag{1.22}$$

and

$$\frac{d}{dt} \langle \sigma_j(t)\sigma_k(t) \rangle = -2\langle \sigma_j(t)\sigma_k(t)\{\omega_j[\sigma_j(t)] + \omega_k[\sigma_k(t)]\} \rangle \tag{1.23}$$

The particular form chosen to represent the nearest neighbor cooperative interactions in the transition probabilities allow these two equations to be solved exactly and independently using generating function or transform techniques. Other forms for this interaction leave the equation coupled.

Glauber utilizes his kinetic model to describe the dynamics of lattice spin waves, investigate the influence of a time dependent magnetic field on the distributions of spins, and to find the frequency-dependent magnetic susceptibility of the lattice in a weak field limit. He also derives the fluctuation-dissipation theorem relating the magnetic susceptibility to the Fourier transform of the time dependent spin-spin correlation function at equilibrium.

Much of the other work concerning reversible events has come in the connection with the study of magnetic spin

systems. A detailed review of this topic is somewhat beyond the range of this thesis, however, it can be mentioned that higher dimensional analogues of the Glauber model and problems involving magnetic spin lattices in an external field have been considered but have not been solved exactly. Huang (28) presents a brief overview of these problems and the various approximation techniques used in their solution.

Literature Survey - Applications

We now examine some applications of the models discussed in previous sections to problems of chemical and physical interest.

Historically, much of the development of one-dimensional kinetic models has come in connection with polymer chemistry. As we have seen, one form of the dimer space-filling model was presented in 1939 by Flory to study the condensation reaction of neighboring ketone groups of poly(methyl-vinyl) ketone. Barron and Boucher (29) have proposed the use of dimer space-filling models to determine whether the reaction mechanisms of the dechlorination of polyvinyl chloride, illustrated in Eqn. 1.24, and the dehydrochlorination of polyvinylidene chloride, illustrated in Eqn. 1.25, are random or self-propagating.

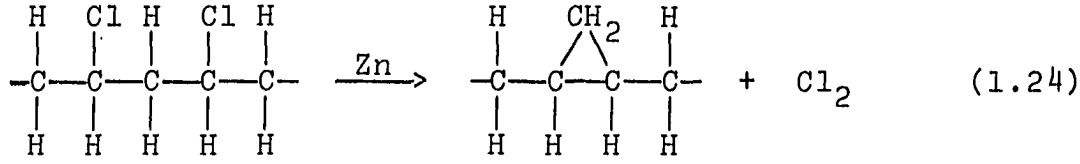

(1.24)

If the model distributions match the experimental results at lattice saturation, then it is assumed that the reaction of

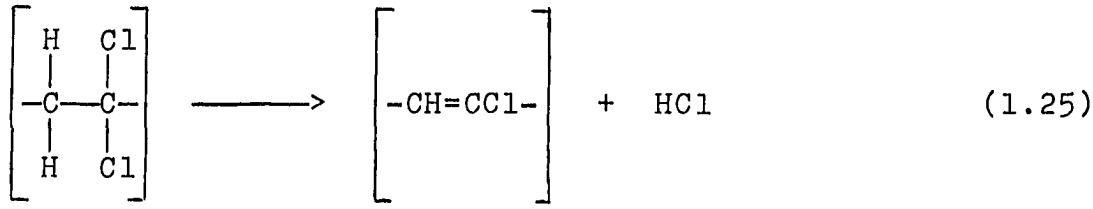

(1.25)

a particular polymer unit is governed by random selection. If a substantially larger fraction of monomer units have reacted than the 13.5% predicted by the space-filling models, then it is assumed that the reaction proceeds along the chain in a highly cooperative, sequential manner. Experimental results are presented by the authors to support the random reaction mechanism for Eqn. 1.24 and the sequential mechanism for Eqn. 1.25.

Cooperative, irreversible models on the linear lattice have been useful in the description of the cooperative reaction of polymer functional groups. Alfrey and Lloyd (30), Arends (31), and Keller (32) present similar models for the kinetics of events with a 0th n.n. blocking potential and 1st n.n. cooperative interactions to describe the kinetic distribution of sequences of n unreacted

functional groups. Alfrey and Lloyd suggest the application of the models to investigate the cooperative nature of such reactions as the dehydrochlorination of polyvinyl chloride, as seen in Eqn. 1.26, or the quaternization of poly(4-vinyl pyridine), illustrated in Eqn. 1.27. For example, in Eqn.

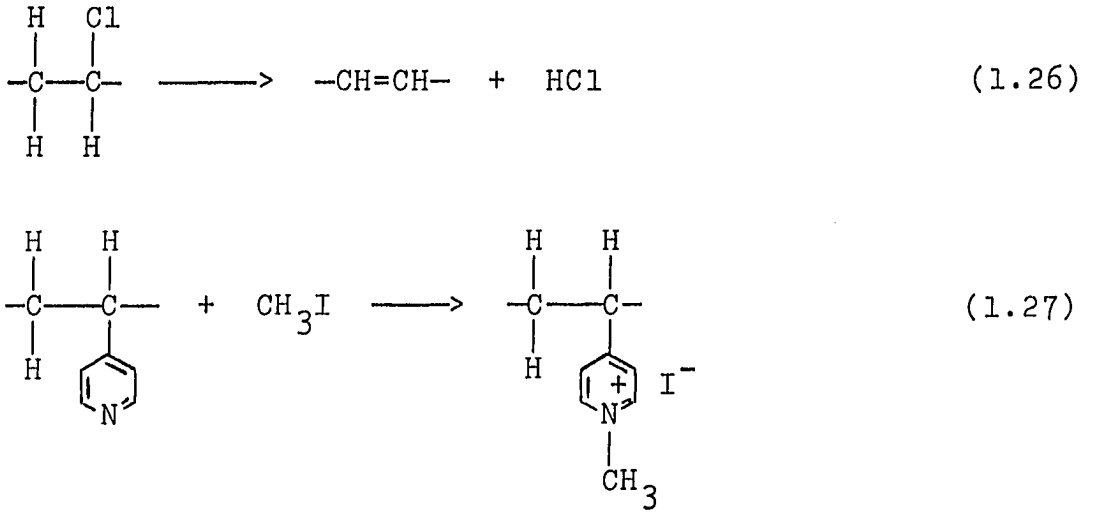

(1.26)

(1.27)

1.26 the loss of HCL from a monomer unit converts the adjacent units to allylic structures, which tends to promote the dehydrochlorination reaction. On the other hand, the charged amine group of Eqn. 1.27 is thought to inhibit the quaternization of adjacent units, especially during the latter stages of the reaction. A comparison of the model and experimental distributions would help clarify the nature and extent of the cooperative behavior. The results of Barron and Boucher, from the application of the space-filling models to the dehydrochlorination of poly-vinylidene chloride, supports the cooperative nature of the similar reaction of polyvinyl chloride.

A variation on the cooperative models we have seen thus far is used by McQuarrie et al. (33) to describe a kinetic version of the equilibrium Zimm-Bragg (34) model that describes the denaturation of a polypeptide. McQuarrie defines the event to be the breakage of a peptide bond and the subsequent loss of helical structure of the polymer unit, where the breaking rate of the peptide bond depends on the average cooperative effect of the condition of a cluster of neighboring segments instead of accounting for the effect of each neighboring segment individually. Distributions of sequences of unbonded segments are calculated from a hierarchy of kinetic equations in the standard manner. No experimental results are presented for comparison. The same problem of polypeptide denaturation is also treated by Gō (35) who uses the path integral formalism which he developed to describe chemical kinetics. The basic model was described in the previous section. We remember that his kinetic equations are derived to describe an arbitrary chemical process in terms of state parameters and path parameters that are analogous to the event distributions and transition probabilities of the lattice models. To model the polypeptide denaturation Gō defines the state parameters as the distribution of configurations of bonded and unbonded segments, but restricts the description to distributions of configurations of three segments or less. (This is

reminescent of the triplet closure approximation invoked by Schwarz which was previously discussed.) The path parameters are specified as the transition probability for an event with 1st n.n. cooperative interactions. The resulting kinetic equations are solved in the linear or near equilibrium approximation. Once again, no experimental results are presented.

Isbister and McQuarrie (3) adopt Glauber's reversible cooperative model to describe the rotational motion of a polymer pendant group about the axis of the monomer segment to which it is attached. It is assumed that the pendant group can take on one of two possible orientations with respect to the axis of the segment and that the dipole moment of the polymer segment will depend on the pendant groups orientation. Thus, the theory can be experimentally tested. The average dipole moment and the dipole-dipole correlation function are obtained directly from the Glauber kinetic equations. The dielectric susceptibility of the polymer chain is then calculated as the Laplace transform of the dipole autocorrelation function, $\langle\sigma_m(0)\sigma_m(t)\rangle$, and plotted versus electric field frequency for various polymer chain lengths to examine the chain length dependence of the rotameric motions.

In other areas of application, kinetic lattice models have been utilized in the study of processes that occur on

the surface or in the bulk of a crystalline solid. We have already seen the application of two-dimensional space-filling and cooperative models in the description of irreversible adsorption processes in the work of Vette, and of Hoffman. However, also of interest are problems involving the reaction of chemical species that occupy neighboring sites on a two- (or three) dimensional lattice. For example, under normal laboratory conditions the surfaces of several metals or metal oxides are strongly hydrated and are essentially lattices with hydroxyl groups attached to each site. On heating these surfaces it is possible for neighboring hydroxyl groups to react with the elimination of water, and to leave either one vacant lattice site or an oxygen atom bridging two adjacent sites. The analogy to the Flory model is obvious. The distribution of reacted sites or unreacted hydroxyl groups can be used to predict various physical properties of the surface such as its catalytic activity. The dependence of the catalytic activity of a surface on the distribution of chemical species on its surface is further discussed in Chapter 6.

A study of the dehydration of metallic surfaces was reported by Fuller *et al.* (1) who model the noncooperative combination and elimination of neighboring hydroxyl groups on a general NxN square lattice. The reaction of neighboring hydroxyl groups proceeds according to Eqn. 1.28. Instead of

utilizing a two dimensional space-filling model, they

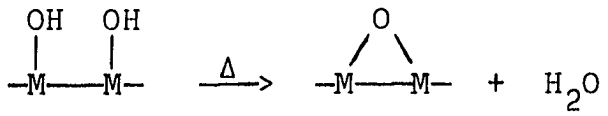

(1.28)

represent the square surface as a composite of finite, one-dimensional lattices that are assembled to comprise the NE-SW diagonals of the lattice. It is then assumed that the elimination reaction occurs only between hydroxyls that lie on one of the diagonal lattices. Each diagonal can then be considered as an independent, finite lattice for which the distribution of events is readily attainable by methods previously discussed. The distribution of events of the square lattice is then obtained as an average of the distributions on the linear lattices. In this manner Fuller obtains the result that at saturation $\theta_{sat} = 0.921$, or approximately 7.9% of the hydroxyl groups remain vacant and isolated. As a comparison he also calculates the saturation distribution by Monte Carlo techniques with the results that $\theta_{sat} = 0.925$, or 7.5% of the hydroxyl groups remain isolated. Monte Carlo simulation of the noncooperative dehydration of a surface was also reported for the surface of silica gel by Peri and Hensley (36), and for the surface of γ-alumina by Peri (37). The fully hydrated surface of silica gel described by Peri and Hensley is composed of silicon atoms, each occupied by a pair of geminal hydroxyl groups. In the dehydration reaction it is thought that one of the two

hydroxyl groups on a silicon atom reacts with one of the geminal pair on an adjacent silicon atom in the same lattice row to form a siloxane link and a vicinal pair of hydroxyl groups. A vicinal and geminal hydroxyl group or two vicinal hydroxyl groups are not allowed to react. The results of this calculation show that at saturation, 15.4% of the hydroxyl groups were left isolated and unreacted. The difference in these results with those obtained by Fuller arise from the difference in reaction geometry of the two problems. Whereas the dehydration of the silica gel occurs along the parallel edges of a unit cell, the dehydration model proposed by Fuller is characterized by the reaction of hydroxyls across the diagonal of the square unit cell.

The model of the dehydration of γ-alumina, described by Peri, has one hydroxyl group per surface site and allows the reaction of a hydroxyl group to occur with either horizontal or vertical nearest neighbor groups. At saturation approximately 9.6% of the groups remain isolated.

Three-dimensional applications of kinetic lattice models are rare, however Jackson and Montroll (38) utilize basic combinatorial techniques to describe the statistics of the recombination of nearest neighbor nitrogen radicals that have been condensed in a solid nitrogen matrix. It is assumed that a radical reacts with a single nearest neighbor radical to form a nitrogen molecule. The average saturation

distribution of free radicals is then calculated for lattices of cubic symmetry from the number of ways the nearest neighbor sites can react without reacting with the site of interest. Since this model describes the distribution of events as an average over all configurations of neighboring sites, it clearly ignores the kinetic, space-filling aspects of the problem and the results must be considered as an upper limit for the possible kinetic distributions. For example, the solution of the model on the linear lattice gives a saturation density of unreacted radicals of 17.7% as compared to 13.5% for the space-filling models. The three dimensional results for the fraction of radicals for simple, face centered, and body centered cubic lattices are reported to be 0.138, 0.122 and 0.102, respectively. A more detailed discussion of this approach to the calculation of lattice distributions can be found in papers by Roberts and Miller (39), and Lichtman and McQuistan (40).

CHAPTER 2. NON-COOPERATIVE, IRREVERSIBLE MODELS

In Chapter 1 we presented a very general overview of kinetic lattice models and their applications. It is the purpose of this chapter to review the development of the non-cooperative models by examining the derivation and solution of the kinetic equations for the infinite, semi-infinite, and finite linear lattices. Many of the ideas and techniques utilized in this chapter are fundamental to the development and discussion of the models with cooperative events presented in Chapter 3.

The Infinite Lattice of Equivalent Sites

As in the previous chapter, we consider an ensemble of linear lattices in which each lattice is composed of an infinite number of equivalent, regularly spaced lattice sites. Each site on a given lattice can be in one of two conditions, 0 or 1, which represent two distinct chemical or physical states of the site. An event is now defined as the transition of a site from condition 0 to condition 1. For allowed transitions, the transition probability for an event is denoted by σ. All sites are initially assumed to be in condition 0. An event with an rth n.n. blocking potential which has occurred on site j prevents transitions from occurring on sites j-r through j+r. As in Chapter 1, we define $f^{(n)}_{\{n\}}(\underline{1})$ and $f^{(n)}_{\{n\}}(\underline{0})$ to be the respective

probabilities that a particular set of n sites, which we denote by {n}, have or have not undergone transition at time t. We can relate these two types of distributions through the following operator formalism. Let $\hat{f}_k(1)$ be defined as an operator that acts on individual ensemble members and takes on a value of 1 if site k on the particular lattice has undergone transition, and takes on the value of 0 if site k is vacant. The operator $\hat{f}_k(1)$ is evidently a projection operator that projects from the ensemble that subset of lattices on which site k has undergone transition. Also, let $\hat{f}_k(0)$ be defined as a similar operator that projects the subset of lattices with a vacancy at site k from the ensemble. We note that these operators satisfy the following relation:

$$\hat{f}_k(1) + \hat{f}_k(0) = 1 \tag{2.1}$$

The event distribution on {n} can then be expressed in terms of these operators as

$$f^{(n)}_{\{n\}}(\underline{1}) = \frac{1}{M} \prod_{k\varepsilon\{n\}} \hat{f}_k(1) \text{ (Ensemble)} \tag{2.2}$$

where (Ensemble) represents all of the members of the ensemble, and M is the number of lattices in the ensemble. The distribution of vacancies on the {n} sites is similarly written as

$$f^{(n)}_{\{n\}}(\underline{0}) = \frac{1}{M} \prod_{k\varepsilon\{n\}} \hat{f}_k(0) \text{ (Ensemble).} \tag{2.3}$$

We can now obtain the formal relation between the two types of distributions by substituting Eqn. 2.1 into Eqn. 2.3 with the result

$$f^{(n)}_{\{n\}}(\underline{0}) = \frac{1}{M} \prod_{k\varepsilon\{n\}} (1 - \hat{f}_k(1)) \text{ (Ensemble)}. \qquad (2.4)$$

By expanding the product we have that

$$f^{(n)}_{\{n\}}(\underline{0}) = \sum_{\{r\}\varepsilon\{n\}} (-1)^r \prod_{k\varepsilon\{r\}} \hat{f}_k(1) \text{ (Ensemble)}$$

$$= \sum_{\{r\}\varepsilon\{n\}} (-1)^r f^{(r)}_{\{r\}}(\underline{1}), \qquad (2.5)$$

where {r} represents a possible subset of {n} (including the nullset), and r is the number of elements of {r}. To illustrate this result, let us explicitly find the distribution of vacancies on three adjacent sites (say sites j, j+1, and j+2) in terms of the distribution of events. For this case we find that Eqn. 2.5 can be written

$$\begin{aligned} f^{(3)}_{\{j,j+1,j+2\}}(\underline{0}) = 1 &- f^{(1)}_{\{j\}}(1) - f^{(1)}_{\{j+1\}}(1) \\ &- f^{(1)}_{\{j+2\}}(1) + f^{(2)}_{\{j,j+1\}}(\underline{1}) + f^{(2)}_{\{j,j+2\}}(\underline{1}) \\ &+ f^{(2)}_{\{j+1,j+2\}}(\underline{1}) - f^{(3)}_{\{j,j+1,j+2\}}(1), \end{aligned}$$

where the doublet and triplet distributions can each be equal to zero depending on the range of the blocking potential exhibited by the event. From this discussion, it should be noted that the set of all distributions of

configurations of events (or by Eqn. 2.5, the set of all distributions of configurations of vacancies) is complete; that is, by the conservation of probability, the distribution of any configuration of events and vacancies can be written entirely in terms of distributions of events (or vacancies).

We begin our derivation of the hierarchy of kinetic equations for this model by considering the manner in which the distribution $f^{(n)}_{\{n\}}(\underline{1})$ changes in time. Because we are modeling an irreversible process, the time rate of change of $f^{(n)}_{\{n\}}(\underline{1})$ is solely determined by the ensemble average of the rate of transition of sites in $\{n\}$ that give rise to the configuration denoted by $(\underline{1})$, i.e., the gain term of Eqn. 1.8. Since we now consider only blocking potentials, this rate at a given site on a particular lattice is zero or σ, depending on the local distribution of events and vacancies. Consider, for example, an ensemble member which, at some time t, has site j vacant. An event can occur at that site thereby changing the ensemble density of events $f^{(1)}(1)$, only if site j is not blocked from transition by an event on a neighboring site which is r or less sites away. The time rate of change of $f^{(1)}_{\{j\}}(1)$ is therefore

$$\frac{df^{(1)}_{\{j\}}(1)}{dt} = \sigma\, f^{(2r+1)}_{\{j-r,\ldots,j+r\}}(\underline{0}). \tag{2.6}$$

The kinetic equations governing the distribution of larger configurations of events depend in a very complicated manner on the set {n}, and r, the range of the blocking potential. We can, however, utilize the operator formalism which we previously introduced to write the general kinetic equation governing the time evolution of an arbitrary configuration of events in the following manner:

$$\frac{df^{(n)}_{\{n\}}(\underline{1})}{dt} = \frac{\sigma}{M}\left[\sum_{j\varepsilon\{n\}}\left\{\prod_{k'\varepsilon\{j-r,\ldots,j+r\}}(1-\hat{f}_{k'}(1))\prod_{k\varepsilon\{n-j\}}\hat{f}_k(1)\right\}\right](\text{Ensemble})$$

$$= \sigma\sum_{j\varepsilon\{n\}}\left\{\sum_{\{k\}\varepsilon\{j-r,\ldots,j+r\}}(-1)^k f^{(p)}_{\{k\}\cup\{n-j\}}(\underline{1})\right\}, \qquad (2.7)$$

where $\cup$ is the standard notation for the union of two sets, and p is the number of elements in the set resulting from the union. Equations 2.6 and 2.7 form the infinite hierarchy of differential equations describing the evolution of distributions of irreversible events on the infinite linear lattice.

In a similar manner we can write equations for the distribution of vacancies as follows:

$$\frac{df^{(n)}_{\{n\}}(\underline{0})}{dt} = \frac{-\sigma}{M}\left[\sum_{j\varepsilon\{n\}}\left\{\prod_{k\varepsilon\{n\}\cup\{j-r,\ldots,j+r\}}\hat{f}_k(0)\right\}\right](\text{Ensemble}),$$

$$= -\sigma\sum_{j\varepsilon\{n\}} f^{(n+2r)}_{\{n\}\cup\{j-r,\ldots,j+r\}}(0). \qquad (2.8)$$

The latter set of equations, in general, involve fewer terms and is therefore less complicated. However, as previously mentioned, the complete set of equations for vacancy distributions is equivalent to the complete set of equations for event distributions. This can be explicitly seen by differentiating Eqn. 2.4 with respect to time and substituting Eqn. 2.7 into the result to obtain Eqn. 2.8. In the case where the distributions describe configurations of consecutive vacant sites, Eqn. 2.8 reduces to the following closed set of kinetic equations:

$$\frac{df(\underline{0})^{(n)}}{dt} = -n\sigma\, f(\underline{0})^{(2r+1)}, \qquad n \leq r+1 \tag{2.9}$$

$$\frac{df(\underline{0})^{(n)}}{dt} = -\sigma(2r-n) f(\underline{0})^{(2r+1)} - 2\sigma \sum_{\ell=0}^{n-r-1} f(\underline{0})^{(2r+1+\ell)}, \qquad r+1<n<2r \tag{2.10}$$

and

$$\frac{df(\underline{0})^{(n)}}{dt} = -\sigma(n-2r) f(\underline{0})^{(n)} - 2\sigma \sum_{\ell=1}^{r} f(\underline{0})^{(n+\ell)}, \qquad n \geq 2r \tag{2.11}$$

Here all the distribution functions refer to consecutive vacant sites, hence the subscript designating the set of lattice sites is superfluous and has been deleted to be consistent with the notation of Chapter 1. Equations 2.9, 2.10, and 2.11 form an infinite hierarchy of equations that can be exactly solved for the distributions of adjacent vacancies.

The distributions of events, or equally well, the associated distributions of vacancies, provide a complete description of lattice processes for the case that an event is represented by the transition at a single site. However, as we noted in Chapter 1, it can also be of interest to study the space-filling characteristics of a distribution of events. In other words, instead of representing an event as a point transition with an associated blocking potential, we wish to consider an event as an entity of finite spatial proportions that occupies a segment of definite length on the lattice. Thus, we consider two different but related lattices; the first being the event lattice we have previously introduced, and the second being a lattice on which an event with an rth n.n. blocking potential occupies a lattice segment which is r+1 event lattice spacings in length. We refer to this second lattice as a space-filling lattice. The space-filling lattice sites are defined to be the centers of the r+1 units into which the occupied length can be divided. The spacing of sites of the space-filling lattice is clearly the same as for the event lattice. (This, however, is only true for a one-dimensional lattice.) By definition, each event occupies r+1 space-filling lattice sites. This situation is illustrated in Fig. 2.1 for the case where r=3. In the dimer adsorption example cited in Chapter 1, the atomic lattice is the space-filling lattice

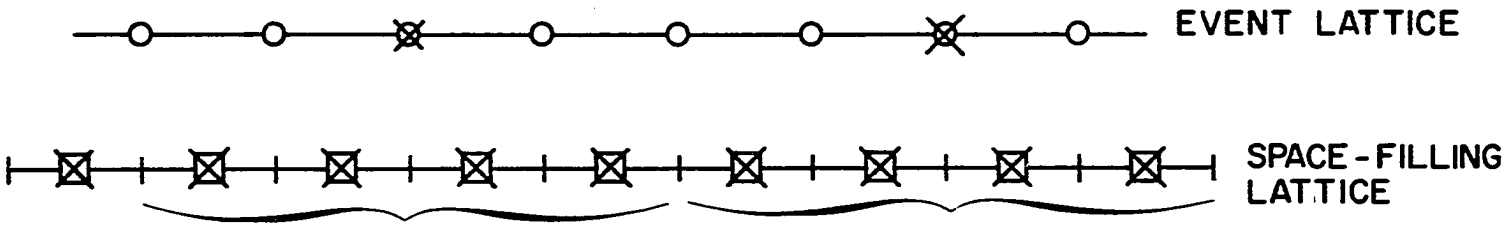

Figure 2.1. Two events with an r=3 blocking potential which are as close as possible on the event lattice. Each event occupies r+1=4 segments and 4 sites on the space-filling lattice

and the molecular lattice is, of course, the event lattice. Note that in this case the two lattices are not coincident, but are offset from each other by half a unit spacing. Some thought will show that this is the situation when r is odd. When r is even, the two lattices are coincident. In certain cases (e.g., the dimer adsorption problem) it is more convenient to know the distribution on the space-filling sites than on the event sites. We denote these distribution functions by $P^{(m)}_{\{m\}}(\underline{y})$ where $\underline{y}$ is the occupation vector for the set of sites {m} on the space-filling lattice.

It is important to note that the kinetic descriptions of a process on the event and space-filling lattices of a particular model are in general not equivalent if we consider only a portion of the lattice. The configurations on the event lattice always uniquely determine a corresponding configuration on the space-filling lattice. However, a particular space-filling configuration on a lattice segment, in general, can result from one of several event configurations. A simple example is given in Fig. 2.2. The space-filling distribution functions for a lattice segment can, therefore, be written as a sum of the event distributions that give rise to the space-filling configuration. However, there is no corresponding converse relationship. Because the space-filling distributions, in general, correspond to a sum of several event distributions, they contain less

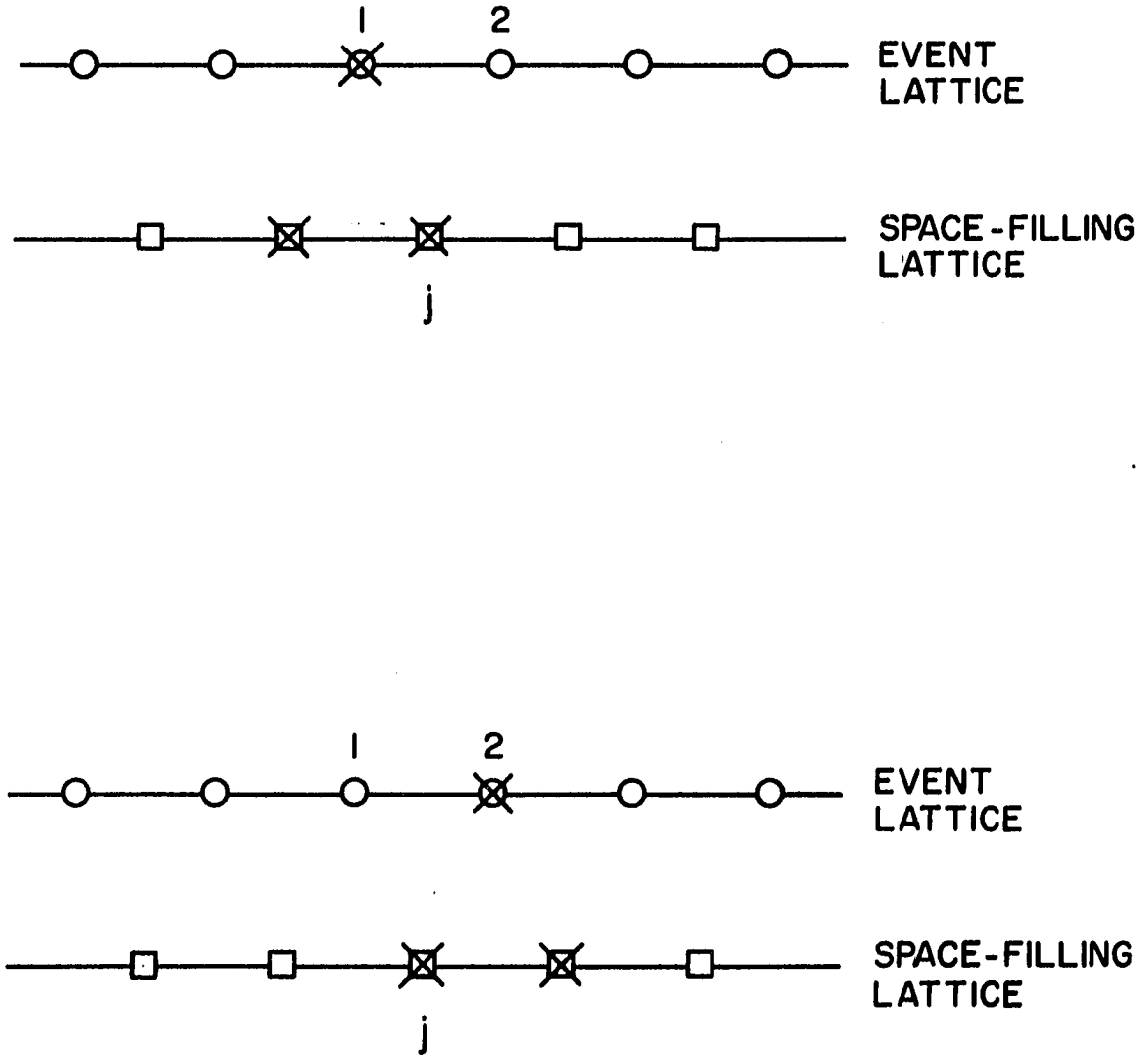

Figure 2.2. Two distributions on the event lattice that give rise to the occupation of site j on the space-filling lattice

information and provide a less complete description of the kinetic process than do the distributions on the event lattice.

Even though distributions on the space-filling lattice do not contain the information of the corresponding distributions on the event or molecular lattice, the space-filling distributions often are related to properties of physical interest. In the Flory model discussed earlier, the event is the reaction of a pair of neighboring pendant groups on the polymer chain. The quantity of interest to Flory was not, however, the number of pairs of reacted groups (i.e., events), but rather the number of unreacted pendant groups, i.e., the space-filling vacancies.

The kinetic equations for the distribution of n consecutive space-filling vacancies, $P^{(n)}(\underline{0})$, are easily derived from Eqns. 2.9, 2.10 and 2.11. (Here, as before, we omit a subscript on the distribution functions for consecutive vacancies.) An examination of the event and space-filling lattices for general r shows that $P^{(1)}(0)$, the density of space-filling vacancies, is related to the density of event vacancies by

$$P^{(1)}(0) = (r+1)\, f^{(1)}(0). \tag{2.12}$$

In addition, we see that

$$P^{(n)}(\underline{0}) = f^{(n+r)}(\underline{0}). \tag{2.13}$$

Differentiating Eqn. 2.12 with respect to time and substituting this result, along with Eqn. 2.13, into Eqn. 2.9 for n=1, we obtain the result

$$\frac{dP^{(1)}(0)}{dt} = -(r+1)\sigma P^{(r+1)}(\underline{0}). \tag{2.14}$$

The remaining kinetic equations in the hierarchy are obtained by making the same substitutions into Eqns. 2.10 and 2.11. These equations are listed below:

$$\frac{dP^{(n)}(\underline{0})}{dt} = -(r-n+2)\sigma P^{(r+1)}(\underline{0}) - 2\sigma \sum_{\ell=1}^{n-1} P^{(r+1+\ell)}(\underline{0}), \quad 1<n\leq r \tag{2.15}$$

and

$$\frac{dP^{(n)}(\underline{0})}{dt} = -(n-r)\sigma P^{(n)}(\underline{0}) - 2\sigma \sum_{\ell=1}^{r} P^{(n+\ell)}(\underline{0}), \quad n\geq r \tag{2.16}$$

These equations can also be derived without explicitly considering the event lattice by directly examining the time rate of change of $P^{(n)}(\underline{0})$.

Equations 2.14, 2.15 and 2.16 form an infinite set of coupled differential equations describing the kinetics of the distribution of vacancies on the space-filling lattice. We now truncate the hierarchy in an exact manner. To this end we define a new variable q_j which is the conditional probability that a given site is vacant given that the preceding j consecutive sites are vacant. That is

$$P^{(j+1)}(\underline{0}) \equiv P^{(j)}(\underline{0})\, q_j. \tag{2.17}$$

Differentiation of Eqn. 2.17 with respect to time gives

$$\frac{dP(\underline{0})^{(j+1)}}{dt} = q_j \frac{dP(\underline{0})^{(j)}}{dt} + P^{(j)} \frac{dq_j}{dt} \tag{2.18}$$

Equation 2.16 can be substituted into Eqn. 2.18 and the result rearranged to give

$$\frac{dq_j}{dt} = -\sigma q_j - 2\sigma \sum_{\ell=1}^{r} \left(P(\underline{0})^{(j+\ell)} / P(\underline{0})^{(j)} \right) \left(q_{j+\ell} - q_j \right), \quad j \geq r, \tag{2.19}$$

which is the general equation governing the time evolution of all q_j, $j \geq r$, and is completely equivalent to the hierarchy defined by Eqn. 2.10. The boundary condition for the problems we consider is $q_j = 1$, at $t=0$, for all j. It is evident that

$$q_j = q_r \tag{2.20}$$

is a solution of Eqn. 2.19 satisfying the boundary condition. Substituting this result back into Eqn. 2.19 yields

$$\frac{dq_r}{dt} = -\sigma q_r, \tag{2.21}$$

which has as its solution

$$q_r = e^{-\sigma t}. \tag{2.22}$$

Using these results we can write Eqn. 2.17 in the form

$$P(\underline{0})^{(j)} = P(\underline{0})^{(r)} \prod_{\ell=0}^{j-r-1} q_{r+\ell} = P(\underline{0})^{(r)} (q_r)^{j-r}, \quad j \geq r \tag{2.23}$$

Equation 2.23 is the exact solution of the infinite hierarchy for all $P^{(j)}(\underline{0})$, where $j \geq r$. Physically, the truncation equation (Eqn. 2.20) says that the sites on which a particular site is conditioned that lie beyond r successive space-filling vacancies do not affect the conditional probability. That is, the r vacancies separating the site of interest from the other sites on the lattice block the influence that the condition of these sites might have on the rate of addition to the site of interest. This truncation procedure reduces the determination of any distribution which can be written in terms of consecutive vacancies to the solution of a finite set of differential equations, namely Eqns. 2.14 and 2.15. In Chapter 3 we will see that distributions involving nonconsecutive vacancies can be obtained in a similar manner.

Equation 2.20 can now be used to solve Eqns. 2.14 and 2.15. These equations form an autonomous system of differential equations, that is, time does not appear explicitly on the right side of the equations. Hence, the time can be completely eliminated by dividing all of the equations by Eqn. 2.21. Thus, Eqn. 2.14 assumes the form

$$\frac{dP^{(1)}(0)}{dq_r} = (r+1)P^{(r)}(\underline{0}), \tag{2.24}$$

where q_r is now the independent variable, and similarly, Eqn. 2.15 has the form

$$\frac{dP^{(n)}(\underline{0})}{dq_r} = \left\{(r+2-n) + 2\sum_{\ell=0}^{n-1}(q_r)^{\ell}\right\}P^{(r)}(\underline{0}), \quad 1<n\leq r \tag{2.25}$$

In particular, for j=r, Eqn. 2.25 can be written

$$\frac{d\ \ell n\ P^{(r)}(\underline{0})}{dq_r} = 2\sum_{\ell=0}^{r-1}(q_r)^{\ell}, \tag{2.26}$$

which has as the particular solution obeying the boundary conditions

$$P^{(r)}(\underline{0}) = \exp\left\{2\sum_{\ell=1}^{r}\frac{1}{\ell}\left(q_r{}^{\ell}-1\right)\right\}. \tag{2.27}$$

This result, when substituted into Eqns. 2.24 and 2.25, yields the results

$$P^{(1)}(0) = 1 + (r+1)\int_1^{q_r} dx\ \exp\left\{2\sum_{\ell=1}^{r}\frac{1}{\ell}\left(x^{\ell}-1\right)\right\}, \tag{2.28}$$

and

$$P^{(n)}(\underline{0}) = 1 + \int_1^{q_r} dx\left[(r-n+2) + 2\sum_{\ell=1}^{n-1}x^{\ell}\right] \times \exp\left\{2\sum_{\ell=1}^{r}\frac{1}{\ell}\left(x^{\ell}-1\right)\right\}, \quad 1<n\leq r. \tag{2.29}$$

Equations 2.23, 2.28 and 2.29 are the consecutive vacancy distributions on the infinite discrete space-filling lattice for events with an rth n.n. blocking potential. In the present form they are functions of the independent variable

q_r. Their time dependence can be established using Eqn. 2.22.

It can be seen in the case where r=1 that these results reduce exactly to those obtained by Cohen and Reiss for dumbbells on the infinite lattice, given in Eqn. 1.11. The saturation limit for the fraction of vacant sites in this model is obtained from Eqn. 2.28 by taking the limit as $q_r \to 0$. We find that

$$P_{sat}^{(1)}(0) = 1 - (r+1) \int_0^1 dx \exp\{2 \sum_{\ell=1}^{r} \frac{1}{\ell} (x^{\ell}-1)\}, \quad (2.30)$$

which is $P_{sat}^{(1)}(0) = e^{-2}$ for r=1, in agreement with previous results.

We will also find it useful for our later discussion of the semi-infinite and finite lattice distributions to solve this model for the distributions of two nonconsecutive vacancies on the space-filling lattice, $P_{\{j,j+\ell\}}^{(2)}(\underline{0})$, in the case where r=1. The kinetic equations for these distributions can be derived from Eqn. 2.8 or can be derived by directly considering the time rate of change of the appropriate distribution. These kinetic equations are given below.

$$\frac{dP_{\{j\}}^{(1)}(0)}{dt} = - 2\sigma \, P_{\{j,j+1\}}^{(2)}(\underline{0}), \quad (2.31)$$

$$\frac{dP^{(2)}_{\{j,j+1\}}(\underline{0})}{dt} = -\sigma P^{(2)}_{\{j,j+1\}}(\underline{0}) - 2\sigma P^{(3)}_{\{j,j+1,j+2\}}(\underline{0}), \qquad (2.32)$$

and

$$\frac{dP^{(2)}_{\{j,j+\ell\}}(\underline{0})}{dt} = -2\sigma P^{(3)}_{\{j,j+1,j+\ell+1\}}(\underline{0}) - 2\sigma P^{(3)}_{\{j,j+1,j+\ell\}}(\underline{0}), \quad j\geq 2. \qquad (2.33)$$

We now define the conditional probability $\bar{q}(\ell)$ to satisfy

$$P^{(2)}_{\{j,j+\ell\}}(\underline{0}) = P^{(1)}_{\{j\}}(0)\ \bar{q}(\ell). \qquad (2.34)$$

the quantity $\bar{q}(\ell)$ is then the probability that a site is vacant, given that a single site ℓ sites away is vacant, irrespective of the condition of the intervening sites. For example, $P^{(2)}_{\{1,4\}}(\underline{0}) = P^{(1)}_{\{1\}}(0)\ \bar{q}(3)$. Using this definition, we can write the triplet vacancy distribution as

$$P^{(3)}_{\{j,j+1,j+\ell\}}(\underline{0}) = P^{(1)}_{\{j\}}(0)\ \bar{q}(1)\bar{q}(\ell-1). \qquad (2.35)$$

Substituting this result into Eqns. 2.32 and 2.33 and rearranging, we obtain

$$\frac{d\bar{q}(1)}{dt} = -\sigma\ \bar{q}(1) \qquad (2.36)$$

and

$$\frac{d\bar{q}(\ell)}{dt} = -2\sigma\ \bar{q}(1)\bar{q}(\ell-1). \qquad (2.37)$$

Dividing Eqn. 2.37 by Eqn. 2.36 and introducing the new variable $x = 2(\bar{q}(1)-1)$, we have that

$$\frac{d\,\bar{q}\,(\ell)}{dx} = \bar{q}\,(\ell-1), \tag{2.38}$$

which has the solution

$$\bar{q}\,(\ell) = e_{\ell-1}(x) + \frac{1}{2}\,\frac{x^{\ell}}{\ell!}\,. \tag{2.39}$$

Here $e_n(x) = \sum_{\ell=0}^{n} \frac{x^{\ell}}{\ell!}$ is the truncated exponential polynomial of degree n. Substituting this result into Eqn. 2.33, we have that

$$P^{(2)}_{\{j,j+\ell\}}(\underline{0}) = P^{(1)}_{\{j\}}(0)\,(e_{\ell-1}(x) + \frac{1}{2}\,\frac{x^{\ell}}{\ell!}). \tag{2.40}$$

Upon obtaining q_1 from Eqn. 2.28 and equating this result with Eqn. 2.39 for r=1 we find that $x = \ell n\,(1-\theta)$.

The Infinite Lattice with a Continuous Distribution of Sites

The distribution of vacancies on a line (a line being a lattice with a continuous distribution of sites) can be calculated as a limiting case of the distribution of vacancies on a discrete space-filling lattice, or it can be obtained directly by the application of the general model to a continuous lattice. In the following discussion, the general model will be applied to the infinite line to describe the kinetics of space-filling events with a blocking

size of length a. The saturation limit of this continuous model will then be compared to the saturation on a discrete lattice in the limit that the event site spacing goes to zero.

Consider an infinite lattice over which events of length a can be continuously distributed. An event can randomly and irreversibly occupy a line segment of length "a" provided it does not overlap events which have previously occurred. We define P(L) as the probability that a line segment of length L is vacant, and $\sigma d\ell$ as the transition rate of an event onto a line segment of length $d\ell$ if no previous event blocks the transition. The time rate of change of P(L) for $L \geq a$ is given by the rate of transition onto the line segment [-L/2,L/2]. This can be written

$$\frac{dP(L)}{dt} = -\sigma \int_{-\frac{(L-a)}{2}}^{\frac{(L-a)}{2}} d\ell\, P(L) - 2\sigma \int_{o}^{a} d\ell\, P(L+\ell), \qquad (2.41)$$

where the integrals replace the sums of the discrete model (compare to Eqn. 2.15). The first integral in Eqn. 2.41 gives the rate of addition of events lying totally within the segment [-L/2,L/2]. The second integral gives the rate of addition of events only partially overlapping the line segment (see Fig. 2.3). Since P(L) is not a function of the integration variable in the first integral, this integral can be explicitly evaluated to obtain

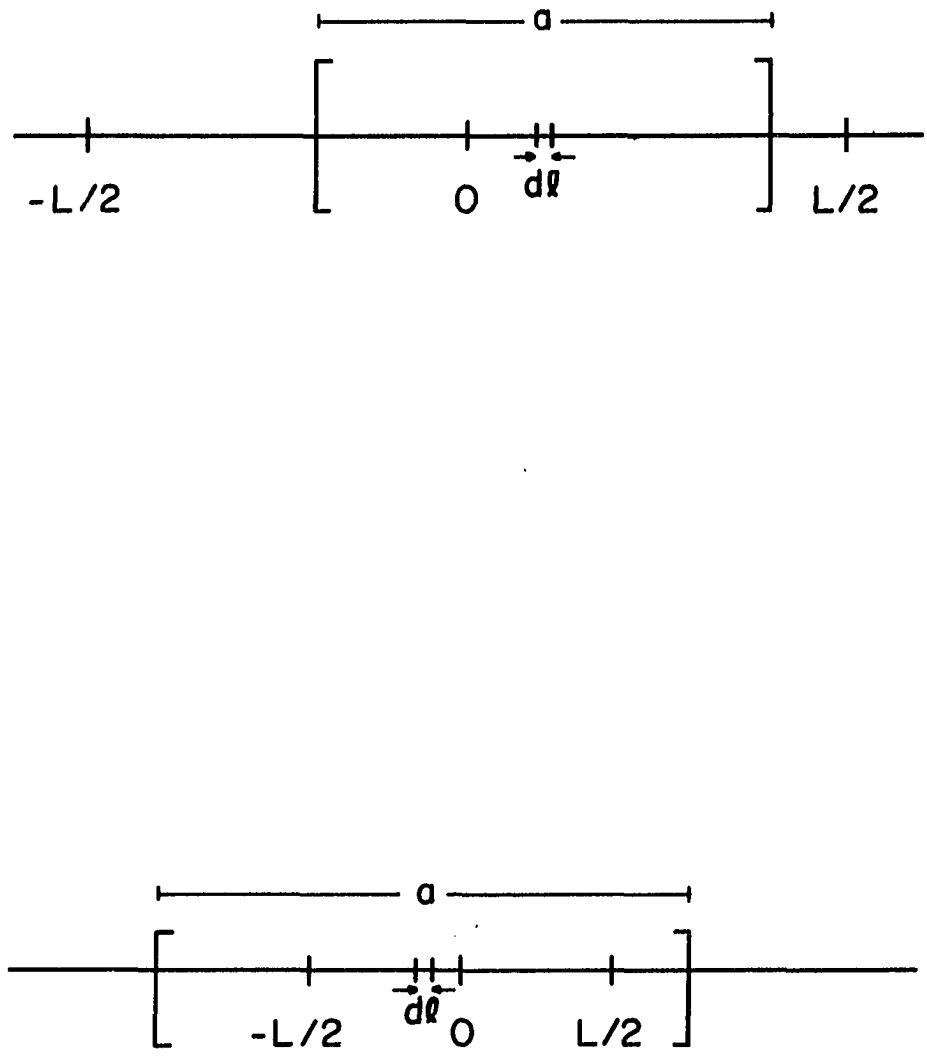

Figure 2.3. Possible configurations of an event of length a on a line segment of length L. In the first configuration, L>a and the event lies entirely on the segment. In the second configuration, L<a and the event encloses the entire segment

$$\frac{dP(L)}{dt} = -(L-a)\ \sigma\ P(L) - 2\sigma \int_0^a d\ell\ P(L+\ell),\ L \geq a. \quad (2.42)$$

The remaining integral will be evaluated later.

When $a \geq L$, the time rate of change of $P(L)$ is given by

$$\frac{dP(L)}{dt} = -\sigma \int_{-\frac{(a-L)}{2}}^{\frac{(a-L)}{2}} d\ell\ P(a) - 2\sigma \int_0^a d\ell\ P(a+\ell),\ a \geq L. \quad (2.43)$$

Here, the first integral gives the rate of addition of events which totally encompasses the interval $[-L/2, L/2]$, while the second integral gives the rate of addition of events which only partially overlap the interval (see Fig. 2.3). Once again, the first integral can be evaluated explicitly to yield

$$\frac{dP(L)}{dt} = -(a-L)\ \sigma\ P(a) - 2\sigma \int_0^L d\ell\ P(a+L), \quad a \geq L. \quad (2.44)$$

Equations 2.42 and 2.44 correspond to the hierarchy defined by Eqns. 2.14 through 2.16 and can be solved in an analogous fashion. For $L \geq a$, the conditional probability $\beta(L|a)$ is defined by

$$P(L) = P(a)\beta(L|a). \quad (2.45)$$

It is the probability that the entire interval of length L is vacant given that an interval of length, a, (which can

be on either side) is vacant. If we differentiate with respect to time and make use of Eqn. 2.42, we obtain

$$\frac{d\beta(L|a)}{dt} = -(L-a)\sigma\beta(L|a) - 2\sigma\int_{o}^{a} d\ell[\beta(L+\ell|a) - \beta(L+a)\beta(\ell+a|a)]. \qquad (2.46)$$

By analogy with the solution of the discrete hierarchy, we propose that

$$\beta(L|a) = e^{-\sigma(L-a)t} \qquad (2.47)$$

is the solution which satisfies the boundary condition $\beta(L)a) = 1$ at $t=0$. This result can be verified by noting that

$$\beta(L+\ell|a) = e^{-\sigma(L+\ell-a)t} = e^{-\sigma(L-a)t}e^{-\sigma(\ell+a-a)t} = \beta(L|a)\beta(\ell+a|a), \qquad (2.48)$$

and substituting this result into Eqn. 2.46. Using Eqns. 2.45 and 2.47 we can explicitly integrate Eqn. 2.44 to obtain

$$\frac{dP(L)}{dt} = -\sigma P(a)[(a-L) + \frac{2}{\sigma t}(1 - e^{-\sigma Lt})], \qquad (2.49)$$

$a \geq L$.

For $L=a$, both the equations for $a \geq L$ and $L \geq a$ give

$$\frac{dP(a)}{dt} = -\frac{2\sigma}{\sigma t} P(a)(1 - e^{-\sigma at}), \qquad (2.50)$$

which can be integrated to obtain

$$P(a) = \exp\{-2f(\sigma at)\}. \tag{2.51}$$

Here,

$$f(x) = \int_0^x dy\, \frac{1}{y}\,(1 - e^{-y}). \tag{2.52}$$

Substituting Eqn. 2.51 into Eqn. 2.49 yields

$$\frac{dP(L)}{dt} = -\sigma \exp\{-2f(\sigma at)\}[(a-L) + \frac{2}{\sigma t}\,(1 - e^{-\sigma Lt})], \tag{2.53}$$

which on integration gives

$$P(L) = 1 - \sigma \int_0^t dt' \exp\{-2f(\sigma at')\}[(a-L) + \frac{2}{\sigma t'}\,(1 - e^{-\sigma Lt'})], \quad a \geq L. \tag{2.54}$$

Equations 2.45, 2.47, 2.51 and 2.54 give the distribution of any length of vacant segment on the infinite line for the events which have a blocking potential of length a.

We now wish to calculate the probability of any point not being covered by an event at saturation. From Eqn. 2.54, P(0), the probability that any given point on the line is vacant, is given by

$$P(0) = 1 - \int_0^{\sigma at} dt' \exp\{-2f(t')\}. \tag{2.55}$$

Thus, in the limit as $t \to \infty$, the probability of any point on the lattice remaining empty is

$$P(0)_{sat} = 1 - \int_0^\infty dt \exp\{-2f(t')\} \approx 0.25502. \quad (2.56)$$

This result has been previously obtained by Rényi (15) and others (16,18).

The saturation vacancy density on the infinite line will now be shown to be equal to the saturation vacancy density on the discrete lattice in the limit $r \to \infty$. To this end, the saturation limit of the discrete lattice can be written as

$$\lim_{r\to\infty} P^{(1)}_{sat}(\underline{0}) = 1 - \lim_{r\to\infty} (r+1) \int_0^1 dq \exp\{2 \sum_{\ell=1}^{r} (q^\ell - 1)\}$$

$$= 1 - \lim_{r\to\infty} r \int_0^1 dq \exp\{2 \sum_{\ell=1}^{r} (q^\ell - 1)\}. \quad (2.57)$$

We define a new variable x by $x = (1-q)(r+1)$, substitute it into Eqn. 2.57, and expand the argument of the exponent to obtain

$$P^{(1)}_{sat}(\underline{0}) = 1 - \lim_{r\to\infty} \int_0^r dx \exp\{-2 \ln x - 2 \sum_{\ell=r}^{\infty} \frac{1}{\ell} (1 - \frac{x}{r})^\ell$$

$$- 2 [\sum_{\ell=1}^{r} \frac{1}{\ell} - \ln r]\}. \quad (2.58)$$

The first sum in the argument of the exponent can be rewritten with the aid of the Euler-MacLaurin sum formula (41) as follows:

$$\sum_{\ell=r}^{\infty} \frac{1}{\ell} \left(1 - \frac{x}{r}\right)^{\ell} = \int_{r}^{\infty} d\ell \, \frac{1}{\ell} \left(1 - \frac{x}{r}\right)^{\ell} + \frac{1}{2r} \left(1 - \frac{x}{r}\right)^{r} + \mathcal{O}(r^{-2}), \qquad (2.59)$$

where $\mathcal{O}(r^{-2})$ represents terms to order r^{-2} and smaller. However,

$$\int_{r}^{\infty} d\ell \, \frac{1}{\ell} \left(1 - \frac{x}{r}\right)^{\ell} = \int_{r}^{\infty} d\ell \, \frac{1}{\ell} \exp\{\ell \, \ell n(1 - \frac{x}{r})\} = E_1(-r \, \ell n \, (1 - \frac{x}{r})), \qquad (2.60)$$

where $E_1(x) \int_{x}^{\infty} dt \, \frac{e^{-t}}{t}$ is the exponential integral (41). Equation 2.59 can then be written

$$\sum_{\ell=r}^{\infty} \frac{1}{\ell} \left(1 - \frac{x}{r}\right)^{\ell} = E_1 \left(- r \, \ell n(1 - \frac{x}{r})\right) + \frac{1}{2r} \left(1 - \frac{x}{r}\right)^{r} + \mathcal{O}(r^{-2}) \qquad (2.61)$$

and substituted into Eqn. 2.58 to obtain

$$P_{sat}^{(1)}(0) = 1 - \lim_{r\to\infty} \int_{0}^{r} dx \exp\{-2 \, \ell n \, x - 2E_1(-r \, \ell n(1 - \frac{x}{r})) - \frac{1}{r} \left(1 - \frac{x}{r}\right)^{r} - 2[\sum_{\ell=1}^{r} \frac{1}{\ell} - \ell n \, r]\}, \qquad (2.62)$$

where terms to the order of r^{-2} vanish in the limit as $r\to\infty$. In this same limit the relations

$$\lim_{r\to\infty} \left(1 - \frac{x}{r}\right)^r = e^{-x} \tag{2.63}$$

$$\lim_{r\to\infty} \left(-r \ln\left(1 - \frac{x}{r}\right)\right) = x \tag{2.64}$$

and

$$\lim_{r\to\infty} \left[\sum_{\ell=1}^{r} \frac{1}{\ell} - \ln r\right] = \gamma = \text{Euler's Constant (41)} \tag{2.65}$$

are applicable. Thus,

$$\lim_{r\to\infty} P^{(1)}_{sat}(0) = 1 - \int_0^\infty dx \exp\{-2[\ln x + E_1(x) + \gamma]\},$$

$$= 1 - \int_0^\infty dx \exp\{-2\, E_{in}(x)\}, \tag{2.66}$$

where $E_{in}(x) = \int_0^x dy \frac{1}{y}(1 - e^{-y})$. In comparing this result with Eqn. 2.56, we find that

$$\lim_{r\to\infty} P^{(1)}_{sat}(0) = P(0)_{sat}. \tag{2.67}$$

This rather lengthy analysis shows that the continuous model can also be treated as a special case of the model on a discrete lattice.

The Semi-Infinite Lattice

The mathematical approach used to derive the kinetic equations for the infinite discrete lattice can also be used to develop the equations for the linear semi-infinite

lattice. The semi-infinite lattice can be described as a lattice which has a definite starting point and extends to infinity in one direction. For convenience, the model will only be developed for lattice events with a 1st n.n. blocking potential in this section and the one that follows. Extension to events with a general blocking potential is straightforward.

Consider an infinite array of equivalent sites on a space-filling lattice with a definite left hand end point. Let the sites be labeled sequentially, with the left end site being number 1 (see Fig. 2.4), and let $P_1^{(j)}(\underline{0})$ be the probability that j consecutive sites are vacant, beginning with site i as the leftmost point. It is necessary to specify the location of the configuration of sites in the distribution functions because of the influence of the end site on the distributions. The time rate of change of $P_1^{(1)}(0)$, the singlet distribution function on the first space-filling site, depends only on the rate at which transitions are made on the pair of sites 1 and 2 (i.e., on the event lattice site farthest to the left) because there are no left neighbors to site 1. This kinetic equation for $P_1^{(1)}(0)$ is

$$\frac{dP_1^{(1)}(0)}{dt} = - \sigma P_1^{(2)}(\underline{0}) = - \sigma P_1^{(1)}(0)\bar{q}(1), \qquad (2.68)$$

where, as before, $\bar{q}(j)$ is the conditional probability on

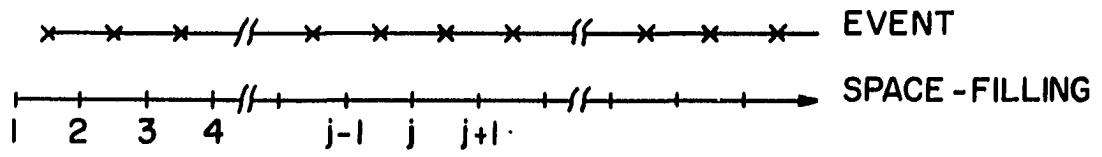

THE SEMI-INFINITE LATTICE

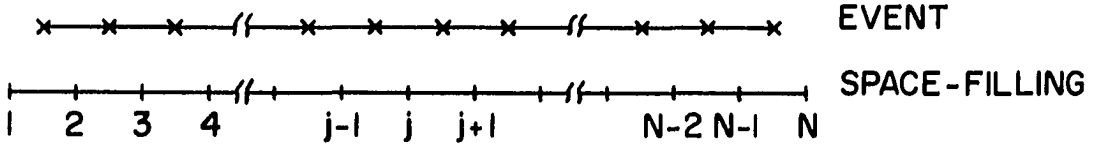

THE FINITE LATTICE

Figure 2.4. The semi-infinite and finite event and space-filling lattices

the infinite lattice that a site is vacant given that a site j lattice vectors away is also vacant. Note that this conditional probability does not depend on the position of the sites relative to the end site. This is true since the conditioning site is to the left or terminal side of the lattice site of interest (i.e., the site at which the probability of a vacancy is of interest). The conditioning site blocks the site of interest from the influence of the end site. Conditional probabilities conditioned on the terminal side of the semi-infinite lattice are therefore not a function of position on the lattice and are equal to the corresponding conditional probabilities on the infinite lattice. Of course, we have given here only a heuristic argument, but this result can be easily proven rigorously by explicitly writing the equations governing the time evolution of the conditional probabilities. However, a conditional probability defined such that the conditioning sites are to the right or infinite side of the lattice is not independent of position on the lattice because the site of interest is not blocked from the terminal site by a conditioning site. These conditional probabilities are denoted by $Q_k(\ell)$, where subscript k is the relative separation of the conditioned site and the terminal site, and as in Eqn. 2.34, ℓ is the relative separation of the conditoned site and the site of interest. Expressions relating the conditional probabilities

conditioned to the left and right are easily derived since

$$P^{(2)}_{\{j,j+\ell\}}(\underline{0}) = P^{(1)}_{j+\ell}(0)\; Q_{j+\ell-1}(\ell)$$

$$= P^{(1)}_{j}(0)\bar{q}(\ell), \qquad (2.69)$$

and thus

$$Q_{(j+\ell-1)}(\ell) = \frac{P^{(1)}_{j}(0)\bar{q}(\ell)}{P^{(1)}_{j+\ell}(0)}, \qquad (2.70)$$

which clearly depends on the position of the end site since $P^{(1)}_{j}(0)$ and $P^{(1)}_{j+\ell}(0)$ depend on the end site position.

Now, dividing Eqn. 2.68 by $P^{(1)}_{1}(0)$ and introducing the new variable, $z = \bar{q}(1)-1$, we have that

$$\frac{d\ \ell n\ P^{(1)}_{1}(0)}{dz} = 1, \qquad (2.71)$$

which has the solution

$$P^{(1)}_{1}(0) = e^{z}. \qquad (2.72)$$

From Eqn. 2.28 for r=1, we have that $\bar{q}(1) = 1+z = 1 + \frac{1}{2}\ \ell n(1-\theta)$ and therefore $P^{(1)}_{1}(0) = e^{z} = (1-\theta)^{1/2}$. This is a result that is to be expected if we conceptually split an infinite lattice in two at a particular site. If the space-filling site at the split is vacant then it must be that the two <u>event</u> lattice sites on either side of this site are vacant and <u>vice versa</u>. But these two event probabilities are just equal to the probability that the end site of the corresponding semi-infinite lattice is vacant. Therefore

$$(1-\theta) = P_1^{(1)}(0)^2, \tag{2.73}$$

or

$$P_1^{(1)} = (1-\theta)^{1/2}, \tag{2.74}$$

which is the desired result.

The kinetic equation for the singlet distribution on site i, when i≠1, is given by

$$\frac{dP_i^{(1)}(0)}{dt} = -\sigma P_i^{(2)}(\underline{0}) - \sigma P_{i-1}^{(2)}(\underline{0})$$

$$= -\sigma q_1 (P_i^{(1)}(0) + P_{i-1}^{(1)}(0)). \tag{2.75}$$

Since the right hand side of these equations involves only $P_i^{(1)}(0)$ and $P_{i-1}^{(1)}(0)$, these equations can be successively solved starting with i=2. The general result is

$$P_i^{(1)}(0) = e^z e_{i-1}(z), \tag{2.76}$$

where, as before, $e_i(z)$ is the truncated exponential polynomial. In the limit as $i \to \infty$, $e_i(z) = e^z$, and $P_1^{(1)}(0) \to e^{2z} = (1-\theta)$, as is to be expected. Making use of this result and Eqn. 2.20, we have that the distribution of j adjacent vacancies on the semi-infinite lattice is

$$P_i^{(j)}(\underline{0}) = P_i^{(1)}(0)(q_1)^{j-1} = e^z e_{i-1}(z)(q_1)^{j-1}. \tag{2.77}$$

Also from Eqn. 2.70, we have that the conditional probabilities conditioned to the right are given explicitly

by

$$Q_n(k) = \frac{e_{n-k}(z)\ \bar{q}(k)}{e_n(z)} . \qquad (2.78)$$

As we shall see in the next section, this relation can be exploited to obtain distributions on the finite lattice.

The Finite Lattice

Finally, let us consider a linear, finite space-filling lattice of N equivalent sites which is labeled numerically from the left end as in Fig. 2.4. As before, the quantity $P_i^{(j)}(\underline{0})$ is defined as the probability that sites i, i+1,..., i+j-1 are vacant. The kinetic equations for this lattice are

$$\frac{dP_1^{(j)}(\underline{0})}{dt} = -\sigma(j-1)\ P_1^{(j)}(\underline{0}) - \sigma\ P_1^{(j+1)}(\underline{0}), \qquad j<N, \qquad (2.79)$$

and

$$\frac{dP_1^{(N)}(\underline{0})}{dt} = -\sigma(N-1)\ P_1^{N}(\underline{0}), \qquad j=N. \qquad (2.80)$$

The solution to this last equation is clearly

$$P_1^{(N)}(\underline{0}) = e^{-\sigma(N-1)t} = (q_1)^{N-1}. \qquad (2.81)$$

Equation 2.79 can be expressed in the form

$$\frac{d}{dt}\left(e^{\sigma(j-1)t}\ P_1^{(j)}(\underline{0})\right) = -\sigma e^{\sigma(j-1)t}\ P_1^{(j+1)}(\underline{0}), \qquad (2.82)$$

or

$$\frac{dK_j}{dt} = -\sigma\, q_1\, K_{j+1}, \tag{2.83}$$

where $$K_j = P_1^{(j)}(\underline{0})e^{\sigma(j-1)t} = P_1^{(j)}(\underline{0})/(q_1)^{j-1}. \tag{2.84}$$

This is an autonomous system of differential equations in the cyclic variable t. Hence, we can divide Eqn. 2.83 by Eqn. 2.20 to obtain

$$\frac{dK_j}{dz} = K_{j+1} \tag{2.85}$$

in which the time no longer explicitly appears. These equations can be solved successively starting with the equation for K_{N-1}, using the fact from Eqn. 2.81 that $K_N=1$. This procedure yields the general result

$$K_{N-j} = e_j(z), \tag{2.86}$$

or $$K_j = e_{N-j}(z). \tag{2.87}$$

Thus, from Eqn. 2.84

$$P_1^{(j)}(\underline{0}) = (q_1)^{j-1}\, e_{N-j}(z), \tag{2.88}$$

and in particular,

$$P_1^{(1)}(0) = e_{N-1}(z). \tag{2.89}$$

In the limit that $N\to\infty$, $P_1^{(1)}(0) \to e^z$, which is the result on the semi-infinite lattice.

Equation 2.88 gives the probabilities that the first j sites on the lattice are empty. All other distributions on

the finite lattice can be obtained from Eqn. 2.89 and the conditional probabilities for the semi-infinite lattice. As before, we can use the fact that a conditioning vacancy blocks the effect of an end site to obtain two expressions for the pair distribution function

$$P^{(2)}_{\{1,j\}}(\underline{0}) = P^{(1)}_1(0)\, Q_{N-1}(j-1)$$

$$= P^{(1)}_j(0)\, Q_{j-1}(j-1). \qquad (2.90)$$

Substituting Eqn. 2.78 and Eqn. 2.89 into this result we find that

$$P^{(2)}_j(\underline{0}) = e_{N-j}(z)\, e_{j-1}(z). \qquad (2.91)$$

This solves the kinetic problem on the finite lattice since any distribution can be written as a product of Eqn. 2.91 and conditional probabilities of the form of Eqn. 2.78.

We now wish to calculate the mean number of vacancies on the lattice, A, and the dispersion in the number of vacancies, σ_A. Let x_i denote the condition of site i, where $x_i=0$ if the site is vacant, and $x_i=1$ if the site is occupied. The average number of vacancies on the lattice of length N is then

$$A = \overline{\sum_{i=1}^{N} (1-x_i)}\ , \qquad (2.92)$$

where the bar denotes an ensemble average. But using the fact that the average of a sum is the sum of the averages,

$$A = \sum_{i=1}^{N} \overline{(1-x_i)} = \sum_{i=1}^{N} P_i^{(1)}(0). \tag{2.93}$$

If, for convenience, we limit our considerations to large N, then over most of the lattice $P_i^{(1)}(0)$ can be approximated by $P^{(1)}(0)$ and A is approximately given by

$$A \simeq NP^{(1)}(0), \tag{2.94}$$

which at saturation is Ne^{-2}. This is the standard result we have mentioned several times previously.

By definition, the variance is given by

$$\sigma_A^2 = \overline{F_N^2} - \bar{F}_N^2, \tag{2.95}$$

where, in this case, $F_N = \sum_{i=1}^{N} (1-x_i)$. On expanding Eqn. 2.95 we obtain

$$\sigma_A^2 = \overline{\sum_{i=1}^{N} \sum_{j=1}^{N} (1-x_i)(1-x_j)} - A^2.$$

By using Eqn. 2.93 we have that

$$\sigma_A^2 = \sum_{i=1}^{N} P_i^{(1)}(0) + 2 \sum_{i} \sum_{j>i} P_{\{i,j\}}^{(2)}(\underline{0}) - A^2. \tag{2.96}$$

Now

$$A^2 = \sum_{i=1}^{N} \sum_{j=1}^{N} P_i^{(1)}(0)P_i^{(1)}(0) = \sum_{i=1}^{N} P_i^{(1)}(0) + 2 \sum_{i} \sum_{j>1} P_i^{(1)}(0)P_j^{(1)}(0), \qquad (2.97)$$

and after substituting this result into Eqn. 2.96, we obtain

$$\sigma_A^2 = \sum_{i=1} \left\{ P_i^{(1)}(0) - P_i^{(1)}(0)P_j^{(1)}(0) \right\} + \sum_{i} \sum_{j>i} \left\{ P_{\{i,j\}}^{(2)}(\underline{0}) - P_i^{(1)}(0)P_j^{(1)}(0) \right\}. \qquad (2.98)$$

For large N we note that $P_i^{(1)}(0) \approx P^{(1)}(0) = (1-\theta)$, and $P_{\{i,j\}}^{(2)}(\underline{0}) \approx P^{(1)}(0)\bar{q}(j-i)$, and so, in this limit,

$$\sigma_A^2 = N\theta(1-\theta) + 2(1-\theta) \sum_{i=1}^{N-1} \sum_{j=i+1}^{N} [\bar{q}(j-i) - (1-\theta)]. \qquad (2.99)$$

Now $\sum_{i=1}^{N-1} \sum_{j=i+1}^{N} = \sum_{i=1}^{N-1} \sum_{k=1}^{N-i}$, where $k = (j-i)$. Using this result and interchanging the order of summation, we can perform the sum over i to obtain

$$\sigma_A^2 = (1-\theta)\left[N\theta + 2 \sum_{k=1}^{N-1} (N-k)[q_1(k) - (1-\theta)] \right]. \qquad (2.100)$$

Since N is assumed to be large, this expression can be written

$$\sigma_A^2 \approx N(1-\theta)\left[\theta + 2 \sum_{k=1}^{\infty} [q_1(k) - (1-\theta)] \right]. \qquad (2.101)$$

However, from the semi-infinite result, we know that $\bar{q}(k) = e_{k-1}(x) + \frac{1}{2}\frac{x^k}{k!}$ and $(1-\theta) = e^x$, where $x = \ell n\ (1-\theta)$. The incorporation of these results into Eqn. 2.101 finally leads to

$$\sigma_A^2 \approx N(1-\theta)\left(2\sum_{k=1}^{\infty}[e_{k-1}(x) - e^x]\right), \qquad (2.102)$$

or

$$\sigma_A^2 \approx 2N(1-\theta)(-x)(1-\theta). \qquad (2.103)$$

Now at saturation $(1-\theta) = e^{-2}$, and hence in this limit $x = -2$. Thus we find that in the limit of large N, the saturation value of the dispersion is

$$\sigma_A^2 \approx 4Ne^{-4}. \qquad (2.104)$$

This result agrees with the results previously obtained by other authors (10,11,18). Two points should be noted here. First, taking the large N limit beginning with Eqn. 2.99 is only for convenience -- the method is valid for any value of N. Secondly, the variance calculation through Eqn. 2.101 can be applied for events with any blocking potential. However, our results are valid only for r=1 since we use $\bar{q}(\ell)$ and the saturation covering fraction appropriate to that problem.

CHAPTER 3. COOPERATIVE MODELS ON AN INFINITE LATTICE

Cooperative models, describing the kinetics of systems of interacting events, can be derived as direct extensions of the non-cooperative models discussed in the previous chapter. For cooperative models, events which have occurred on the lattice affect the activation energy barrier for the occurrence of events on neighboring sites. The rate of transition can be either increased or decreased. A negative change in the activation energy will increase the rate of transition at a site, while a positive change will have the opposite effect. For the sake of simplicity, it is assumed that the contributions of neighboring sites to the activation energy are pairwise additive, although the mechanistic nature of the interaction and its explicit numerical value is arbitrary. Thus, the net change in the activation barrier due to the distribution of events near the site of interest is obtained by summing over the contribution of all neighboring sites to the site of interest. For our numerical computations we shall assume that the transition rate has the Arrhenius form

$$\tau = A \exp\{-\beta E_{act}\}, \tag{3.1}$$

where A is the pre-exponential frequency factor (which is assumed to be independent of events on neighboring sites), $\beta = (kT)^{-1}$, and E_{act} is the energy of activation for the

transition including the contributions from the events in the vicinity of the site. This particular form is specified for numerical convenience and has little bearing on the general mathematical development.

In this Chapter, we consider events on an infinite linear lattice. First, we discuss the case where events have a 0th n.n. blocking potential and a 1st n.n. cooperative interaction. Next, we consider the general equations governing the time dependence of the distribution of events for the case of an rth n.n. blocking potential and an r+1st n.n. cooperative interactions (cf. Chapter 1 for the convention used to describe the range of the interaction). These equations are solved for the case when r=1 (i.e., the interacting dimer problem). Some general considerations of the case with longer range interactions are also discussed.

Cooperative Events with a 0th n.n. Blocking Potential

We now discuss events on a linear lattice with a 0th n.n. blocking potential and 1st n.n. cooperative interaction. This model can be used to represent such physical processes as the adsorption of atoms onto a linear substrate or the change in state of a monomer unit of a polymer chain. Since we have a 0th n.n. blocking potential, the event lattice and space-filling lattice are identical, as discussed in Chapter 2.

Again we consider an infinite linear lattice composed of equivalent, equally spaced lattice sites. We now introduce a new quantity, τ_{ij}, which is the transition probability at a site with left 1st n.n. site in condition i and right 1st n.n. site in condition j, where i,j = 0 or 1. In Arrhenius form with pairwise activation energy this can be written

$$\tau_{ij} = A \exp\{-\beta(\phi_i+\phi_j)\}, \tag{3.2}$$

where ϕ_i and ϕ_j are the pairwise additive contributions to the activation energy due to sites to the left and right, respectively, of the site of interest. Because of lattice symmetry, $\tau_{ij} = \tau_{ji}$. The transition probability can now be written in the form

$$\tau_{ij} = \sigma \exp\{-\beta(i+j)(\phi_1-\phi_0)\} = \sigma(1+\alpha)^{i+j}, \tag{3.3}$$

where $$\sigma \equiv \tau_{00} = A \exp\{-2\beta\phi_0\} \tag{3.4}$$

is the transition probability of the noncooperative models discussed in Chapter 2, and

$$\alpha = \exp\{-\beta(\phi_1-\phi_0)\} - 1. \tag{3.5}$$

The quantity α reflects the cooperative influence of an event at one site on the transition probability at a neighboring site. For the noncooperative case $\alpha=0$, for a positive interaction (corresponding to a negative change in the activation energy) $\alpha>0$, and for a negative interaction (a positive change in the activation energy) $\alpha<0$. Table 3.1

illustrates the variation in activation energy with α. The value of ϕ_0, the contribution of a nearest neighbor vacancy to the transition activation energy of a site, is a measure of the temperature dependence of the initial rate as can be seen from the equation $d\sigma/dT = 2\phi_0 A(kT^2)^{-1}\exp\{-2\beta\phi_0\}$. This parameter can take on values representing an activated transition ($\phi_0>0$) or a nonactivated transition ($\phi_0=0$). The effects of this parameter are eliminated if the kinetic equations are solved as a function of the dimensionless time $\tau_{00}t$. Hence, ϕ_0 sets the time scale of the kinetic process but has no effect on the various distributions of interest when they are considered as functions of the density of events.

Table 3.1. The variation of the activation energy difference $(\phi_1-\phi_0)$ with the interaction parameter α, at T = 300°K

α	$(\phi_1-\phi_0)$, kcal/mole	α	$(\phi_1-\phi_0)$, kcal/mole
0.0	0.0	0.5	-0.242
-0.1	0.063	1.0	-0.413
-0.3	0.213	2.0	-0.655
-0.5	0.413	3.0	-0.826
-0.7	0.717	5.0	-1.068
-0.9	1.372	10.0	-1.429
-0.99	2.744	100.0	-2.750

It has been assumed in our expressions for the rate constants that the pre-exponential frequency factor, A, is not a function of event configuration. This assumption would break down if the local distribution of events had an entropic effect on the transition probability at the site of interest. When a multistep mechanism is represented as a single event, it is necessary to introduce an effective pre-exponential factor, A, which is an implicit function of time. An example of this will be considered in Chapter 5. However, for the present, we will consider A to be a constant that is independent of configuration and time.

As previously mentioned, the mechanism through which an event changes the activation energy for transition at a neighboring site is immaterial to the mathematical development of the models. It is, however, of interest to note that these changes can be attributed to a variety of mechanisms. For example, the condition of a neighboring site can directly interact with the site of interest to induce a temperature independent change in the activation energy. The interactions can also be transmitted through the lattice with mechanisms of varying degrees of complexity. These effects can be temperature dependent according to the specific mechanism; examples are changes due to an increase in the helicity of a polymer in the case of the denaturation of a polypeptide (see Chapters 1 and 6) or the shift in the Fermi

level of the electrons near the surface of a semiconductor in chemisorption.

We now derive the kinetic equations for this model. The time rate of change of $f^{(1)}(0) = P^{(1)}(0)$ is given by

$$\frac{dP^{(1)}(0)}{dt} = -\tau_{00}P^{(3)}(000) - 2\tau_{01}P^{(3)}(100) - \tau_{11}P^{(3)}(101). \quad (3.6)$$

By expressing all probabilities in terms of vacancy probabilities as discussed in the previous chapter, we have that

$$\frac{dP^{(1)}(0)}{dt} = -\tau_{11}P^{(1)}(0) - 2(\tau_{01}-\tau_{11})P^{(2)}(\underline{0}) - (\tau_{00}-2\tau_{01}+\tau_{11})P^{(3)}(\underline{0}), \quad (3.7)$$

where as before $P^{(n)}(\underline{0})$ is the probability of finding n adjacent vacant sites. The kinetic equations governing the time evolution of other distributions of vacant sites are derived similarly, and as in the case of the noncooperative models previously developed, the equation for consecutive vacancies form a closed hierarchy. Specifically,

$$\frac{dP^{(2)}(0)}{dt} = -2\tau_{01}P^{(2)}(\underline{0}) - 2(\tau_{00}-\tau_{01})P^{(3)}(\underline{0}), \quad (3.8)$$

and

$$\frac{dP^{(n)}(0)}{dt} = -(n-2)\tau_{00}P^{(n)}(\underline{0}) - 2\tau_{01}P^{(n)}(\underline{0}) - 2(\tau_{00}-\tau_{01})P^{(n+1)}(\underline{0}), \quad n\geq 2. \quad (3.9)$$

The kinetic equations for event distributions not decomposable into distributions of consecutive sites are derived in an analogous fashion. These equations, of course, form a larger hierarchy; they are discussed later in this Chapter.

As in Chapter 2, conditional probabilities can now be introduced through the defining equation

$$P^{(n+1)}(\underline{0}) = P^{(n)}(\underline{0})\, q_n, \tag{3.10}$$

where the subscript, n, on q_n refers to the number of conditioning sites. On differentiating this expression with respect to time, substituting Eqns. 3.7 and 3.8 into this result, and rearranging, we obtain the alternate, equivalent hierarchy

$$\frac{dq_1}{dt} = -(2\tau_{01}-\tau_{11})q_1 - 2(\tau_{00}-\tau_{01})q_1q_2 + 2(\tau_{01}-\tau_{11})q_1^2 + (\tau_{00}-2\tau_{01}+\tau_{11})q_1^2q_2, \tag{3.11}$$

and

$$\frac{dq_n}{dt} = -\tau_{00}\, q_n - 2(\tau_{00}-\tau 0_1)(q_nq_{n+1}-q_n^2),\ n\geq 2. \tag{3.12}$$

The solution to equation 3.12, which satisfies the boundary conditions $q_j=1$ at $t=0$, is clearly

$$q_n = q_2, \tag{3.13}$$

for all $n\geq 2$. Equation 3.12 then becomes

$$\frac{dq_2}{dt} = -\tau_{00}\, q_2, \tag{3.14}$$

which has the solution

$$q_2 = e^{-\tau_{00}t}. \tag{3.15}$$

With this result we have exactly solved the alternate hierarchy for all cases where $n \geq 2$.

The remaining kinetic equations in the hierarchy (Eqns. 3.7 and 2.11) form an autonomous system of equations in the cyclic variable t. As in Chapter 2, the explicit time dependence of these equations can be eliminated by dividing each equation by the truncation equation, in this case, Eqn. 2.14. We can then solve Eqn. 3.8 as a function of q_2 to obtain the result

$$P^{(2)}(\underline{0}) = {q_2}^{2\rho_{01}} \exp\{2(1-\rho_{01})(q_2-1)\}, \tag{3.16}$$

where ρ_{01} is the reduced rate constant τ_{01}/τ_{00}. Equation 3.11 is solved in a similar manner. After dividing through Eqn. 3.11 by Eqn. 3.14, we obtain

$$\begin{aligned}\frac{dq_1}{dq_2} = {} & (2\rho_{01}-\rho_{11})q_1/q_2 - 2(1-\rho_{01})q_1 \\ & + 2(\rho_{01}-\rho_{11}){q_1}^2/q_2 + (1-2\rho_{01}+\rho_{11}){q_1}^2,\end{aligned} \tag{3.17}$$

where ρ_{11} is the reduced rate constant τ_{11}/τ_{00}. This equation has the general form

$$\frac{dq_1}{dq_2} = q_1\, f(q_2) + {q_1}^2 q(q_2), \tag{3.18}$$

which is one form of the Ricatti equation (42). Introducing the new variable $r = q_1^{-1}$, rearranging and solving the resulting equation, we have that

$$q_1 = q_2^{(2\rho_{01}-\rho_{11})}\exp\{2(1-\rho_{01})(q_2-1)\}\cdot$$

$$\left[\int_1^{q_2} dq' \exp\{2(1-\rho_{01})(q'-1)\}\{2(\rho_{01}-\rho_{11})q'^{(2\rho_{01}-\rho_{11}-1)} + (1-2\rho_{01}+\rho_{11})q'^{(2\rho_{01}-\rho_{11})}\} + 1\right]^{-1}. \quad (3.19)$$

Finally, Eqn. 3.7 can also be put into the form of the Ricatti equation and solved for $P^{(1)}(0)$ as a function of q_2. However, instead of directly solving this equation, we can utilize previously derived results to obtain an expression for $P^{(1)}(0)$. We know by Eqn. 3.10 that $P^{(2)}(\underline{0}) = P^{(1)}(0)q_1$, and hence, $P^{(1)}(0) = P^{(2)}(\underline{0})q_1^{-1}$. Equations 3.8 and 3.9 are now substituted into this result yielding $P^{(1)}(0)$ as a function of q_2; namely

$$P^{(1)}(0) = [q_1]^{-1} q_2^{2\rho_{01}} \exp\{2(1-\rho_{01})(q_2-1)\}. \quad (3.20)$$

Equations 3.15, 3.19 and 3.20 (or equivalently, Eqns. 3.15, 3.16 and 3.20) completely solve this kinetic model for an event with a 1st n.n. cooperative interaction. The time dependence of these equations is established by eliminating q_2 using Eqn. 3.15.

The integral in Eqn. 3.19 can be numerically integrated to satisfactory accuracy using a twenty point Gauss-Legendre integration scheme. The resulting expressions for q_1 can then be used to evaluate $P^{(1)}(0)$ by means of Eqn. 3.20. The results of these calculations are shown in Figs. 3.1 and 3.2. The particular values of α used in these calculations have been chosen to represent moderate changes in the activation energy of approximately equal magnitude, but opposite sign. Hence, as noted in Table 3.1, $\alpha = 1.0$ is equivalent to $(\phi_1-\phi_0) \approx -0.413$ kcal/mole, and $\alpha = -0.5$ is equivalent to $(\phi_1-\phi_0) \approx 0.413$ kcal/mole, for T=300°K.

The use of the quantity q_2 as an independent variable in this discussion is mathematically convenient because it allows us to easily solve the kinetic equations; however, it is often desirable to express these results in terms of the physically more intuitive variable $P^{(1)}(0)$ as shown in Figs. 3.3 and 3.4. It is seen that the probability of a distribution of vacancies at a given covering fraction (recall that $\theta = 1-P^{(1)}(0)$) is increased or decreased relative to the corresponding result for the noncooperative case according to the value of α. For $\alpha>0$, an occupied site favors the transition of the neighboring sites, and events tend to occur in clusters, thereby increasing the probability that a site is vacant given that one or two conditioning sites are vacant. For $\alpha<0$, the occupation of a site

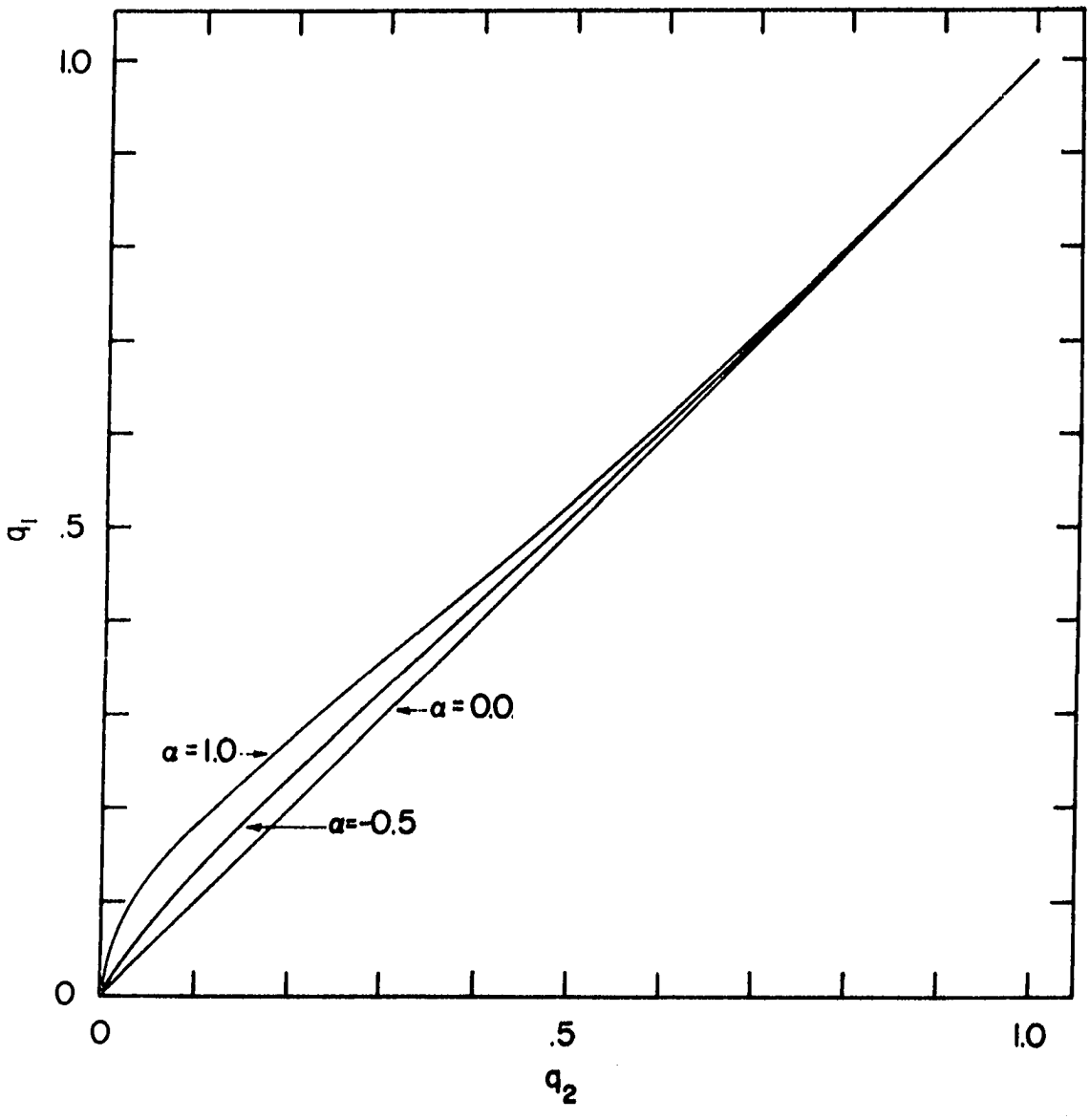

Figure 3.1. The q_1 conditional probability as a function of q_2 for the case where r=0

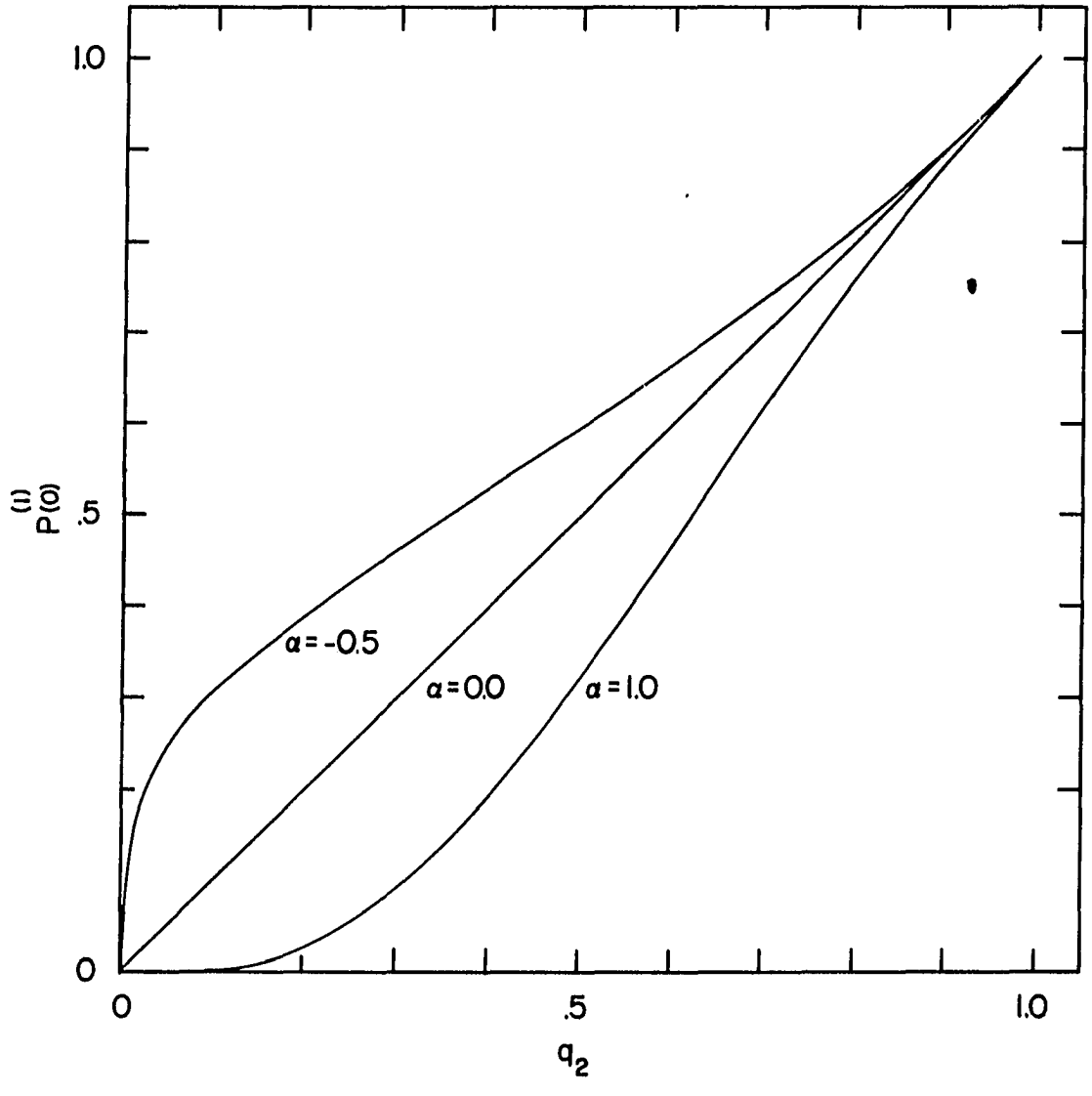

Figure 3.2. The density of vacant space-filling sites as a function of q_2, where r=0

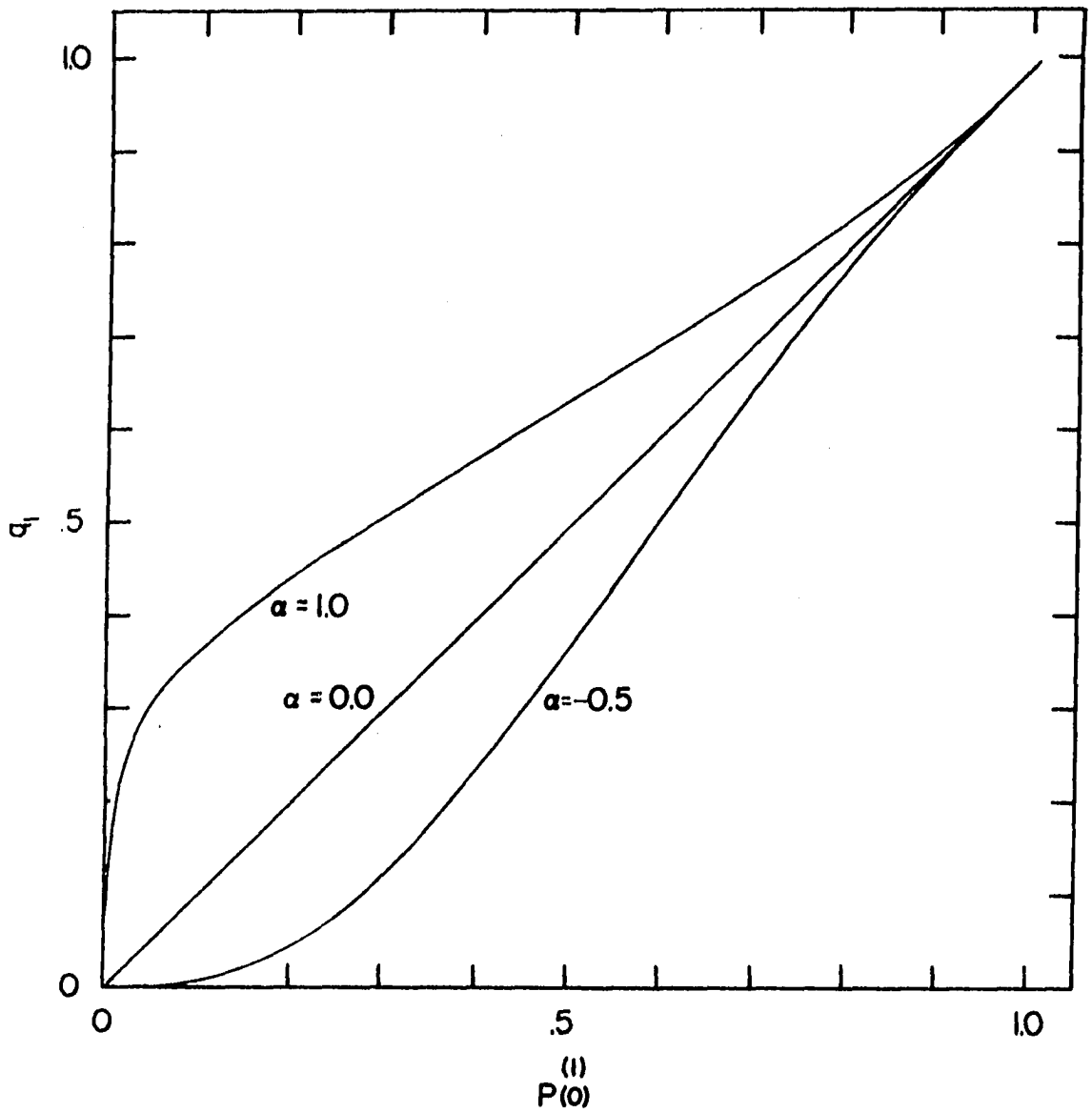

Figure 3.3. The q_1 conditional probability as a function of $P(0)^{(1)}$, where r=0

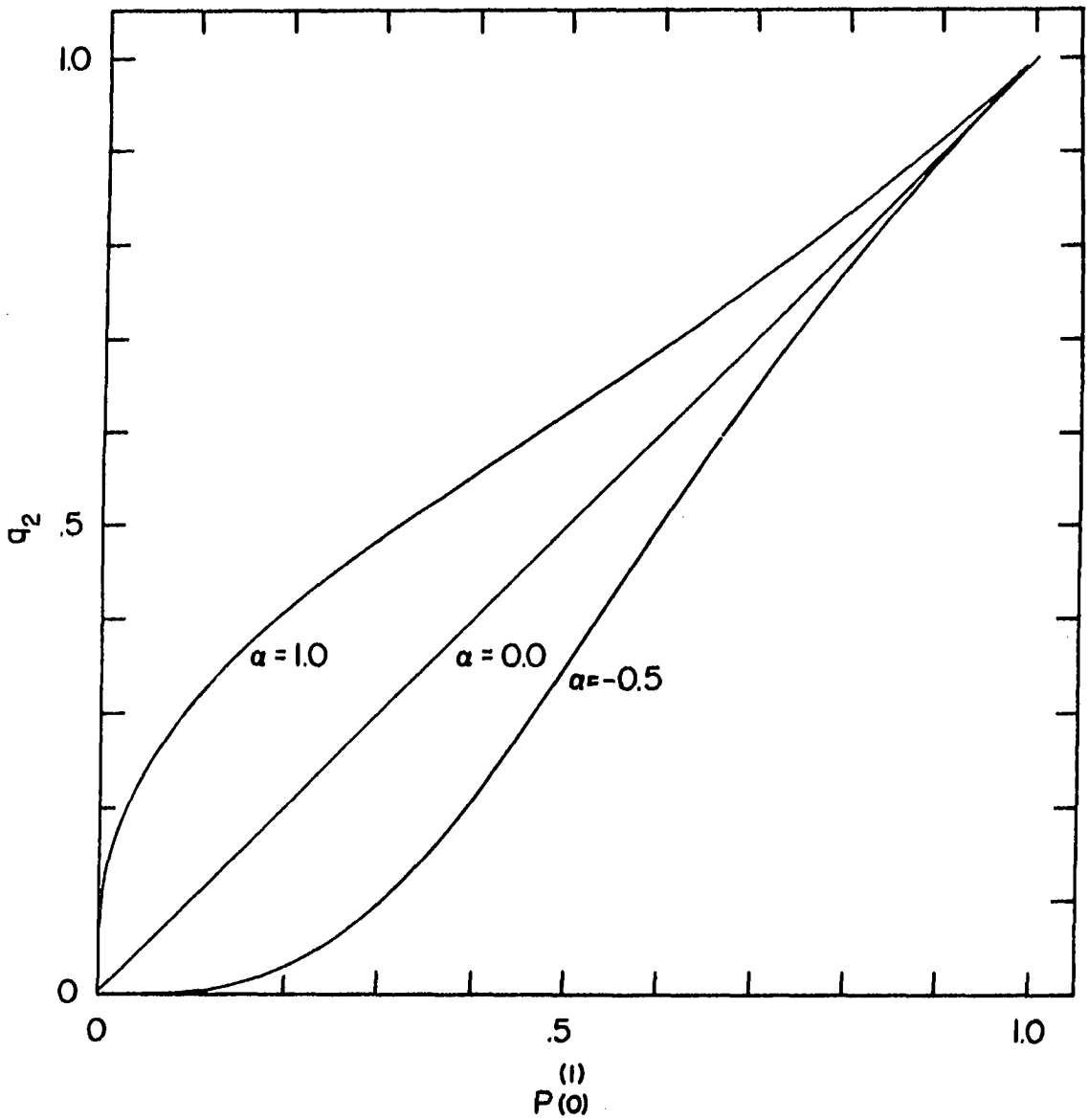

Figure 3.4. The q_2 conditional probability as a function of $P(0)^{(1)}$, where r=0

disfavors the transition of the neighboring sites, which results in a dispersal of the distribution of events as compared with the noncooperative case, and leads to smaller values of q_1 and q_2 at the same density of events. It is evident from these figures that all distributions of vacancies go to zero at lattice saturation, i.e., $P^{(1)}(0) = 0$. This is to be expected since the r=0 blocking potential does not exclude neighboring sites from transition. This is true for all finite interactions; however, in the limit as $\alpha \to -1$ (i.e., $\phi_1 - \phi_0 = \infty$), this model reduces to the noncooperative model with 1st n.n. blocking potentials as discussed in Chapter 2.

Instead of numerically integrating the quadrature in Eqn. 3.19, we can directly solve the truncated hierarchy of coupled equations using other numerical techniques. We note in comparing Eqns. 3.7, 3.11 and 3.14 with Eqn. 3.3 that the rate constants τ_{00}, τ_{01} and τ_{11}, which govern the time evolution of the distributions, differ from one another by powers of $(1+\alpha)$, and in many physically interesting problems this quantity can be large. Differential equations are said to be stiff if they contain two or more rate constants that vary widely in magnitude. The solution to such equations contain terms that change rapidly, with a small change in the independent variable, and others that change much more slowly. The solution is then typically a function which

changes rapidly in a small portion of the domain of the independent variable and much more slowly elsewhere. (For example; the equation $dy/dx = -\{100\ e^{-100x} + 0.05\ e^{-0.05x}\}$, which has the general solution of $y = e^{-100x} + e^{-0.05x}$, is stiff.) Stiff differential equations are not efficiently solved by standard fixed step size methods because of the strong variations in the behavior of the function and therefore require special techniques. The method we utilize to solve the kinetic equations is based on a predictor-corrector method with automatically determined step size developed by C. W. Gear (43) to solve systems of stiff, coupled, first order differential equations. In comparing the Gear method with the Gauss-Legendre numerical integration of the quadratures, we find that large values of α require an inordinately large number of integration points (and hence, the amount of computer time) to adequately sample the rapidly changing integrand. Numerical solution of the equations by the Gear method in this range of α is much more efficient. The subprogram we use to solve the system of stiff differential equations in this thesis is a version of the Gear procedure due to A. C. Hindmarsh (44), which will be referred to as GEAR. This program can be directly applied to Eqns. 3.7, 3.11 and 3.14 to obtain the distributions directly as a function of the reduced time $\tau_{00}t$.

All distributions of interest are, of course, not decomposable into distributions of <u>consecutive</u> vacancies and are therefore not determined by Eqns. 3.7, 3.11 and 3.14. The distribution

$$P^{(3)}(010) = P^{(2)}(0\_0) - P^{(3)}(000) \tag{3.21}$$

is an important example which arises in Chapter 6. Here, the symbol (0_0) denotes the configuration where two vacancies are separated by a site of unspecified condition. Such distributions are governed by a set of kinetic equations which is larger than the previously derived hierarchy of equations for consecutive vacancies, and in fact, include this hierarchy as a subset. The truncation condition, Eqn. 2.13, is applicable to this larger hierarchy since q_2 does not depend on the configuration of lattice sites beyond the two conditioning sites. The additional kinetic equations contained in this second hierarchy (after truncation) are given below.

$$\begin{aligned}\frac{dP^{(2)}(0\_0)}{dt} = -2\{&(\tau_{00}-2\tau_{01}+\tau_{11})P^{(2)}(\underline{0})q_2^{\,2} + (\tau_{01}-\tau_{11})P^{(3)}(\underline{0})\\ &- (\tau_{01}-\tau_{11})P^{(3)}(00\_0)\\ &- \tau_{11}P^{(2)}(0\_0)\},\end{aligned} \tag{3.22}$$

$$\frac{dP^{(3)}(00\_0)}{dt} = -(\tau_{00}-2\tau_{01}+\tau_{11})P^{(2)}(\underline{0})q_2^3 - (\tau_{01}-\tau_{11})P^{(4)}(\underline{0})$$
$$- (\tau_{00}-\tau_{01})P^{(3)}(00\_0)q_2 - (2\tau_{01}-\tau_{11})P^{(3)}(00\_0$$
$$- (2\tau_{01}-\tau_{11})P^{(3)}(00\_0)$$
$$- (\tau_{01}-\tau_{11})P^{(4)}(00\_00), \qquad (3.23)$$

and
$$\frac{dP^{(4)}(00\_00)}{dt} = -2\{(\tau_{00}-\tau_{01})P^{(2)}(\underline{0})q_2^3 - 2\tau_{01}P^{(4)}(00\_00)$$
$$- (\tau_{00}-\tau_{01})P^{(4)}(00\_00)q_2\}. \qquad (3.24)$$

We now define the following conditional probabilities:

$$P^{(2)}(0\_0) \equiv P^{(1)}(0)\nu_1, \qquad (3.25)$$

$$P^{(3)}(00\_0) \equiv P^{(2)}(\underline{0})\nu_2, \qquad (3.26)$$

and
$$P^{(4)}(00\_00) \equiv P^{(2)}(\underline{0})\nu_2\nu_3. \qquad (3.27)$$

When these relations are differentiated with respect to time, substituted into Eqns. 3.22, 3.23 and 3.24 and the result rearranged, we obtain the alternate, equivalent set of differential equations

$$\frac{d\nu_1}{dt} = -2(\tau_{00}-2\tau_{01}+\tau_{11})q_1q_2^2 - 2(\tau_{01}-\tau_{11})q_1q_2$$
$$- 2(\tau_{01}-\tau_{11})q_1\nu_2 - \tau_{11}\nu_1 + 2(\tau_{01}-\tau_{11})q_1\nu_1$$
$$+ (\tau_{00}-2\tau_{01}+\tau_{11})q_1q_2\nu_1, \qquad (3.28)$$

$$\frac{d\nu_2}{dt} = -(\tau_{00}-2\tau_{01}+\tau_{11})q_2^3 - (\tau_{00}-\tau_{01})q_2^2 + (\tau_{00}-\tau_{01})\nu_2 q_2 - (\tau_{01}-\tau_{11})\nu_2\nu_3, \tag{3.29}$$

and

$$\frac{d\nu_3}{dt} = -2(\tau_{00}-\tau_{01})q_2^3/\nu_2 - (2\tau_{01}-\tau_{11})\nu_3 - (\tau_{00}-\tau_{00})\nu_3 q_2 + (\tau_{00}-2\tau_{01}+\tau_{11})\nu_3 q_2^3/\nu_2 + (\tau_{00}-\tau_{11})\nu_3 q_2^2/\nu_2 + (\tau_{01}-\tau_{11})\nu_3^2. \tag{3.30}$$

These equations, along with Eqn. 3.14, form a closed, coupled set of differential equations that can be solved analytically with the solutions expressed as quadratures. They can also be solved numerically via the GEAR program. These functions are plotted as a function of $P(0)^{(1)}$ in Fig. 3.5. The solutions to Eqns. 3.28, 3.29 and 3.30, and the solutions to the initial hierarchy of equations (Eqns. 3.7, 3.11 and 3.14) completely describe the kinetics of distributions of configurations of sites containing a single, enclosed, unspecified site (as well as the distributions of consecutive vacancies). The configurations of vacant and unspecified sites of Eqns. 3.28, 3.29 and 3.30 do not exhaust the possibilities of physical interest which give rise to fundamentally different kinetic equations (i.e., require the definition of new conditional probabilities). Every configuration that begins (at both

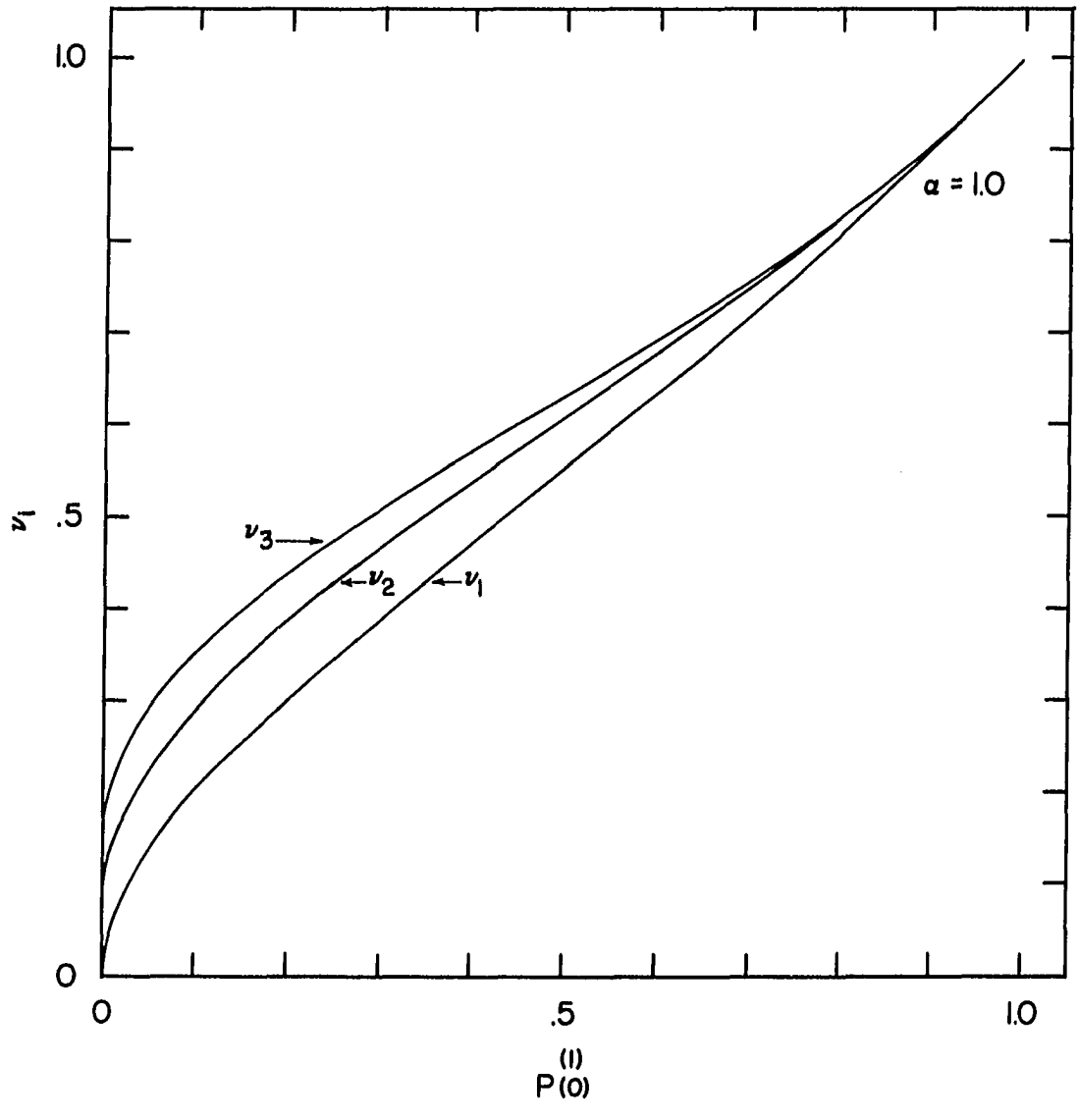

Figure 3.5. The ν_i (i=1,2,3) conditional probabilities as a function of $P^{(1)}(0)$, where r=0

ends) with two vacant sites followed by an unspecified site gives rise to a hierarchy of equations which couple all configurations which can be obtained from the initial configurations by:

1) replacing any internal unspecified site by a vacancy, or
2) replacing an end vacancy at either end by an unspecified site.

The truncation condition of Eqn. 3.13 can be applied in any situation where three or more consecutive vacancies occur. Thus, as we have seen, the configuration (00_00) of Eqn. 3.24 gives rise to the hierarchy which couples the configurations (00_00), (0_00), (0_0), (00), and (0). As another example, we can consider the coupling scheme for the configuration (00_0_00). On application of the above rules, we find that this configuration is coupled to the configurations (0_0_00), (0_0_0), (00_00), and all configurations from the first example. There is no largest hierarchy, but each hierarchy contains a finite number of configurations (after truncation) and larger hierarchies contain totally imbedded smaller hierarchies. It is important to realize, however, that the same truncation condition (i.e., Eqn. 3.13) is used to exactly truncate all of the hierarchies.

Cooperative Events with a 1st n.n. Blocking Potential

Another cooperative model of specific interest is the model describing the kinetics of events exhibiting a 1st n.n. blocking potential and 2nd n.n. cooperative interaction. Physically, this model is of interest because it is applicable to the description of such problems as the cooperative adsorption of homonuclear diatoms or the cooperative reaction of pendant groups on a substrate. Theoretically, this is the simplest cooperative model which saturates at an event density of $\eta<1$ (i.e., isolated vacancies can remain at lattice saturation).

The kinetic equations for the distribution of events in this model are derived using considerations similar to those employed for the previous model, and we therefore present the kinetic equations for the distributions of vacancies on the space-filling lattice below, without derivation.

$$\frac{dP^{(1)}(\underline{0})}{dt} = \frac{-d\theta}{dt} = -2\{\tau_{11}P^{(2)}(\underline{0}) + 2(\tau_{01}-\tau_{11})P^{(3)}(\underline{0}) + (\tau_{00}-2\tau_{01}+\tau_{11})P^{(4)}(\underline{0})\}, \tag{3.31}$$

$$\frac{dP^{(2)}(\underline{0})}{dt} = -\tau_{11}P^{(2)}(\underline{0}) + 2(2\tau_{01}-\tau_{11})P^{(3)}(\underline{0}) + (3\tau_{00}-4\tau_{01}+\tau_{11})P^{(4)}(\underline{0}), \tag{3.32}$$

and $$\frac{dP^{(n)}(\underline{0})}{dt} = -(n-3)\tau_{00}P^{(n)}(\underline{0}) - 2\tau_{01}P^{(n)}(\underline{0}) - 2\tau_{00}P^{(n+1)}(\underline{0})$$
$$-2(\tau_{00}-\tau_{01})P^{(n+2)}(\underline{0}), \quad n\geq 3 \qquad (3.33)$$

With the substitution $P^{(n+1)}(\underline{0}) = P^{(n)}(\underline{0})q_n$ we can derive equations for $P^{(1)}(0)$ and the conditional probabilities, q_n. We find that the equations for q_n, where $n\geq 3$, are all satisfied by the same function when the boundary condition $q_n=1$ at $t=0$ is applied. As in the previous section, this allows us to truncate the hierarchy exactly to obtain the set of four equations;

$$\frac{dP^{(1)}(0)}{dt} = -2P^{(1)}(0)\{\tau_{11}q_1 + 2(\tau_{01}-\tau_{11})q_1q_2$$
$$+ (\tau_{00}-2\tau_{01}+\tau_{11})q_1q_2q_3\}, \qquad (3.34)$$

$$\frac{dq_1}{dt} = -q_1\{\tau_{11}+2(2\tau_{01}-\tau_{11})q_2 + (3\tau_{00}-4\tau_{01}+\tau_{11})q_2q_3$$
$$- 2\tau_{11}q_1 - 4(\tau_{01}-\tau_{11})$$
$$- 2(\tau_{00}-2\tau_{01}+\tau_{11})q_1q_2q_3\}, \qquad (3.35)$$

$$\frac{dq_2}{dt} = -q_2\{2\tau_{01}+2\tau_{00}q_3 + 2(\tau_{00}-\tau_{01})q_3^2 - \tau_{11}$$
$$- 2(2\tau_{01}-\tau_{11})q_2 - (3\tau_{00}-4\tau_{01}$$
$$+\tau_{11})q_2q_3\}, \qquad (3.36)$$

$$\text{and} \quad \frac{dq_3}{dt} = -\tau_{00} q_3, \; q_n = q_3 = e^{-\tau_{00} t}, \; n \geq 3, \tag{3.37}$$

where, in the latter equation we have also included the truncation condition.

The closed form solutions to this kinetic hierarchy are obtained by dividing Eqn. 3.37 into Eqns. 3.34, 3.35 and 3.36 and solving the resulting equations as a function of q_3. As in the previous section, these equations can be put into the general form of the Ricatti equation and solved directly using standard techniques. The solutions in terms of quadratures are presented below:

$$q_2 = q_3^{(2\rho_{01}-\rho_{11})} \exp\{2(q_3-1) + (1-\rho_{01})(q_3^2-1)\}$$
$$\times \left[\int_1^q dq' \left\{\frac{2(2\rho_{01}-\rho_{11})}{q'} + (3-4\rho_{01}-\rho_{11})\right\} q'^{(2\rho_{01}-\rho_{11})} \exp\{2(q'-1) + (1-\rho_{01})(q'^2-1)\} + 1\right]^{-1}, \tag{3.38}$$

$$\text{and} \quad q_1 = q_3^{\rho_{11}} \exp\{2(2\rho_{01}-\rho_{11}) II(q_3, 2\rho_{01}-\rho_{11}-1) + (3-4\rho_{01}+\rho_{11}) II(q_3, 2\rho_{01}-\rho_{11})\}$$
$$\times \left[\int_1^{q_3} dq' \left\{\frac{2\rho_{11}}{q'} + \frac{q'^{(2\rho_{01}-\rho_{11})} \exp\{2(q'-1) + (1-\rho_{01})(q'^2-1)\}}{I(q') + 1} \times \left[\frac{4(\rho_{01}-\rho_{11})}{q'}\right] + 2(1-2\rho_{01}-\rho_{11})\right\} q'^{\rho_{11}}\right.$$
$$\left. \times \exp\{2(2\rho_{01}-\rho_{11}) II(q', 2\rho_{01}-\rho_{11}-1) + (3-4\rho_{01}-\rho_{11}) II(q^1, 2\rho_{01}-\rho_{11})\} + 1\right]^{-1}, \tag{3.39}$$

$$\text{where} \quad I(x) = \int_1^x dq' \left[\frac{2(2\rho_{01}-\rho_{11})}{q'} + (3-4\rho_{01}-\rho_{11}) \right] q'^{(2\rho_{01}-\rho_{11})} \times \exp\{2(q'-1) + (1-\rho_{01})(q'^2-1)\}, \quad (3.40)$$

$$\text{and} \quad II(x,a) = \int_1^x dq' \, \frac{q'^a \exp\{2(q'-1)+(1-\rho_{01})(q'^2-1)\}}{I(q') + 1}. \quad (3.41)$$

The singlet vacancy distribution, $P^{(1)}(0)$, can be obtained by directly integrating Eqn. 3.34, but a simpler procedure is to solve Eqn. 3.33 for $n=3$, as a function of q_3, with the result

$$P^{(3)}(\underline{0}) = q_3^{2\rho_{01}} \exp\{2(q_3-1) + (1-\rho_{01})(q_3^2-1)\}. \quad (3.42)$$

Then, using the definition $P^{(3)}(\underline{0}) = P^{(1)}(0) q_1 q_2$ and the expression for q_1 and q_2 of Eqns. 3.38 and 3.39, we obtain the result

$$P^{(1)}(0) = (q_1 q_2)^{-1} q_3^{2\rho_{01}} \exp\{2(q_3-1) + (1-\rho_{01})(q_3^2-1)\}. \quad (3.43)$$

The quadratures of Eqns. 3.35 and 3.36 can be evaluated to satisfactory accuracy using a twenty point Gauss-Legendre integration scheme, or the hierarchy of Eqns. 3.34 through 3.37 can be solved numerically using the GEAR program.

Representative results for q_3, q_2 and q_1 as a function of $P^{(1)}(0)$ are given in Figs. 3.6 and 3.7. The feature of note

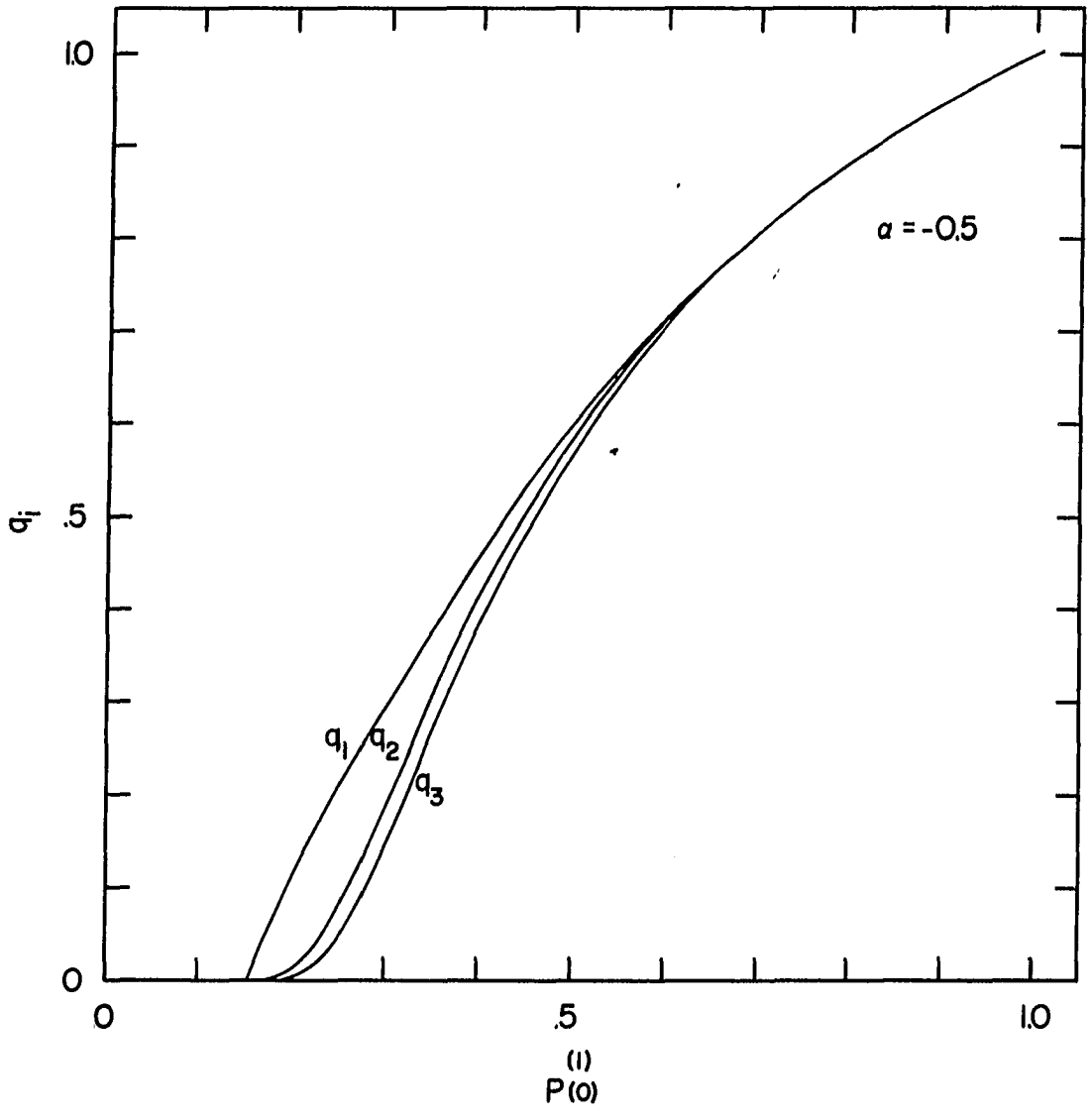

Figure 3.6. The q_i (i=1,2,3) conditional probabilities for a dimer event (r=1) as a function of the density of space-filling vacancies. In this plot $\alpha=-0.5$

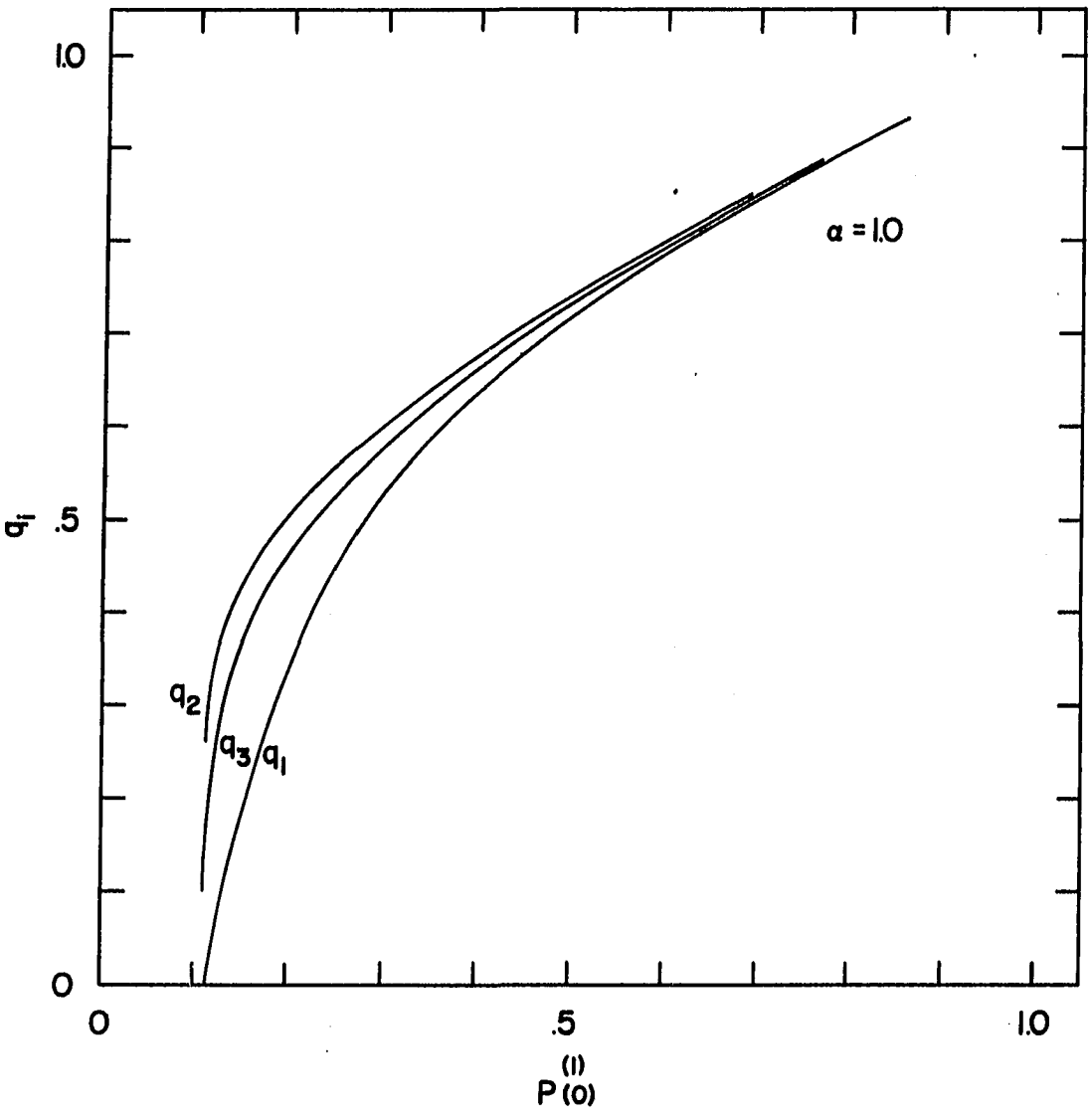

Figure 3.7. The conditional probabilities q_i (i=1,2,3) as a function of $P^{(1)}(0)$, where r=1 and α=1.0

in these plots is the variation in the (nonzero) saturation limit with variations in α. For the special case of $\alpha = 0.0$, the three conditional probabilities are equal and lattice saturation is attained at the expected value of $P^{(1)}(0) = e^{-2} \approx 0.135$. As α becomes positive, the saturation value of $P^{(1)}(0)$ decreases due to the increasing tendency of transitions to occur adjacent to an existing event. This leads to the clustering of events on the lattice. Indeed, in the limit as $\alpha \to \infty$, we see that the rate constants $\rho_{01} = \tau_{01}/\tau_{00}$ and $\rho_{11} = \tau_{11}/\tau_{00}$ become infinitely large, and hence transitions effectively only occur on sites adjacent to events on the lattice. In this case, the rate determining step is the nucleation caused by the first event. After this event, the lattice immediately fills. Also in this limit, the infinitely large rate constants lead to perfect sequential transition of the lattice sites beginning at the nucleated site, and result in a perfectly packed lattice at saturation, i.e., there are no vacant space-filling sites at saturation. On the other hand, negative values of α favor the dispersal of events due to the repulsive interactions. This tends to increase the saturation limit of $P^{(1)}(0)$. It can easily be shown that in the limit as $\alpha \to -1$, the kinetic model for this event directly reduces to the model for an event with a simple 2nd n.n. blocking interaction. The extension of this model to

configurations of vacancies and unspecified sites is straightforward.

The kinetic equations of events with longer range cooperative interactions can also be derived and, under certain conditions which we will later discuss, solved in the manner just described. As is to be expected, the equations become more complicated as the interaction range increases. As an example of such equations, we write the first few equations from the hierarchy describing the kinetics of distribution of events with a 1st n.n. blocking potential and 2nd and 3rd n.n. cooperative interactions.

In these equations a slightly different notation is used for the transition probabilities for notational convenience. Here we let $\tau(i,j)$ represent the transition probability for an event with i 2nd n.n. events and j 3rd n.n. events, where i and j can take on the values 0, 1 or 2. (Note that this notation is unambiguous since it is impossible to have both 2nd and 3rd n.n. sites occupied on the same side of the site of interest.) The first few kinetic equations are as follows:

$$\frac{dP^{(1)}(0)}{dt} = -(\tau(0,0)-2\tau(1,0)+2\tau(1,1)+\tau(2,0)+\tau(0,2))P^{(7)}(\underline{0})$$
$$+ 2(\tau(0,1)+\tau(1,1)+\tau(0,2))P^{(6)}(\underline{0}) - (2\tau(0,1)-\tau(0,2))P^{(5)}(\underline{0})$$
$$- 2(\tau(1,0)-\tau(1,1)-\tau(2,0))P^{(6)}(0\_00000) - 2\tau(1,1)P^{(5)}(0\_0000)$$
$$- \tau(2,0)P^{(5)}(0\_000\_0), \qquad (3.44)$$

$$\frac{dP^{(2)}(\underline{0})}{dt} = 2\,\frac{dP^{(1)}(0)}{dt}\,, \tag{3.45}$$

and

$$\begin{aligned}\frac{dP^{(3)}(\underline{0})}{dt} &= -(3\tau(0,0)-4\tau(1,0)+4\tau(1,1)+\tau(2,0)+3\tau(0,2))P^{(7)}(\underline{0}) \\ &+ (6\tau(0,1)+4\tau(1,1)+6\tau(0,2))P^{(6)}(\underline{0}) - (6\tau(0,1)-3\tau(0,2))P^{(5)}(\underline{0}) \\ &- (4\tau(1,0)-4\tau(1,1)-2\tau(2,0))P^{(6)}(0\_00000) - 4\tau(1,1)P^{(5)}(0\_0000) \\ &- \tau(2,0)P^{(5)}(0\_000\_0).\end{aligned} \tag{3.46}$$

We defer comment on the solution of these equations until the next section.

Cooperative Events with an rth n.n. Blocking Potential

The kinetic equations of the previous section are easily generalized to describe events with an rth n.n. blocking potential and r+1st n.n. cooperative interactions. The kinetic equations governing the time evolution of distributions of atomic vacancies are listed below.

$$\begin{aligned}\frac{dP^{(1)}(0)}{dt} &= -(r+1)\tau_{11}P^{(r+1)}(\underline{0}) - 2(r+1)\tau_{01}P^{(r+2)}(\underline{0}) \\ &- (r+1)(\tau_{00}-2\tau_{01}+\tau_{11})P^{(r+3)}(\underline{0})\,,\end{aligned} \tag{3.47}$$

$$\frac{dP(\underline{0})^{(n)}}{dt} = -2(\tau_{00}-\tau_{01})\sum_{\ell=0}^{n-3} P(\underline{0})^{(r+n-\ell+1)} - 2\tau_{01}\sum_{\ell=0}^{n-3} P(\underline{0})^{(r+n-\ell)}$$

$$-(r+2-n)\tau_{11}P(\underline{0})^{(n+1)} - 2\{(r+3-n)\tau_{01}-(r+2-n)\tau_{11}\}P(\underline{0})^{(r+2)}$$

$$-\{(r+4-n)\tau_{00}-2(r+3-n)\tau_{01}+(r+2-n)\tau_{11}\}P(\underline{0})^{(r+3)},$$

$$2\leq n\leq r+2, \tag{3.48}$$

and $$\frac{dP(\underline{0})^{(n)}}{dt} = -(n-r+2)\tau_{00}P(\underline{0})^{(n)} - 2(\tau_{00}-\tau_{01})\sum_{\ell=0}^{r} P(\underline{0})^{(n+\ell+1)}$$

$$-2\tau_{01}\sum_{\ell=0}^{r} P(\underline{0})^{(n+\ell)}, \quad n\geq r+2. \tag{3.49}$$

The truncation equation for the exact solution of this hierarchy, for general r, is given by

$$\frac{dq_{r+n}}{dt} = \frac{dq_{r+2}}{dt} = -\tau_{00}q_{r+2}, \tag{3.50}$$

which has the solution

$$q_{r+n} = q_{r+2} = e^{-\tau_{00}t}, \tag{3.51}$$

for all cases where $n\geq 2$.

We now consider the problem of whether any hierarchy describing the kinetics of events with an arbitrary cooperative interaction range can be exactly truncated. Within the mathematical formalism adopted in this thesis, the answer is unfortunately no, as we will now show. Let

us consider an n site configuration of consecutive vacant sites denoted by

$$(\underset{x}{0}000\ldots\underset{n}{00}),$$

where n is large, but finite, and x marks the site of interest. We will specifically examine the lattice configurations in the case where the loss of $P^{(n)}(\underline{0})$ is due to an event overlapping only the end site, because this event requires the specification of the largest configuration of sites, and if this event causes no truncation problems, then events that overlap more of the n sites won't either. For an event of length r+1 (which is the length of an rth n.n. blocking potential) to occur as described above requires that r sites beyond the end site of interest are necessarily vacant, as shown below:

$$\overbrace{(1\,1\ldots1)}^{r+1}$$

$$(0\,0\ldots\underset{r}{000})(\underset{x}{000}\ldots\underset{n}{00}).$$

However, because of the cooperative interactions we must specify the condition of c+r sites beyond the site of interest, where c is the range of the cooperative interactions. This is illustrated below:

$$(\underset{c}{aaa\ldots a})(\underset{r}{00\ldots000})(\underset{x}{000}\ldots\underset{n}{00}).$$

Here, a denotes an arbitrary site condition. If c is larger than a complete event (i.e., r+1 sites) then the configuration cannot be written in terms of consecutive, vacant site configurations. Hence, the maximum range of the cooperative interaction for which our exact truncation procedure is applicable is

$$c_{max} = r+1.$$

Thus, for the 0th n.n. blocking potential, we can have only 1st n.n. cooperative interactions, which is the case we have discussed. For the "dimer" problem (i.e., r=1), the cooperative interactions can at most include the 2nd and 3rd n.n. sites, etc.

The truncation of hierarchies of kinetic equations for an irreversible event with 1st n.n. cooperative interactions is also addressed in an article by Schwarz (21) in which he presents a relation, which he refers to as the triplet closure rule. This relation supposedly allows an arbitrary distribution of events and vacancies on the space-filling lattice to be expressed as a quotient of distributions of sets of two and three adjacent lattice sites. If we define the conditional probabilities $Q(x_i | x_1,x_2,\ldots,x_{i-1})$ such that they satisfy the relation

$$P^{(i)}(x_1,x_2,\ldots,x_i) = P^{(i-1)}(x_1,x_2,\ldots,x_{i-1}) \times Q(x_i | x_1,x_2,\ldots,x_{i-1}), \quad (3.52)$$

then the triplet closure rule can be written as

$$P^{(n)}(\underline{x}) = P^{(3)}(x_1,x_2,x_3)Q(x_4|x_2,x_3)\ldots Q(x_n|x_{n-2},x_{n-1}). \quad (3.53)$$

In other words, the triplet closure rule states that any kinetic hierarchy can be exactly truncated through probabilities that are conditioned on only two adjacent, consecutive sites of arbitrary condition. This rule is, however, not exact except in those instances where it is equivalent to the truncation rules we have already given. We will now prove this result.

The kinetic equation governing the distribution of a general configuration of vacancies and events with 1st n.n. cooperative interactions on a set of n adjacent sites (n>2) is given by

$$\frac{dP^{(n)}(\underline{x})}{dt} = \sum_x \sigma_1 P^{(n+1)}(\underline{x}_1) + \sum_{i=2}^{n-1} \sigma_1 P^{(n)}(\underline{x}_i) + \sum_{x_{n+1}} \sigma_n P^{(n+1)}(\underline{x}_n)$$
$$- \sum_x \sigma_1' P^{(n+1)}(\underline{x}) - \sum_{i=2}^{n-1} \sigma_i P^{(n)}(\underline{x}) - \sum_{x_{n+1}} \sigma_n' P^{(n+1)}(\underline{x}), \quad (3.54)$$

where $\underline{x}_j$ is the occupation vector that differs from $\underline{x}$ by the condition of site j, σ_i and σ_i' are the transition probabilities for an event on site i (these are a function of the condition of sites i+1 and i-1 because of the 1st n.n. interactions), $P^{(n)}(\underline{x})$ is the distribution of the configuration $\underline{x}$ (as before), and the sums over x_0 and x_{n+1} denote a sum over the possible configurations of the sites

o and n+1. The first three terms of this expression are gain terms that describe the increase in $P^{(n)}(\underline{x})$ due to the transition of previously vacant sites to form the configuration $\underline{x}$, while the remaining loss terms describe the decrease in the distribution $P^{(n)}(\underline{x})$ due to the transition of vacancies in the configuration $\underline{x}$. Note that this equation on the space-filling lattice is analogous to Eqn. 1.8 for the event lattice. Equation 3.54 can be used to describe reversible processes with minor changes in the definitions of the transition probabilities and $P^{(n)}(\underline{x}_{-1})$. As in previous cases, we now note that

$$\frac{d\ \ell n\ Q(x_n|\underline{x}^{n-1})}{dt} = \frac{d\ \ell n\ P^{(n)}(\underline{x})}{dt} - \frac{d\ \ell n\ P^{(n-1)}(\underline{x})}{dt} \qquad (3.55)$$

Substituting Eqn. 3.54 into this result and assuming for the moment that the triplet closure rule is valid, we obtain

$$\frac{d\ \ell n\ Q(x_n|x_{n-2},x_{n-1})}{dt} = \sum_{x_{n+1}} \left[\sigma_n \frac{Q(\bar{x}_n|x_{n-2},x_{n-1})Q(x_{n+1}|x_{n-1},\bar{x}_n)}{Q(x_n|x_{n-2},x_{n-1})} - \sigma_{n-1} \frac{Q(\bar{x}_{n-1}|x_{n-3},x_{n-2})Q(x_{n+1}|x_{n-2},x_{n-1})}{Q(x_{n-1}|x_{n-3},x_{n-2})} \right]$$

$$+ \sigma_{n-2} \left[\frac{Q(\bar{x}_{n-2}|x_{n-4},x_{n-3})Q(x_{n-1}|x_{n-3},\bar{x}_{n-2})Q(x_n|\bar{x}_{n-2},x_{n-1})}{Q(x_{n-2}|x_{n-4},x_{n-3})Q(x_{n-1}|x_{n-3},x_{n-2})Q(x_n|x_{n-2},x_{n-1})} - \frac{Q(\bar{x}_{n-2}|x_{n-4},x_{n-3})Q(x_{n-1}|x_{n-3},\bar{x}_{n-2})}{Q(x_{n-2}|x_{n-4},x_{n-3})Q(x_{n-1}|x_{n-3},x_{n-2})} \right]$$

$$+ \sigma_{n-1}\left[\frac{Q(\bar{x}_{n-1}|x_{n-3},x_{n-2})Q(x_n|x_{n-2},\bar{x}_{n-1})}{Q(x_{n-1}|x_{n-3},x_{n-2})Q(x_n|x_{n-2},x_{n-1})}\right] - \sigma'_{n-1}$$

$$- \sum_{x_{n+1}}\left[\sigma'_n\, Q(x_{n+1}|x_{n-1},x_n) - \sigma'_{n-1}\, Q(x_{n+1}|x_{n-2},x_{n-1})\right] \qquad (3.56)$$

where $\bar{x}_i$ specifically denotes a vacancy on site i. It is now clear that with the use of the triplet closure rule we have reached a contradiction. The rule would have that the conditional probability on the left-hand side depends only on conditioning sites x_{n-1} and x_{n-2}; however, the right-hand side also depends explicitly on conditioning sites x_{n-3} and x_{n-4}. Hence, the triplet closure rule is inconsistent and cannot be valid as an exact truncation relation for a general hierarchy. In the special case when only the loss terms contribute to the kinetic equation, that is <u>for totally vacant configurations of sites</u>, Eqn. 3.56 reduces to

$$\frac{d\ \ell n\ Q(0|00)}{dt} = -\sigma'_n \qquad (3.57)$$

and we see that the triplet closure rule is an exact truncation relation. This special case is, of course, just the case we considered in an earlier section of this Chapter. Attempts to extend the triplet closure rule (Eqn. 3.53) to include probabilities conditioned on larger configurations

of sites will suffer the same problems encountered in the above analyses.

In spite of the fact that the triplet closure rule is exact in only one case, it is a useful approximation, particularly in those cases where the distributions involve complicated configurations of events and vacancies. The use of the rules in such cases can circumvent the necessity of deriving and solving very complicated sets of kinetic equations. We would expect the triplet closure rule to be a good approximation for noncooperative events and low event density, while in cases where α is large and the event density high, we would expect a poorer approximation. Figure 3.8 shows the fractional deviation, $D = \frac{P_{Exact}-P_{TCR}}{P_{Exact}}$, of the triplet closure rule from the exact solution for the distribution $P^{(4)}(0100)$, as a function of the covering fraction.

Cooperative Models - Expansion Solutions

It is the purpose of this section to solve the kinetic equations for the 0th n.n. blocking potential and 1st n.n. cooperative interaction in expansion form so that the solutions can be directly compared to the virial expansions obtained by Hoffman, which are discussed in the first Chapter. In addition to this comparison, the convergence properties of the expansion solutions are investigated and

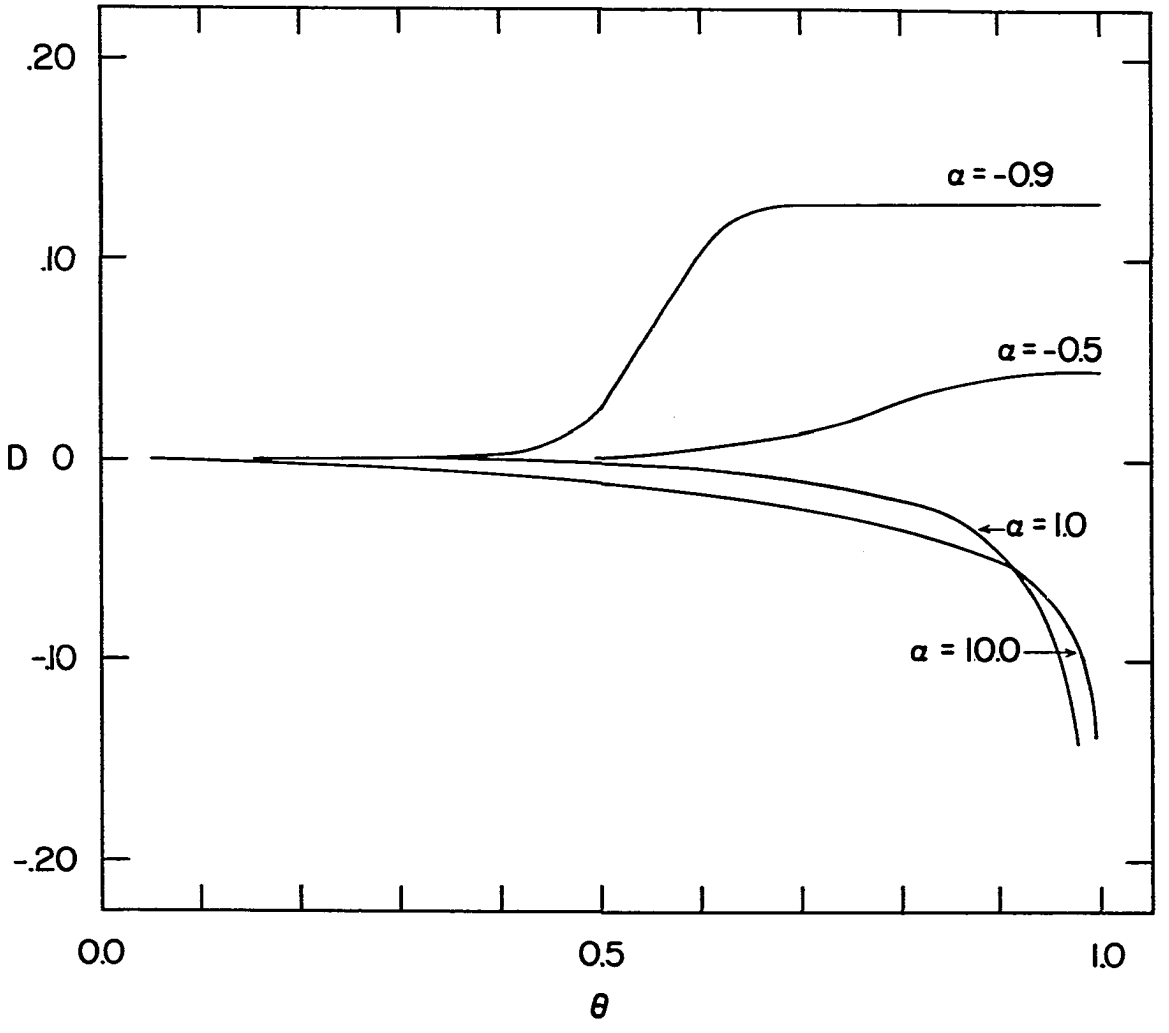

(4)

Figure 3.8. The fractional error, D, in the P(0100) distribution arising from the use of the triplet closure rule to approximately truncate the kinetic hierarchy (see text for definition of D)

a method for improving the convergence properties of such solutions is discussed.

To obtain exact expansion solutions to the kinetic model, the kinetic equations must first be written as infinite expansions. To this end, we can introduce the new variables $Z_i = 1-q_i$, i=1,2, and $\theta = 1-P^{(1)}(0)$ into Eqns. 3.7, 3.11 and 3.14 with the following result:

$$\frac{dZ_1}{dZ_2} = \frac{(1-Z_1)}{(1-Z_2)}\left\{1 + bZ_2 - cZ_1 - cZ_1Z_2\right\}, \tag{3.58}$$

and

$$\frac{d\theta}{dZ_2} = \frac{(1-\theta)}{(1-Z_2)}\left\{1 + bZ_1 - cZ_2 + cZ_1Z_2\right\}, \tag{3.59}$$

where $b = -1+\rho_{11}$ and $c = 1 - 2\rho_{01}+\rho_{11}$. The term $(1-Z_2)^{-1}$ can now be expanded in powers of Z_2 and substituted into Eqns. 3.58 and 3.59. To terms of third degree in Z, these expansions are

$$\begin{aligned}\frac{dZ_1}{dZ_2} = {} & 1 + (1+b)Z_2 - (1+b)Z_1 - (2b+c+1)Z_1Z_2 + (1+b)Z_2^2 \\ & + bZ_1^2 - (2b+c+1)Z_1Z_2^2 + (1+c)Z_1^2Z_2 \\ & + (1+b)Z_2^3 + \ldots,\end{aligned} \tag{3.60}$$

and

$$\begin{aligned}\frac{d\theta}{dZ_2} = {} & 1 + bZ_1 + (1-c)Z_2 - \theta + (b+c)Z_1Z_2 + (1-c)Z_2^2 \\ & - bZ_1\theta - (1-c)Z_2\theta + (b+c)Z_1Z_2^2 - (b+c)Z_1Z_2\theta \\ & - (1-c)\theta Z_2^2 + (1-c)Z_2^3 + \ldots .\end{aligned} \tag{3.61}$$

The solution to Eqn. 3.60 can be obtained by first writing Z_1 as a Taylor series in Z_2, differentiating the expansion with respect to Z_2, and equating the coefficients of the powers of Z_2 of the result with coefficients of like powers of Z_2 on the right hand side of Eqn. 3.60. This procedure gives explicit expressions for the coefficients of Z_2 in the original Taylor series expansion of Z_1. Equation 3.61 can be solved in a similar manner to give θ as a function of Z_2. The solutions of these equations, to fourth degree in Z_2, are presented below:

$$Z_1 = Z_2 - \tfrac{1}{3}\, cZ_2^{\,3} + \tfrac{1}{12}(1+b)cZ_2^{\,4}, + \ldots, \qquad (3.62)$$

and

$$\theta = Z_2 + \tfrac{1}{2}(b-c)Z_2^{\,2} - \tfrac{1}{6}(b-3c)Z_2^{\,3} + \tfrac{1}{4}(\tfrac{2}{3}bc-\tfrac{1}{3}b-\tfrac{1}{2}b^2-\tfrac{1}{2}c^3)Z_2^{\,4} + \cdots . \qquad (3.63)$$

The variables Z_1 and Z_2 can now be expressed as a function of θ by the reversion of the expansion for $Z_2(\theta)$, and by the substitution of this result into $Z_1(Z_2)$. After evaluating the coefficients of these equations in terms of the interaction parameter α, we finally obtain the expansion (explicitly written to fourth order)

$$q_1 = (1-Z_1) = 1-\theta+\alpha\theta^2 - \tfrac{1}{3}(\alpha+4\alpha^2)\theta^3 - \tfrac{1}{6}(\alpha-6\alpha^2-12\alpha^3+\alpha^4)\theta^4 + \cdots, \qquad (3.64)$$

and $$q_2 = (1-Z_2) = 1-\theta+\alpha\theta^2 - \frac{1}{3}(\alpha+5\alpha^2)\theta^3 - \frac{1}{12}(2\alpha-13\alpha^2-38\alpha^3+\alpha^4)\theta^4 + \cdots . \qquad (3.65)$$

The labor involved in this process increases rapidly with the number of terms retained in the power series. The expansions themselves, however, provide easily evaluated alternatives to the exact solutions. Figures 3.9 and 3.10 compare the four term density expansions of q_1 and q_2 to the exact solutions for representative values of α. It is seen that the expansions give good approximations in the regions of low density, and the approximation is best for small values of α. However, as might be expected, the approximations deviate from the exact results quite markedly near $\theta=1$. A method for improving the convergence properties of these expansions, known as the Padé approximant, is discussed later in this section.

These results can now be compared to the virial expansions obtained by Hoffman. Specifically, we examine the q_2 function as an example. Since the space-filling and event lattices for the case of a 0th n.n. blocking potential and 1st n.n. cooperative interactions are the same, the virial expansions, which are expansions on the event lattice, can be applied directly. To obtain the virial expansion of q_2 we write the conditional probability in the following form:

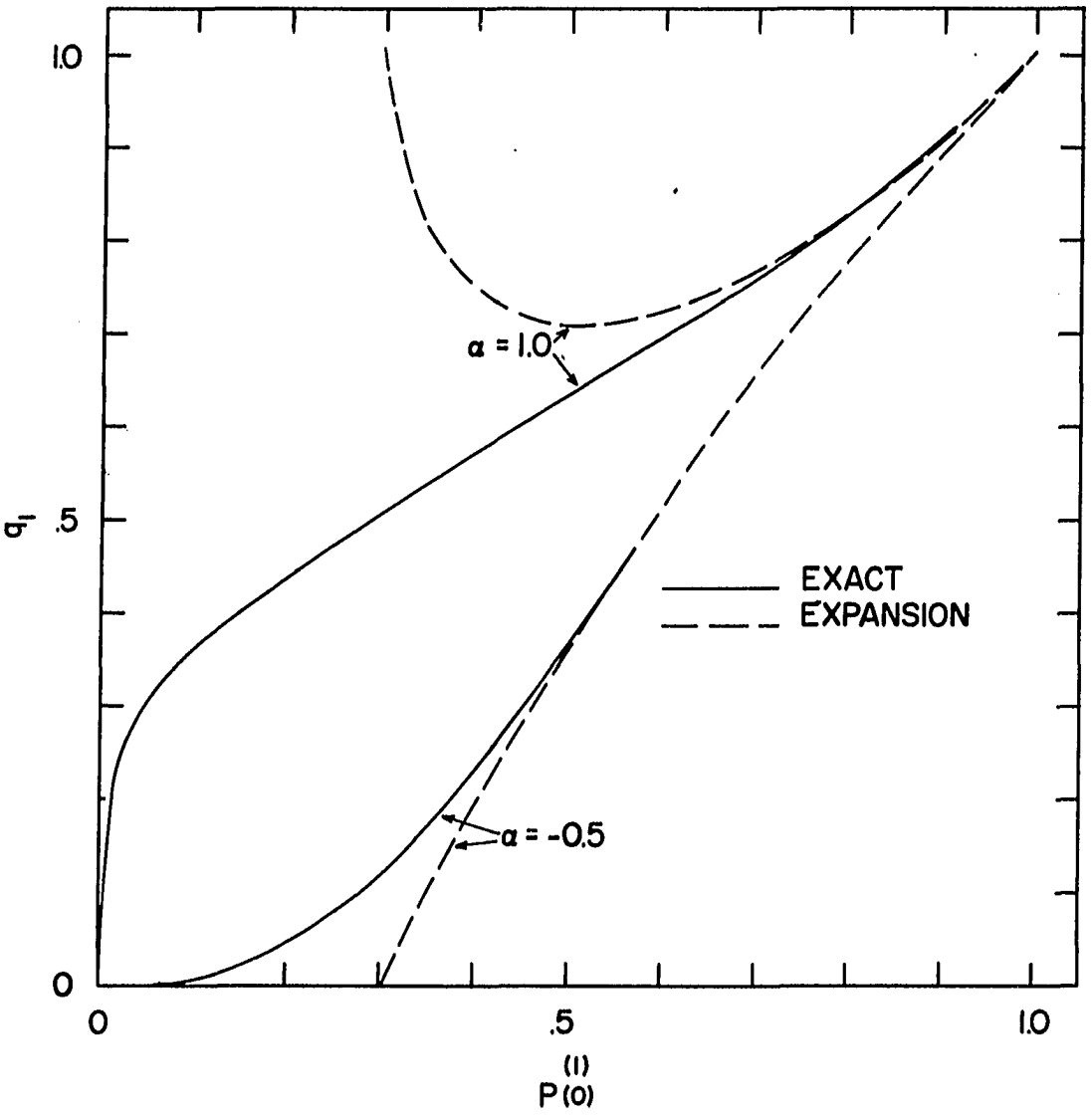

Figure 3.9. The exact solution and the fourth degree density expansion for q_1

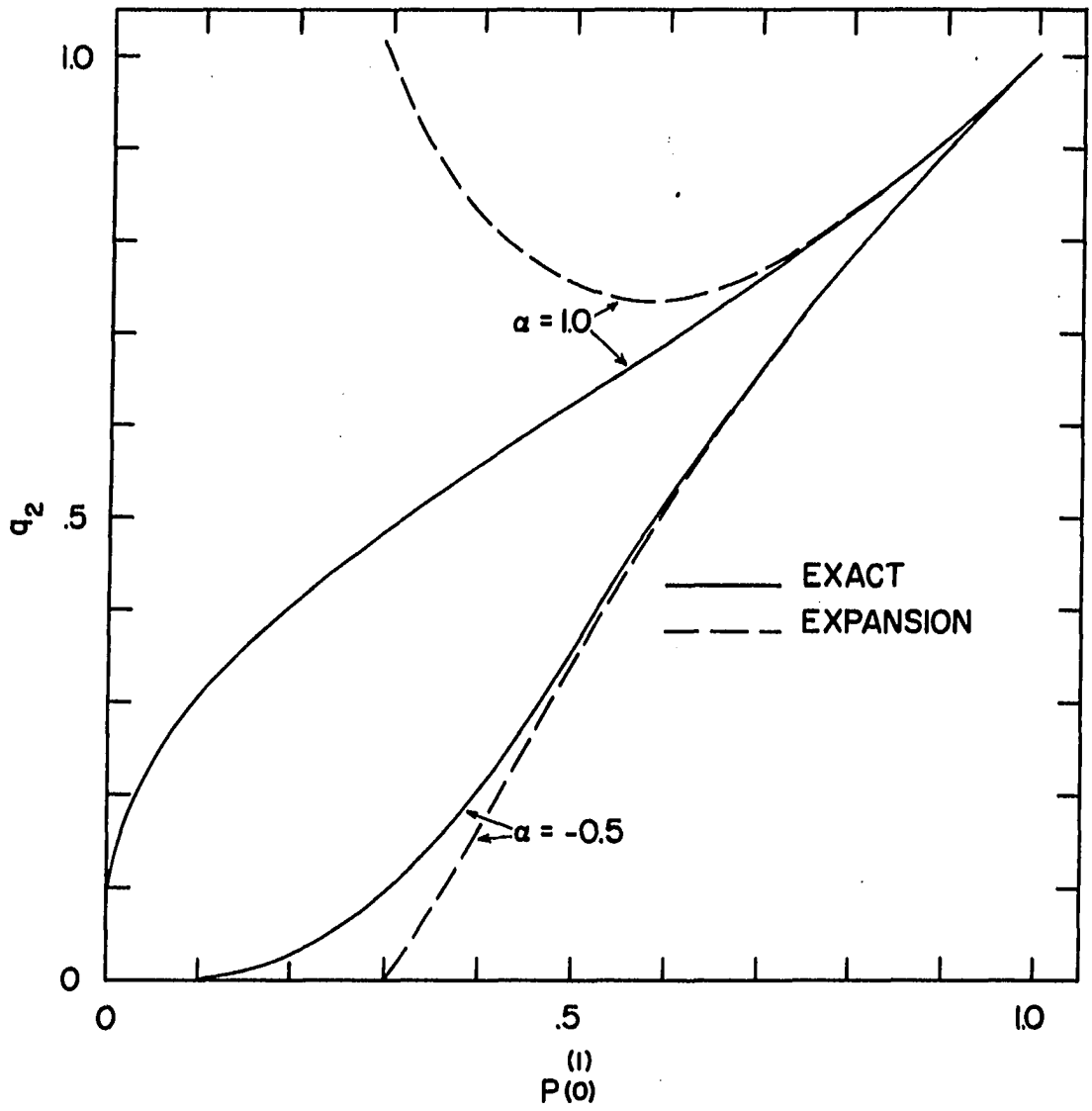

Figure 3.10. The exact solution and the fourth degree density expansion for q_2

$$q_2 = \frac{P^{(3)}(\underline{0})}{P^{(2)}(\underline{0})} \tag{3.66}$$

We now substitute for the distributions of vacant sites with the results of Eqn. 2.5 for n=3 and n=2 to obtain an expression for q_2 in terms of distributions of configurations of occupied sites; namely

$$q_2 = \frac{1 - 3f^{(1)}(1) + 2f^{(2)}(11) + f^{(2)}(1\text{-}1) - f^{(3)}(111)}{1 - 2f^{(1)}(1) + f^{(2)}(11)} . \tag{3.67}$$

Substituting for the f-functions in terms of the virial expansions for a 0th n.n. blocking potential and 1st n.n. interactions, we again obtain the result given in Eqn. 5.8. We recall from Chapter 1 that the virial formalism is not restricted to one-dimensional applications, but can be used to obtain density expansions of the distribution functions for lattices of arbitrary dimensionality. We will use this fact in our discussion of sticking coefficients in Chapter 5.

The convergence properties of these and other truncated expansions can be improved through the use of Padé approximants (45). The Padé method seeks to approximate an exact function, f(x), by a quotient of polynomials whose coefficients are directly related to the coefficients of the Taylor series expansion of the function. We now apply the Padé approximant technique, making use of the coefficients

of the expansion of Eqn. 3.65, to obtain better approximations for q_2.

The basic Padé relation is expressed in the following form:

$$f(x) = \sum_{k=0}^{\infty} a_k x^k = R_L(x)/T_M(x) + \sum_{j=L+M+1}^{\infty} b_j x^j, \quad (3.68)$$

where $R_L(x)$ is a polynomial of degree L, $T_M(x)$ is a polynomial of degree M, and the final sum can be considered an error term. The quotient of the two polynomials, $R_L(x)/T_M(x)$, is the Padé approximant. A thorough discussion of Padé approximants and their applications is presented in a monograph by Baker (46), to which the reader is directed for more information on this topic. We now multiply through Eqn. 3.68 by $T_M(x)$, and, keeping terms of order $\leq$ L+M, we have that

$$\left(1 + \sum_{k=1}^{M} t_k x^k\right)\left(\sum_{k=0}^{L+M} a_k x^k\right) - \sum_{k=0}^{L} r_k x^k = 0, \quad (3.69)$$

where t_k and r_k are the kth order coefficients of $T_M(x)$ and $R_L(x)$, respectively. For a given Taylor series, the Padé approximant is calculated simply by choosing integer L and M, multiplying out the polynomials, and equating like powers of x, to obtain the coefficients of R and T in terms of the Taylor series coefficients, a_k, of f(x) where $0 \leq k \leq L+M$. It is seen that to carry out this procedure, the coefficients

of the Taylor series of f(x) must be known to order L+M. Several different approximants are now possible by making various choices for L and M. As an empirical rule, it is generally found that the best approximations are obtained when L=M or L=M+1 (46). Since the expansion of Eqn. 3.65 is a fourth degree polynomial in θ, we choose L=M=2 in Eqn. 3.69. This gives rise to the Padé approximant

$$q_2 \approx \frac{\{(1+2\alpha)+\frac{1}{4}(-6+\alpha+18\alpha^2-\alpha^3)\theta+\frac{1}{12}(8-24\alpha-94\alpha^2-72\alpha^3+2\alpha^4)\theta^2\}}{\{(1+2\alpha)+\frac{1}{4}(-2+9\alpha+18\alpha^2-\alpha^3)\theta-\frac{1}{12}(4-8\alpha-127\alpha^2-164\alpha^3-7\alpha^4)\theta^2\}} . \tag{3.70}$$

Figure 3.11 shows the approximant for q_2 as compared to the exact function. Comparing these results with Fig. 3.10, we see that the Padé method gives a much better representation of the conditional probability in the large θ region.

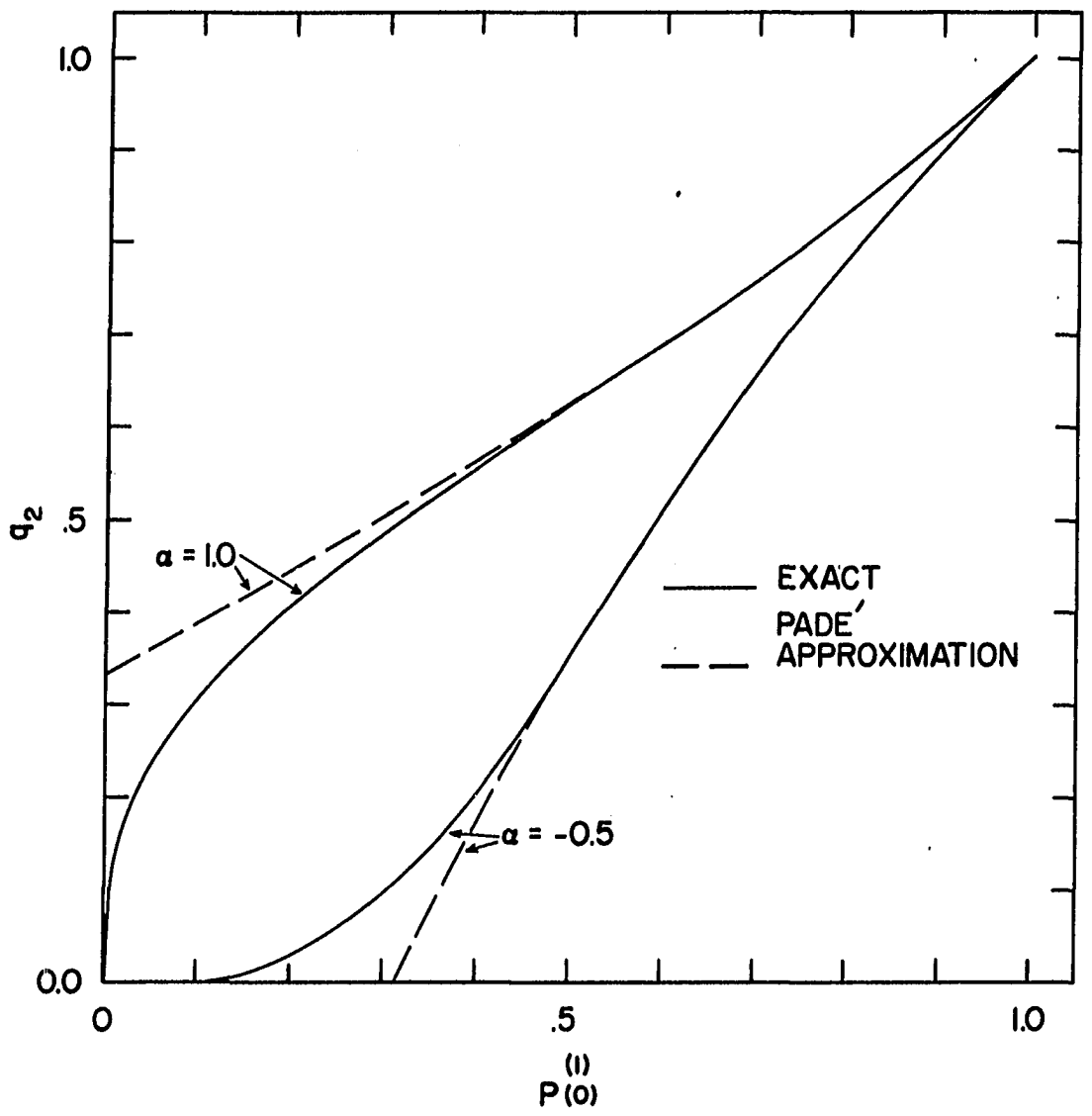

Figure 3.11. The exact solution and the Padé approximant for q_2

CHAPTER 4. A COOPERATIVE MODEL ON A SEMI-INFINITE LATTICE

In Chapter 2 we saw that the end sites of the semi-infinite and finite lattices can have a marked effect on the distribution of events on the respective lattices. The objective of this chapter is to consider cooperative events on a semi-infinite lattice, where the transition probability of the end site can be independently varied with respect to the transition probability of other lattice sites. The hierarchy of site dependent kinetic equations for a 0th n.n. blocking potential and 1st n.n. cooperative interactions are presented and solved from two different approaches. The solutions are used to examine the effects of the variable end site transition rate on the distribution of events on this lattice.

As in Chapter 2, we define $P_i^{(n)}(\underline{0})$ to be the probability of n adjacent vacancies with leftmost vacancy (i.e., the one nearest the terminal end) being at site i. The transition probabilities, τ_{ij}, for all sites except site 1, are defined as in Chapter 3. Site 1, however, has only one neighboring site and is assumed to have different transition probabilities, which we now define to be ε_0 and ε_1. These are written in Arrhenius form as

$$\varepsilon_0 = Ae^{-\beta\phi_0'}, \tag{4.1}$$

and

$$\varepsilon_1 = Ae^{-\beta\phi_1'}, \tag{4.2}$$

where ϕ_0' and ϕ_1' are the activation energies for the transition of site 1 in the cases where site 2 is in condition 0 and 1, respectively. The kinetic equations for site 1 are

$$\frac{dP_1^{(1)}(0)}{dt} = -(\varepsilon_0-\varepsilon_1)P_1^{(2)}(\underline{0}) - \varepsilon_1 P_1^{(1)}(0), \tag{4.3}$$

and

$$\frac{dP_1^{(2)}(\underline{0})}{dt} = -(\tau_{00}-\tau_{01})P_1^{(2)}(\underline{0})q_2 - (\tau_{01}+\varepsilon_0)P_1^{(2)}(\underline{0}), \tag{4.4}$$

where we have made use of the truncation condition of Eqn. 3.13. These two equations form a closed set which we can solve by dividing Eqns. 4.3 and 4.4 by Eqn. 3.14 and integrating to obtain

$$P_1^{(1)}(0) = q_2^{\eta_1}\left\{(\eta_0-\eta_1)\int_1^{q_2} dq\, q^{(\rho_{01}+\eta_0-\eta_1-1)} \exp\{(1-\rho_{01})(q-1)\} + 1\right\}, \tag{4.5}$$

and

$$P_1^{(2)}(\underline{0}) = q_2^{(\rho_{01}+\eta_0)} \exp\{(1-\rho_{01})(q_2-1)\}. \tag{4.6}$$

Here, $\eta_o = \varepsilon_0/\tau_{00}$ and $\eta_1 = \varepsilon_1/\tau_{00}$ are the reduced transition probabilities for the end site.

The kinetic equations for distributions beginning on site K are similar to those for the corresponding cooperative events on the infinite lattice (i.e., Eqns. 3.7 and 3.8), but now are parametrized on the lattice position. These

equations are as follows:

$$\frac{dP_K^{(1)}(0)}{dt} = -\tau_{11}P_K^{(1)}(0) - (\tau_{01}-\tau_{11})P_K^{(2)}(\underline{0}) - (\tau_{01}-\tau_{11})P_{K-1}^{(2)}(\underline{0}) - (\tau_{00}-2\tau_{01}+\tau_{11})P_{K-1}^{(2)}(\underline{0})q_2, \tag{4.7}$$

and

$$\frac{dP_K^{(2)}(\underline{0})}{dt} = -2\tau_{01}P_K^{(2)}(\underline{0}) - (\tau_{00}-\tau_{01})P_{K-1}^{(2)}(\underline{0})q_2 - (\tau_{00}-\tau_{01})P_K^{(2)}(\underline{0})q_2. \tag{4.8}$$

We now solve these equations by two different techniques.

A Semi-Infinite Lattice Model - Iterative Solutions

We note that Eqns. 4.7 and 4.8 have the same general form as Eqn. 2.75, that is, the equations indexed on site K are coupled only to site K-1. We can therefore utilize the general iterative procedure that was employed to solve Eqn. 2.75.

We begin by rewriting Eqn. 4.8 in the following form:

$$\frac{d\chi_K}{dt} = -(\tau_{00}-\tau_{01})q_2(\chi_{K-1}+\chi_K), \tag{4.9}$$

where $\chi_K = P_K^{(2)}(\underline{0})e^{2\tau_{01}t}$. Now, dividing this result by Eqn. 3.14 and introducing the variable $Z_2 = 1-q_2$, we obtain

$$\frac{d\chi_K}{dZ_2} = -\gamma(\chi_{K-1} + \chi_K), \tag{4.10}$$

where $\gamma = (1-\rho_{01})$. This equation can then be rearranged to yield

$$\frac{d\kappa_K}{dZ_2} = -\gamma\kappa_{K-1}, \quad K>1. \tag{4.11}$$

Here, $\kappa_K = \chi_K \; e^{\gamma Z_2}$. We can solve this set of equations in an iterative manner by first substituting $\kappa_1 = (1-Z_2)^{\delta}$, where $\delta = \eta_0-\rho_{01}$, into Eqn. 4.11, and solving for κ_2, the expression for κ_1 being obtained from Eqn. 4.6. We can repeat the process for successive values of K. The first four solutions are given below:

$$\kappa_1 = (1-Z_2)^{\delta}, \qquad \kappa_2 = \frac{\gamma}{\delta+1}\{(1-Z_2)^{\delta+1} - 1\} + 1,$$

$$\kappa_3 = \frac{\gamma^2}{(\delta+1)(\delta+2)}\{(1-Z_2)^{\delta+2}\} - \gamma(1 - \frac{\gamma}{\delta+1})Z_2 + 1,$$

and $$\kappa_4 = \frac{\gamma^3}{(\delta+1)(\delta+2)(\delta+3)}\{(1-Z_2)^{\delta+3} - 1\} + \frac{\gamma^3}{(\delta+1)(\delta+2)} Z_2$$

$$+ \frac{\gamma^2}{2}(1 - \frac{\gamma}{\delta+1})Z_2^{\,2} - \gamma Z_2 + 1.$$

Generalizing these results to arbitrary K, we obtain

$$\kappa_K = \frac{\gamma^{K-1}}{\prod_{j=1}^{K-1}(\delta+j)} \left\{ (1-Z_2)^{\delta+K-1} - 1 \right\} + \sum_{n=1}^{K-2} \frac{(\gamma Z_2)^n (-1)^{n+1}}{n!} \left\{ \frac{\gamma^{K-n-1}}{\prod_{j=1}^{K-n-1}(\delta+j)} - 1 \right\} + 1, \quad K>1 \tag{4.12}$$

This result can be rearranged to give

$$\kappa_K = e^{-\gamma Z_2} + \gamma^{K-1} \sum_{n=0}^{\infty} \frac{(-Z_2)^{n+K-1}}{(n+K-1)!} \left(\frac{\Gamma(\delta-m)}{\Gamma(\delta+2)} - \gamma^n \right), \tag{4.13}$$

where $\Gamma(a)$ is the gamma function. Equation 4.13 is the general solution to Eqn. 4.11, expressed as an exponential in Z_2 with correction terms containing the site dependence of the distribution. We note from this discussion that the pair vacancy distribution is given by

$$P_K^{(2)}(\underline{0}) = (1-Z_2)^{2\rho_{01}} e^{-\gamma Z_2} \kappa_K, \tag{4.14}$$

and hence,

$$P_K^{(2)}(\underline{0}) = (1-Z_2)^{2\rho_{01}} e^{-\gamma Z_2} \left(e^{-\gamma Z_2} + \gamma^{K-1} \sum_{n=0}^{\infty} \frac{(-Z_2)^{n+K-1}}{(n+K-1)!} \left(\frac{\Gamma(\delta-m)}{\Gamma(\delta+2)} - \gamma^n \right) \right). \tag{4.15}$$

The time dependence of Eqn. 4.15 is established through the relation $Z_2 = 1-q_2 = 1-e^{-\tau_{00} t}$.

Sites far from the end of the lattice should be affected very little by the termination of the lattice. Therefore, in the limit as $K \to \infty$, the distribution on the semi-infinite lattice should go over to the corresponding distribution on the infinite lattice. In this limit we obtain

$$\kappa_\infty = e^{-2\gamma Z_2}, \tag{4.16}$$

or by Eqn. 4.14,

$$P_\infty^{(2)}(\underline{0}) = (1 - Z_2)^{2\rho_{01}} e^{-2\gamma Z_2}, \tag{4.17}$$

which is precisely the expression given in Eqn. 3.16 for the pair vacancy distribution on the infinite lattice.

Equation 4.15 can now be substituted into Eqn. 4.7 to obtain an expression for the time rate of change of $P_K^{(1)}(0)$ as a function of $Z_2 = 1-q_2$. The resulting set of equations is, however, much more complicated than Eqn. 4.11 and it becomes advantageous to seek an alternate method of solution.

A Semi-Infinite Lattice Model - Transform Solutions

A second method for solving the kinetic equations, Eqns. 4.7 and 4.8, is based on transforming the site dependence of the kinetic equations. This transform method reduces the infinite set of coupled, site-dependent equations to a single differential equation for a transform function. The specific distributions are then obtained as an inverse transform.

Fourier transforms offer a familiar example of a similar transform technique.

Once again, the equations for the pair vacancy distributions are solved first since they form a closed set. Beginning with Eqn. 4.11, we define the following transforms:

$$f(\zeta,Z_2) = \sum_{j=1}^{\infty} \zeta^j \kappa_{j+1} \tag{4.18}$$

and $$g(\zeta,Z_2) = \sum_{j=1}^{\infty} \zeta^j \kappa_j \tag{4.19}$$

where ζ is a general complex transform variable. From these relations we note that $g(\zeta,Z_2) = \zeta\{f(\zeta Z_2) + \kappa_1\}$. Transforming Eqn. 4.11, we obtain

$$\frac{df(\zeta,Z_2)}{dZ_2} = -\gamma g(\zeta,Z_2) = -\gamma\zeta\{f(\zeta,Z_2) + (1-Z_2)^{\delta}\}, \tag{4.20}$$

which has the general solution

$$f(\zeta,Z_2) = e^{-\gamma\zeta Z_2}\{-\gamma\zeta \int_0^{Z_2} dZ\, e^{\gamma\zeta Z} (1-Z)^{\delta} + C\}. \tag{4.21}$$

The integration constant, C, is evaluated using the boundary conditions $\kappa_K = 1$ at $t = Z_2 = 0$, for all K. Substituting this condition into the definition of the transform $f(\zeta,Z_2)$, we have that

$$f(\zeta,0) = C = \frac{\zeta}{1-\zeta}, \tag{4.22}$$

where the magnitude of ζ is now restricted to the range $|\zeta|<1$ to ensure the convergence of the transform. Equations 4.21 and 4.22 together yield

$$f(\zeta,Z_2) = e^{-\gamma\zeta Z_2}\{-\gamma\zeta \int_0^{Z_2} dZ e^{\gamma\zeta Z}(1-Z)^{\delta} + \frac{\zeta}{1-\zeta}\}. \qquad (4.23)$$

The pair vacancy distribution functions can now be obtained as inverse transforms of this function using the theory of complex variables. Thus, we have that

$$P_K^{(2)}(\underline{0}) = (1-Z_2)^{2\rho_{01}} e^{-\gamma Z_2} \frac{1}{2\pi i} \int_C d\zeta\ \zeta^{-K} f(\zeta,Z_2), \qquad (4.24)$$

where C is a circular contour with radius $r<1$. Substituting Eqn. 4.23 into this result we obtain

$$P_K^{(2)}(\underline{0}) = (1-Z_2)^{2\rho_{01}} e^{-\gamma Z_2} \frac{1}{2\pi i} \int_C d\zeta\ \zeta^{-K} \{e^{-\gamma\zeta Z_2}(-\gamma\zeta \int_0^{Z_2} dZ e^{\gamma\zeta Z}(1-Z)^{\delta} + \frac{\zeta}{1-\zeta})\}. \qquad (4.25)$$

The complex integrals appearing in this expression are readily evaluated by the Cauchy integral formula, or the theory of residues (47), yielding Eqn. 4.12, as expected.

Transform solutions for the singlet distributions can now be obtained directly from Eqn. 4.7. We can define the following transforms on the site dependence of the singlet vacancy distributions:

$$Z(\zeta,q_2) = \sum_{j=1}^{\infty} \zeta^j P_{j+1}^{(1)}(0), \tag{4.26}$$

$$H(\zeta,q_2) = \sum_{j=1}^{\infty} \zeta^j P_{j+1}^{(2)}(\underline{0}), \tag{4.27}$$

and $$T(\zeta,q_2) = \sum_{j=1}^{\infty} \zeta^j P_j^{(2)}(\underline{0}),$$

or $$T(\zeta,q_2) = \zeta(H(\zeta,q_2) + P_1^{(2)}(\underline{0})).$$

Note that from Eqn. 4.14,

$$H(\zeta,q_2) = e^{-\gamma(1-q_2)} q_2^{2\rho_{01}} f(\zeta,q_2). \tag{4.28}$$

After dividing Eqn. 4.7 by Eqn. 3.14 to eliminate the explicit time dependence of the left side, we can transform the resulting equations to give

$$\begin{aligned}\frac{dZ(\zeta,q_2)}{dq_2} = \rho_{11} \frac{Z(\zeta,q_2)}{q_2} &+ (1-2\rho_{01}+\rho_{11})\zeta H(\zeta,q_2) \\ &+ (1-2\rho_{01}+\rho_{11})\zeta P_1^{(2)}(\underline{0}) + (\rho_{01}-\rho_{11})\zeta \frac{P_1^{(2)}(\underline{0})}{q_2} \\ &+ (1+\zeta)(\rho_{01}-\rho_{11}) \frac{H(\zeta,q_2)}{q_2},\end{aligned} \tag{4.29}$$

which has solutions of the form

$$Z(\zeta,q_2) = q_2^{\rho_{11}}\Big\{(1-2\rho_{01}+\rho_{11})\zeta \int_1^{q_2} dq\; q^{-\rho_{11}} H(\zeta,q)$$
$$+ (1-2\rho_{01}+\rho_{11})\zeta \int_1^{q_2} dq\; q^{-\rho_{11}} P_1^{(2)}(\underline{0})$$
$$+ (\rho_{01}-\rho_{11})(1+\zeta) \int_1^{q_2} dq\; q^{-(1+\rho_{11})} H(\zeta,q)$$
$$+ (\rho_{01}-\rho_{11})\zeta \int_1^{q_2} dq\; q^{-(1+\rho_{11})} P_1^{(2)}(\underline{0}) + C\Big\}. \qquad (4.30)$$

Equations 4.6 and 4.23 can now be substituted into this result and the integration constant, C, determined by applying the boundary conditions $P_K^{(n)}(\underline{0}) = 1$ at t=0 for all n and K. The transform function of the singlet vacancy distributions so obtained is

$$Z(\zeta,q_2) = q_2^{\rho_{11}}\Big\{\int_1^{q_2} dq\; q^{-(1+\rho_{11})}\Big[(1-2\rho_{01}+\rho_{11})\zeta q^{(\rho_{01}+\eta_0+1)}$$
$$\times e^{(1-\rho_{01})(q-1)} + (\rho_{01}-\rho_{11})\zeta q^{(\rho_{01}+\eta_0)} e^{(1-\rho_{01})(q-1)}$$
$$+ \big((1-2\rho_{01}+\rho_{11})\zeta q + (\rho_{01}-\rho_{11})(1+\zeta)\big)e^{\gamma(q-1)} q^{2\rho_{01}} e^{\gamma\zeta(q-1)}$$
$$\times \Big(\gamma\zeta \int_1^{q} dq' q'^{\delta} e^{-\gamma\zeta(q'-1)} + \frac{\zeta}{1-\zeta}\Big)\Big] + \frac{\zeta}{1-\zeta}\Big\}. \qquad (4.31)$$

The inverse transform of Eqn. 4.31 is given by the contour integral

$$P_K^{(1)}(0) = \frac{1}{2\pi i}\int_C d\zeta\ \zeta^{-K}\ Z(\zeta,q_2),\ K\geq 2. \tag{4.32}$$

The solution of this equation for various K leads to the general solutions for the singlet distributions,

$$P_2^{(1)}(0) = q_2^{\rho_{11}}\Bigg\{\int_1^{q_2} dq\ q^{-(1+\rho_{11})}\Bigg[(1-2\rho_{01}+\rho_{11})q^{(\rho_{01}+\eta_0+1)} \times e^{\gamma(q-1)} + (\rho_{01}-\rho_{11})q^{(\rho_{01}+\eta_0)}e^{(1-\rho_{01})(q-1)} + (\rho_{01}-\rho_{11})e^{+\gamma(q-1)}q^{2\rho_{01}}\Big\{\gamma\int_1^q dq'q'^{\delta} + 1\Big\}\Bigg] + 1\Bigg\}, \tag{4.33}$$

and, for K>2,

$$P_K^{(1)}(0) = q_2^{\rho_{11}}\Bigg\{\int_1^{q_2} dq\ q^{-(1+\rho_{11})}\Bigg[\Big\{(1-2\rho_{01}+\rho_{11})q + (\rho_{01}-\rho_{11})\Big\}q^{2\rho_{01}}e^{\gamma(q-1)} \times \Big\{\gamma^{K-2}\int_1^q dq'\ q'^{\delta}\ \frac{(q-q')^{K-3}}{(K-3)!} + e_{K-3}(\gamma(q-1)\Big\} + (\rho_{01}-\rho_{11})e^{\gamma(q-1)}q^{2\rho_{01}}\Big\{\gamma^{K-1}\int_1^q dq'\ q'^{\delta}\ \frac{(q-q')^{K-2}}{(K-2)!} + e_{K-2}(\gamma(q-1))\Big\}\Bigg] + 1\Bigg\}, \tag{4.34}$$

where $e_K(x)$ is the truncated exponential series. In the limit as $K \to \infty$, Eqn. 4.34 properly reduces to Eqn. 3.20, which gives the singlet vacancy distribution on the infinite lattice.

The above distribution functions can be utilized to study the effect of various end site transition rates on the lattice distributions. As previously mentioned, the end site transition rates are independent of the transition probabilities on the other sites of the lattice. We can therefore adjust ε_0 and ε_1, the end site transition probabilities, so as to promote or inhibit the transition at site 1 and examine the effect that this has on the lattice distributions.

For the numerical calculations of this Chapter, we can write the reduced transition probabilities η_0 and η_1 as

$$\eta_0 = \varepsilon_0/\tau_{00} = e^{-\beta(\phi_0'-2\phi_0)} \tag{4.35}$$

and

$$\eta_1 = \varepsilon_1/\tau_{00} = \eta_0\, e^{-\beta(\phi_1-\phi_0)} = \eta_0(1+\alpha). \tag{4.36}$$

For convenience, we have assumed that $(\phi_1'-\phi_0') = (\phi_1-\phi_0)$ in our calculations, but this is not required.

Figures 4.1 and 4.2 illustrate the effects of various end site transition rates on $P_1^{(1)}(0)/P_\infty^{(1)}(0)$ and $P_2^{(1)}(0)/P_\infty^{(1)}(0)$ as a function of $P_\infty^{(1)}(0)$. The end site transition probabilities

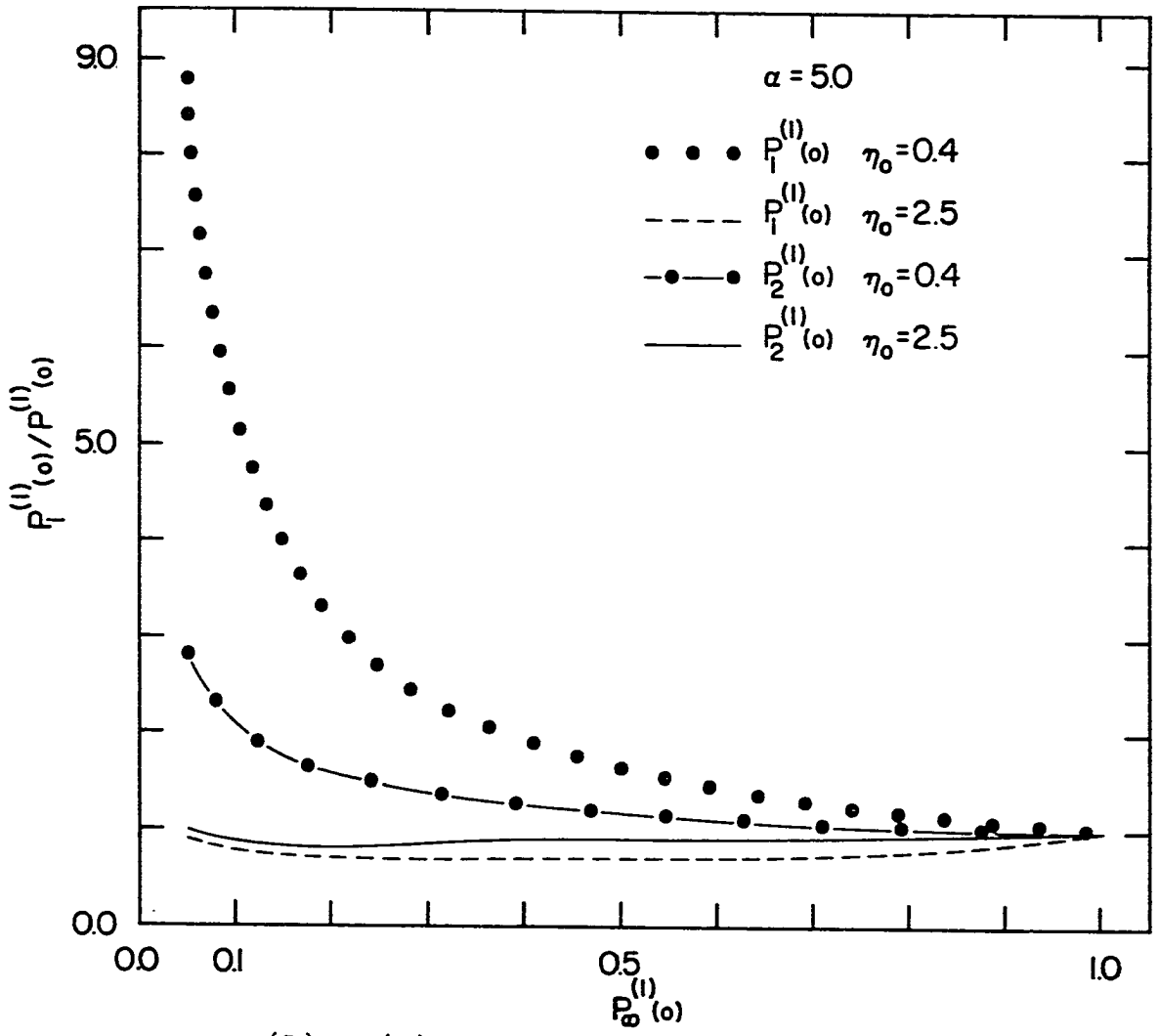

Figure 4.1. The quantity $P_i^{(1)}(0)/P_\infty^{(1)}(0)$ (i=1,2) as a function of $P_\infty^{(1)}(0)$ for α=5.0, and η_0 = 0.4 and 2.5

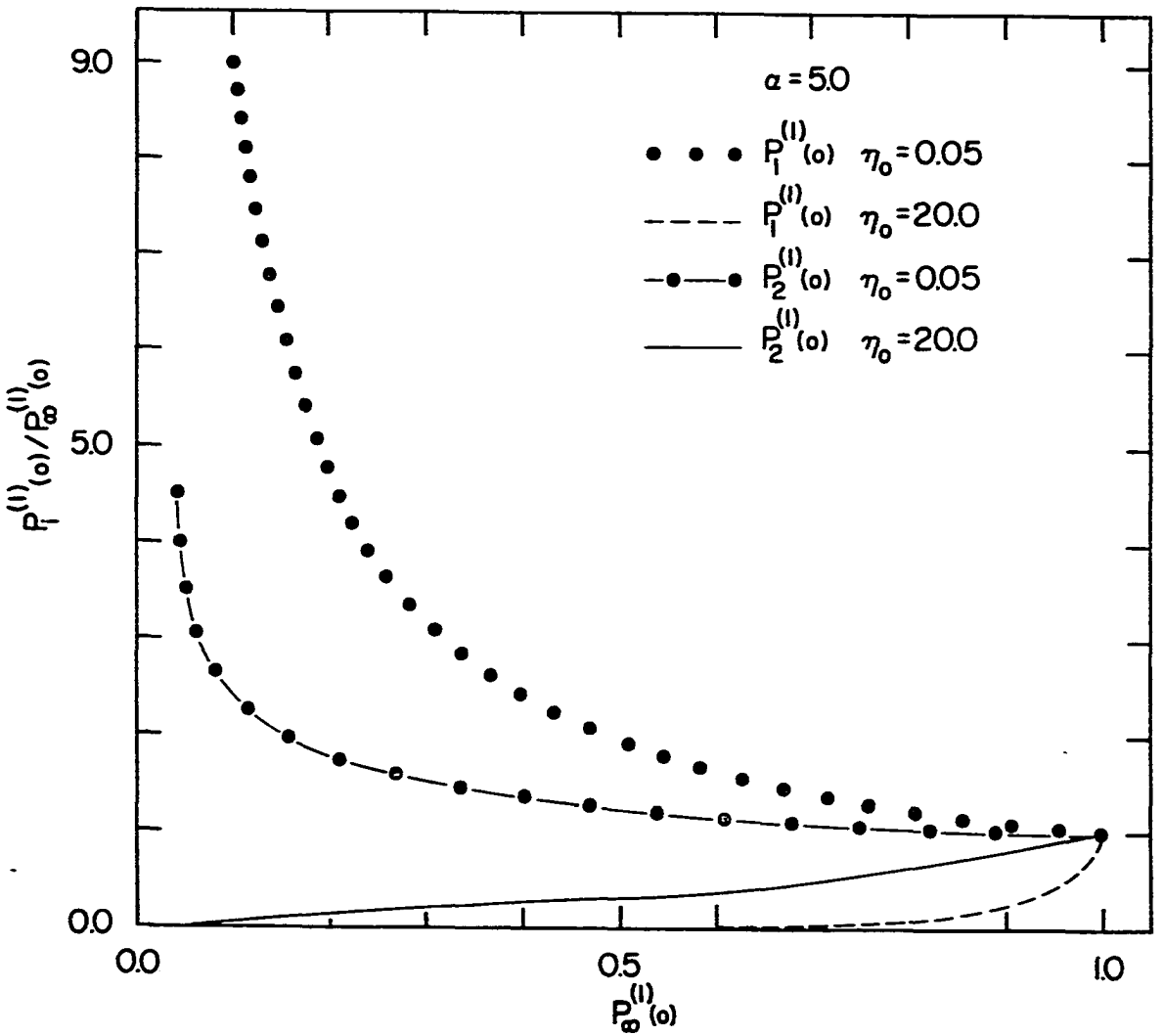

Figure 4.2. The quantity $P_i^{(1)}(0)/P_\infty^{(1)}(0)$ (i=1,2) as a function of $P_\infty^{(1)}(0)$ for α=5.0, and η_0 = 0.05 and 20.0

in these figures are $\eta_0 = \varepsilon_0/\tau_{00} = 0.4$ and 2.5, and $\eta_0 = 0.05$ and 20.0, respectively. In all cases $\alpha = 5.0$. The effect of η_0 is greatest at the end site, as is to be expected, but we also note a somewhat smaller effect on the singlet vacancy distribution at site 2. Figure 4.3 is a plot of the same functions for several values of α at a fixed value of $\eta_0 = 20.0$. Here we note only small variations in the site 1 functions with α, while the ratio of distributions at site 2 is markedly affected. From these three figures we can therefore conclude that the value of η_0 determines the magnitude of the influence of the end site and the value of α determines the range of the influence of the end site on the lattice distributions. Ultimately, for large values of α and η_0, the lattice will fill sequentially from the nucleation at site 1. Figure 4.4 shows the effect of the end site on pair vacancy distribution functions beginning at sites 1, 2, 3, 4, 5 and ∞. For the values of $\eta_0 = 20.0$ and $\alpha = 5.0$, we note that the range of influence of the end site is approximately five sites.

Possible applications of this semi-infinite lattice model are considered in Chapter 6. However, we can mention here that the semi-infinite lattice model can be used to describe such diverse problems as the increased activity of terraces and kinks on catalytically active crystals (48) or the influence of the condition of the end site on the helix to random coil transitions in a polypeptide (34).

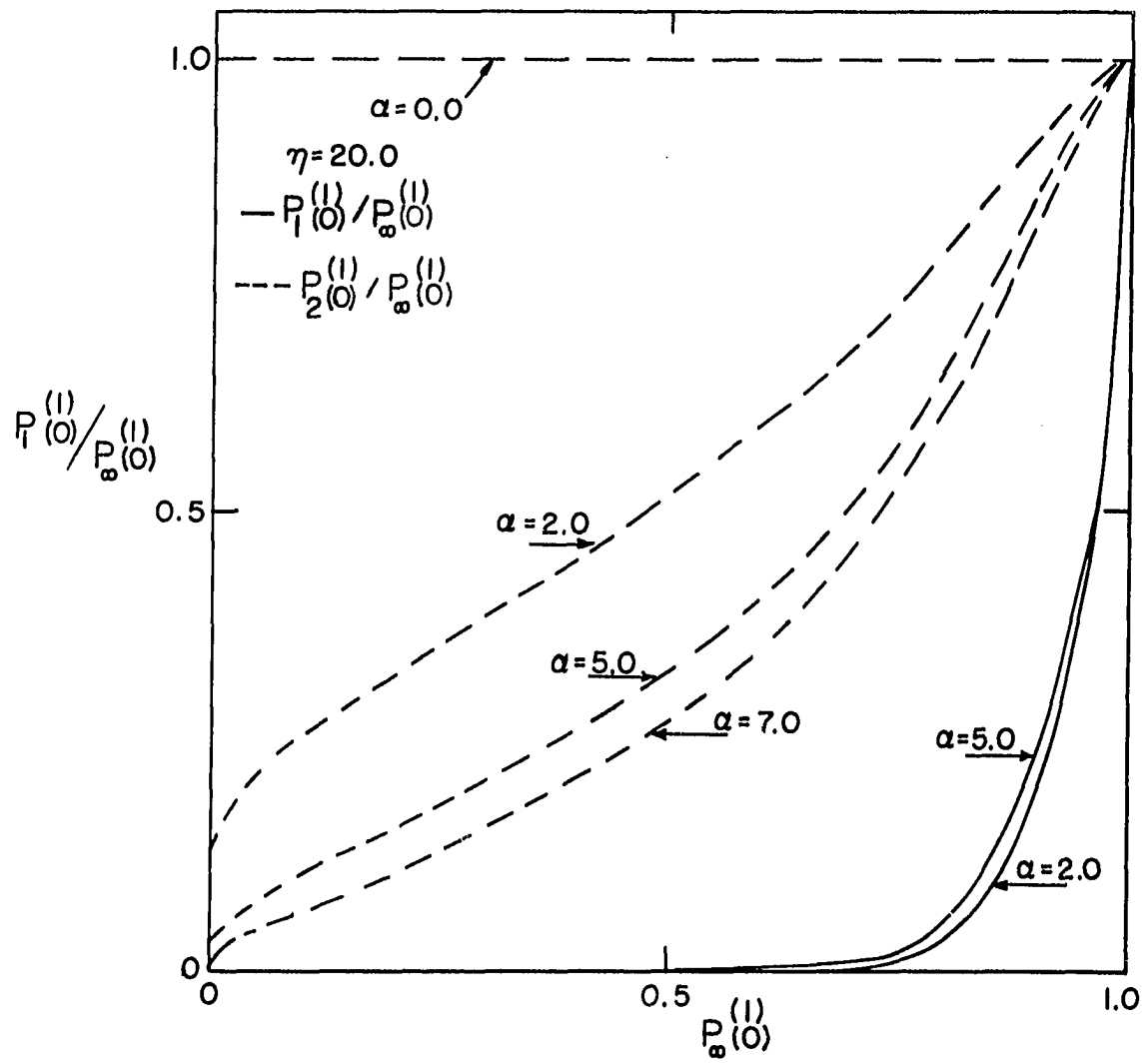

Figure 4.3. The quantity $P_i^{(1)}(0)/P_\infty^{(1)}(0)$ (i=1,2) as a function of $P_\infty^{(1)}(0)$ for η_0 = 20.0, and α = 2.0, 5.0 and 7.0

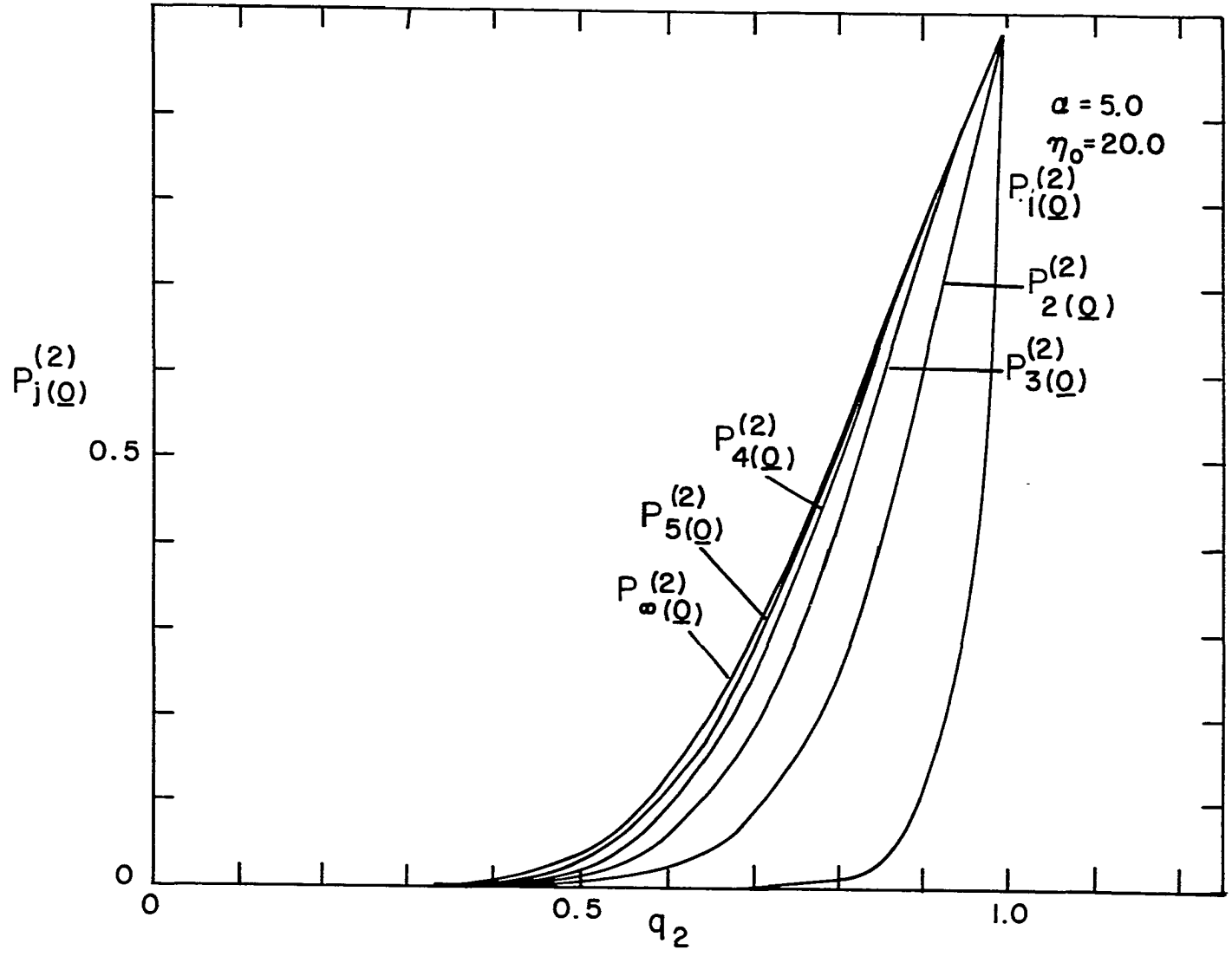

Figure 4.4. The distribution function $P_j^{(2)}(\underline{0})$ (j = 1,2,3,4,5,∞) as a function of q_2

CHAPTER 5. THE STICKING COEFFICIENT

The final test of any model is to compare its predictions with experimental results. In this Chapter, we test our kinetic models by calculating the sticking coefficient for molecular chemisorption as a function of atomic covering fraction and temperature. We compare our calculated results to data taken from various experimental studies of molecular chemisorption on metal surfaces. Of the several phenomena which can be treated by lattice models, we choose to consider chemisorption in detail because of the relevance of adsorption phenomena to the modern analysis of catalytic processes; and, in particular, because of the availability of sticking coefficient data. In addition, chemisorption provides a convenient context in which to illustrate the effects of system dimensionality.

It is usually the case that adsorbed molecules exist in one of two broadly defined adsorption states, which we refer to as physisorbed and chemisorbed. A physisorbed molecule is loosely bound to the surface by van der Waals forces. This means that it easily desorbs and is fairly free to move about on the surface. On the other hand, a chemisorbed molecule is chemically bonded to the atoms of the surface and for the purposes of this discussion we assume that is irreversibly adsorbed. We will assume that a molecule must first be physisorbed before chemisorption occurs, as is

widely believed to be the usual situation (49). The sticking coefficient is defined as the fraction of molecules which collide with the surface and eventually become chemisorbed. Thus, we can define the sticking coefficient in terms of the change of the molecular covering fraction of chemisorbed species. That is, the sticking coefficient, S, is given by

$$S \propto \frac{d\bar{f}^{(1)}(1)}{dt} , \tag{5.1}$$

where $\bar{f}^{(1)}(1)$ is the average distribution of molecules (i.e., chemisorption events) over all sites of the surface.

The Exact Sticking Coefficient on an Infinite Lattice

For the first part of our analysis we assume that the chemisorption step of the kinetic process is rate determining and that the sticking coefficient is not a function of the concentration of physisorbed species. This assumption will be eliminated in a more general analysis later in this section.

Since we are ultimately interested in the concentration dependence of the sticking coefficient, and not its absolute magnitude, we now define a normalized sticking coefficient, S', by

$$S' = \frac{df^{(1)}(1)}{\tau_{00} dt}, \tag{5.2}$$

where S' is normalized to one at t=θ=0. Here, we have made use of the fact that $f^{(1)}(1)$ is site independent and the fact that τ_{00} is the rate of addition to an empty lattice (i.e., the sticking coefficient for the empty lattice). From Eqn. 2.12, we have that

$$f^{(1)}(1) = -\frac{1}{(r+1)}\left(1-P^{(1)}(0)\right) \tag{5.3}$$

for a molecule composed of r+1 atoms. Substituting this result into the expression for the normalized sticking coefficient, we have that

$$S' = -\frac{1}{(r+1)\tau_{00}}\frac{dP^{(1)}(0)}{dt} . \tag{5.4}$$

The time derivative of $P^{(1)}(0)$, as given by Eqn. 3.47, when substituted into Eqn. 5.4 gives an expression for the sticking coefficient in terms of distributions introduced in Chapter 3. This substitution yields

$$S' = \rho_{11}P^{(r+1)}(\underline{0}) + 2\rho_{01}P^{(r+2)}(\underline{0}) + (1-2\rho_{01}+\rho_{11})P^{(r+3)}(\underline{0}) . \tag{5.5}$$

We now evaluate this expression for monomer (r=0) and for dimer (r=1) adsorption, using the results from Chapter 3.

Figures 5.1 and 5.2 give the results of these calculations for values of the interaction parameter of $\alpha = -0.8$,

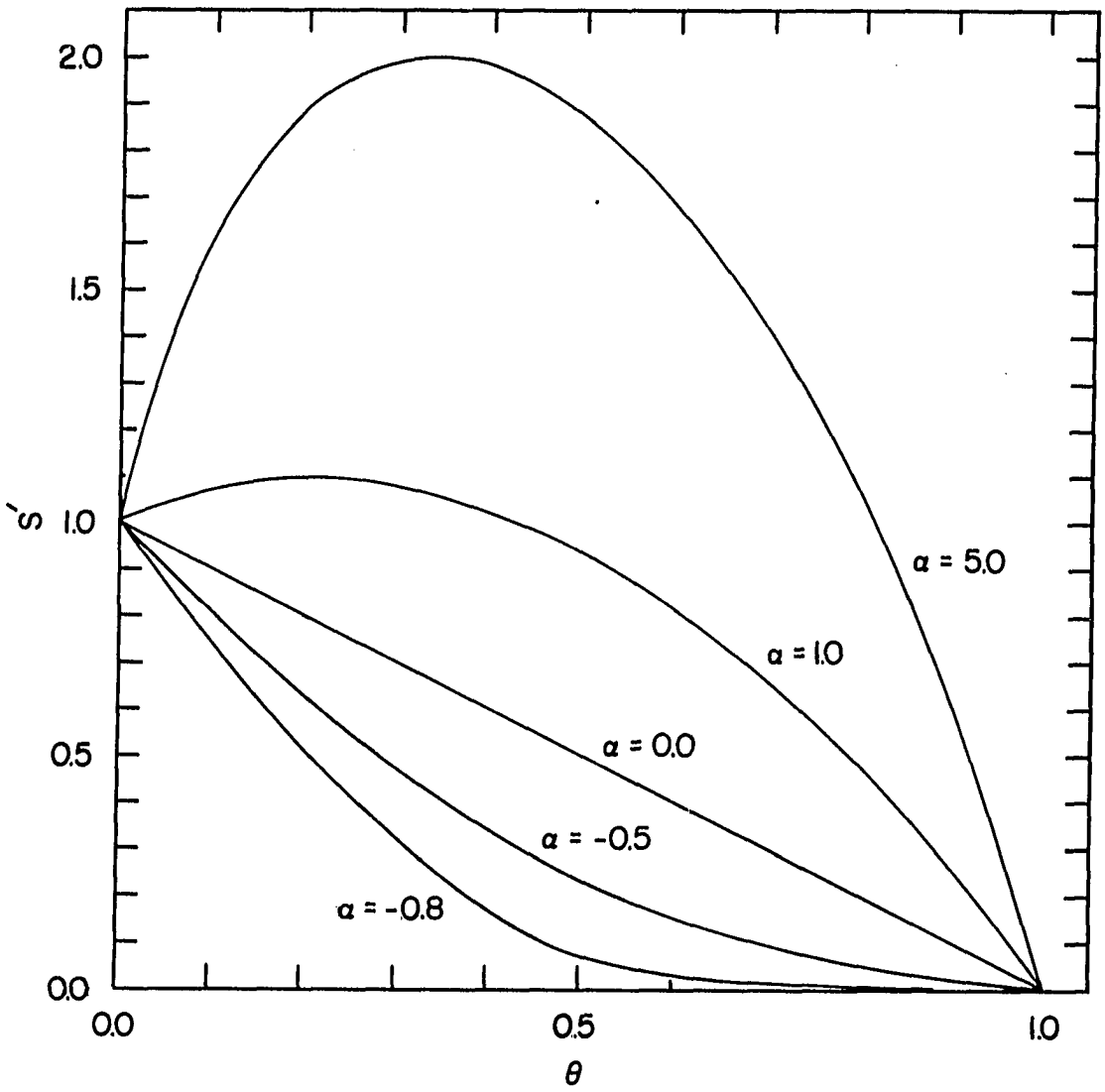

Figure 5.1. Theoretical sticking coefficient curves (S' vs θ) for the adsorption of a monomer

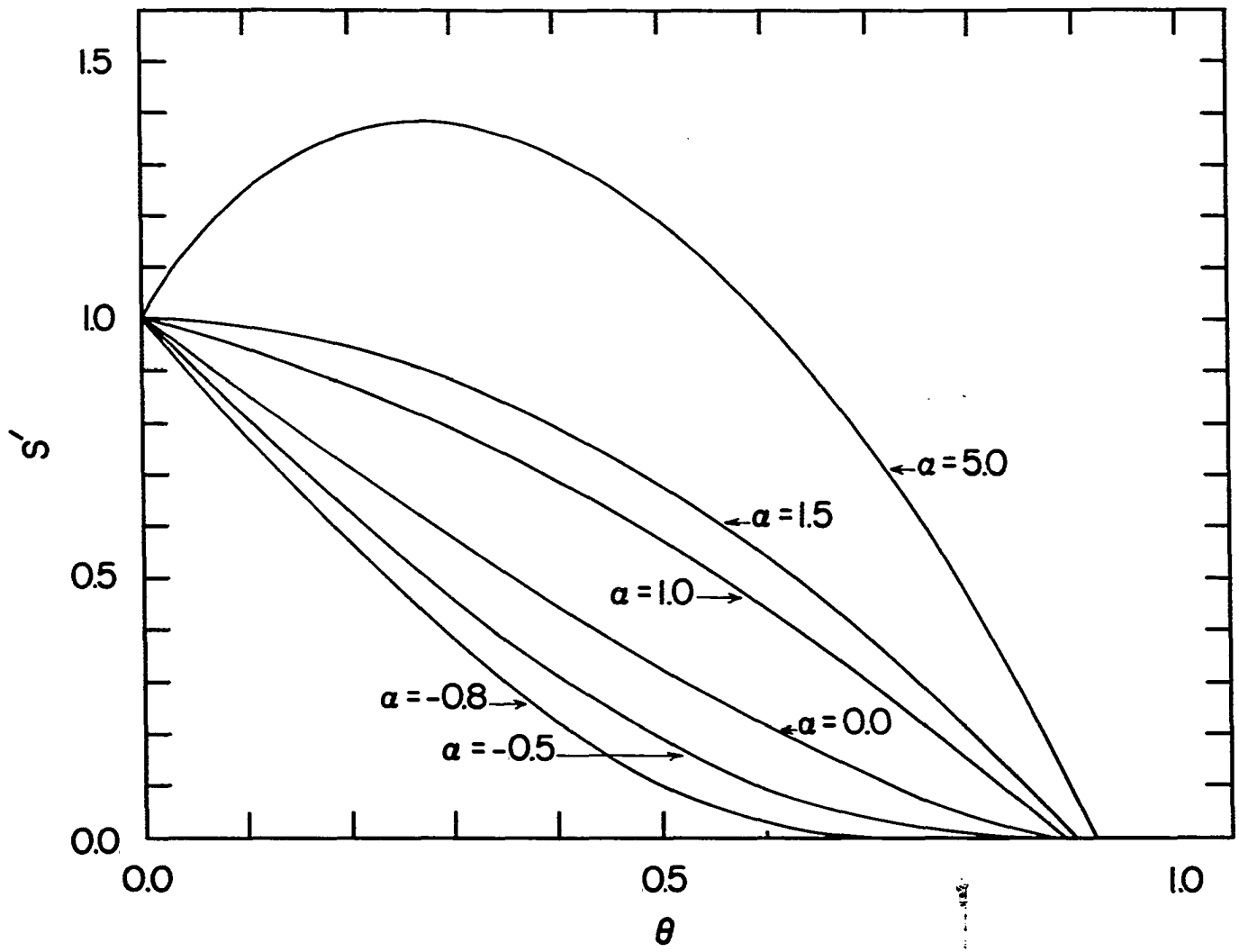

Figure 5.2. Theoretical sticking coefficient curves (S' vs θ) for the adsorption of a dimer

-0.5, 0.0, 1.0 and 5.0. These plots clearly show the differing effects of the attractive and repulsive interactions on the adsorption process. For values of $\alpha>0$, the activation energy is lowered at sites next to an adsorbed molecule, thereby increasing the tendency for molecules to stick. In fact, large positive values of α result in a normalized sticking coefficient that can be larger than one due to the strong attractive influence of previously adsorbed molecules. For $\alpha<0$, adsorbed molecules raise the adsorption activation energy on neighboring sites and therefore lower the probability that a molecule will stick. The point at which the sticking coefficient goes to zero is the saturation covering fraction for the lattice. These coverages are, of course, the same as those shown in Figs. 3.3 and 3.6 when $q_r=0$.

Three experimental sticking coefficient curves for dimer adsorption on various metal surfaces are illustrated in Fig. 5.3. These curves are, in general, typical of sticking coefficient curves reported in the literature and represent the adsorption of molecules exhibiting repulsive and attractive cooperative interactions. The sticking coefficient curve for O_2 on a Ag film (50) is characterized by the strongly negative initial slope and positive first derivative indicative of a strong repulsive interaction. The adsorption of cyanogen (C_2N_2) on Pt(110) (51), on the

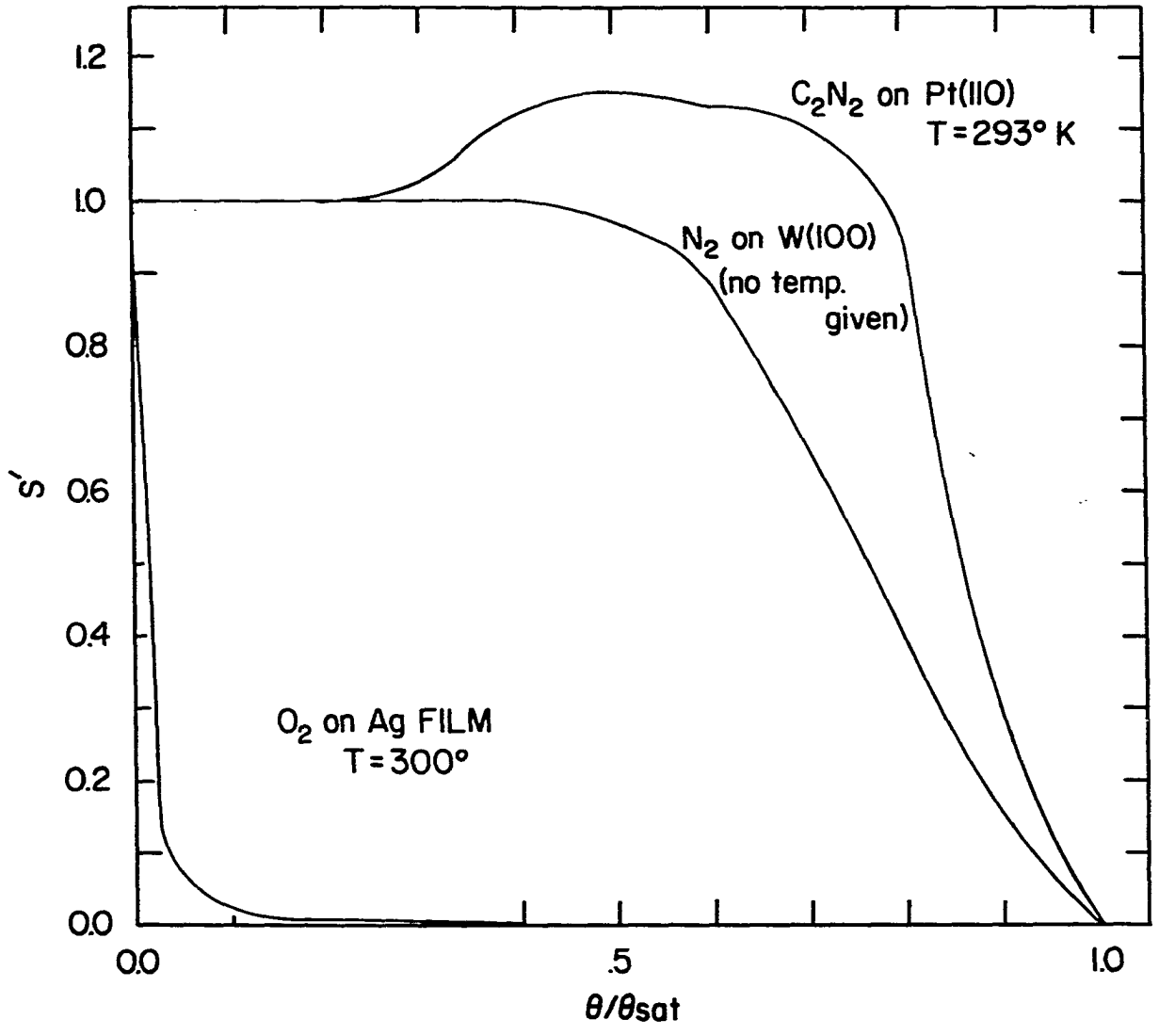

Figure 5.3. Three experimentally determined sticking coefficient curves for the comparison of theoretical and experimental results

other hand, gives a sticking coefficient curve that has a shape indicative of an attractive interaction. Cyanogen is, of course, not a simple diatomic molecule; however, it is a dimer and one of a few examples to exhibit a maximum in the sticking coefficient curve. The final curve illustrated in this figure describes the adsorption on N_2 on W(100) (52) and is characterized by a nearly zero initial slope and a sharp drop off near $\theta=0.5$. This extended flat region is not seen in the model curves of Figs. 5.1 and 5.2 even though it is possible to choose parameters such that initial slope is zero (see for example, Fig. 5.2, $\alpha = 1.5$). Clearly, this seemingly anomalous behavior is not directly described by our models. However, as we shall now see, a slight generalization of the kinetic models, which utilizes all the previously derived mathematical results, is adequate to explain this behavior.

As previously mentioned, adsorbed molecules can be in a physisorbed or a chemisorbed state. We assume that all molecules initially adsorb in the physisorbed state, and from this state they can chemisorb or desorb. In general, the rate of chemisorption now depends on the concentration of physisorbed molecules. Let ξ be the surface concentration of physisorbed molecules. This quantity is governed by the kinetic equation

$$\frac{d\xi}{dt} = k_1 P - k_2 \xi - k_3 \overset{(1)}{\frac{df(1)}{dt}} \qquad (5.6)$$

where P is the gas pressure. The rate constants k_1 and k_2 govern the adsorption and desorption processes, respectively, and $df^{(1)}/dt$ gives the rate at which the physisorbed state changes due to chemisorption. Presumably, the lattice undergoes relaxation after each chemisorption event (e.g., dissipation of a local excess of energy). If such relaxation is very rapid compared to the rate of chemisorption, then $df^{(1)}/dt$ should be just proportional to ξ, and we can write Eqn. 5.6 in the form

$$\frac{d\xi}{dt} = k_1 P - k_2 \xi - k_3 \xi S' \tag{5.7}$$

Here, k_3 is a rate constant serving the role of τ_{00} in our previous discussion, and S' is given by Eqn. 5.5. In this equation, $S'=S'(\theta)$ can be interpreted as the normalized sticking coefficient for a hypothetical process occurring at some fixed value of ξ. By the above argument, if relaxation following chemisorption is rapid, S' is independent of the chosen, fixed value of ξ. However, the value of ξ can change as a function of θ, and hence the true normalized sticking coefficient, S, is

$$S = \left(\frac{\xi(\theta)}{\xi(\theta=0)}\right) S' \ . \tag{5.8}$$

To find $\xi(\theta)$, it is necessary to solve Eqn. 5.7, which in turn requires knowing θ as a function of t. The kinetic equation governing θ is coupled to the kinetic equations for

other distributions of chemisorbed species, as indicated in Eqns. 3.31, 3.32,and 3.33. By the above discussion, we must now take the rate constants, τ_{ij}, occurring in these equations to be proportional to ξ. Since ξ changes as a function of time, the chemisorbed distributions will now have a different time dependence than in the previous case. However, since $dP^{(n)}(\underline{0})/d\theta$ is independent of ξ (i.e., the ξ dependence divides out), the chemisorbed distributions, as a function of covering fraction, are exactly the same as in the previous case. This should always be true as long as lattice relaxation following a chemisorption event occurs on a much shorter time scale than the rate of chemisorption itself.

We could solve Eqn. 5.7 numerically, using the known functional form of S' to evaluate the normalized sticking coefficient, S. However, for low gas pressures we can obtain an approximate solution to Eqn. 5.7 by invoking the steady state approximation. That is, if ξ is assumed to be small and approximately constant, then $\frac{d\xi}{dt} \simeq 0$, and we find that

$$\xi(\theta) = \frac{k_1 P}{(k_2+k_3 S')} , \tag{5.9}$$

or, by Eqn. 5.8

$$S = \frac{(1+y)S'}{1+yS'} . \tag{5.10}$$

Here, $y = k_3/k_2$ is the ratio of the rate of chemisorption to the rate of desorption. We wish to emphasize that the steady state approximation is not being invoked here for any

essential reason, but simply because it leads to a simple mathematical expression without altering the basic physics of the situation.

It should be noted from this expression that the rate determining step of the adsorption process determines the basic shape of the sticking coefficient curve. This is a specific example of the more general fact that the primary source of information in a kinetic process is the rate determining step. For example, at small values of y, chemisorption is the rate determining step and the shape of the sticking coefficient curves is dominated by the effects of the chemisorption process. In particular, in the limit as $y \to 0$, the sticking coefficient curves are completely determined by the chemisorption process and the results of our irreversible models are directly applicable. In the opposite limit, where $y \to \infty$, the physisorption step is rate determining and over most of the range of θ the sticking coefficient curves contain little or no information concerning the chemisorption step of the process. The sticking coefficient curves in this limit are flat and rather featureless. It is important to note that for any value of y, the lattice eventually fills and the effective rate of chemisorption decreases due to the lack of available surface vacancies. Ultimately, chemisorption is always the rate limiting step, and in this limit

$$S \to (1+y)S'. \qquad (5.11)$$

Thus, we can always gain information about the chemisorption process by studying the saturation region of the sticking coefficient curves.

Figure 5.4 shows examples of the modified sticking coefficient curves for noninteracting monomers in order to illustrate the effect of different values of y. As has been explained, the curves become flatter in the low density region as y increases, but they will ultimately saturate at the same value of θ. This is in general true since saturation occurs at the value of θ for which $P_{(0)}^{(r+1)} = 0$, where r+1 is the number of atoms in the molecule.

The quantity S also depends on the interaction between adsorbing molecules through the parametric dependence on α of S'. Figures 5.5 and 5.6 illustrate the influence of these interactions on the sticking coefficient for dimer adsorption on a linear lattice in the cases where y=10 and y=100. It is apparent from these curves that the primary influence of the interactions is in the region of high covering fraction where the probability of chemisorption is diminished due to the lack of surface vacancies. Near lattice saturation, curves for molecules with repulsive interactions are typically concave and reach saturation at a lower covering fraction than do noncooperative molecules. Slightly convex curves at saturation, with slopes more negative than for the

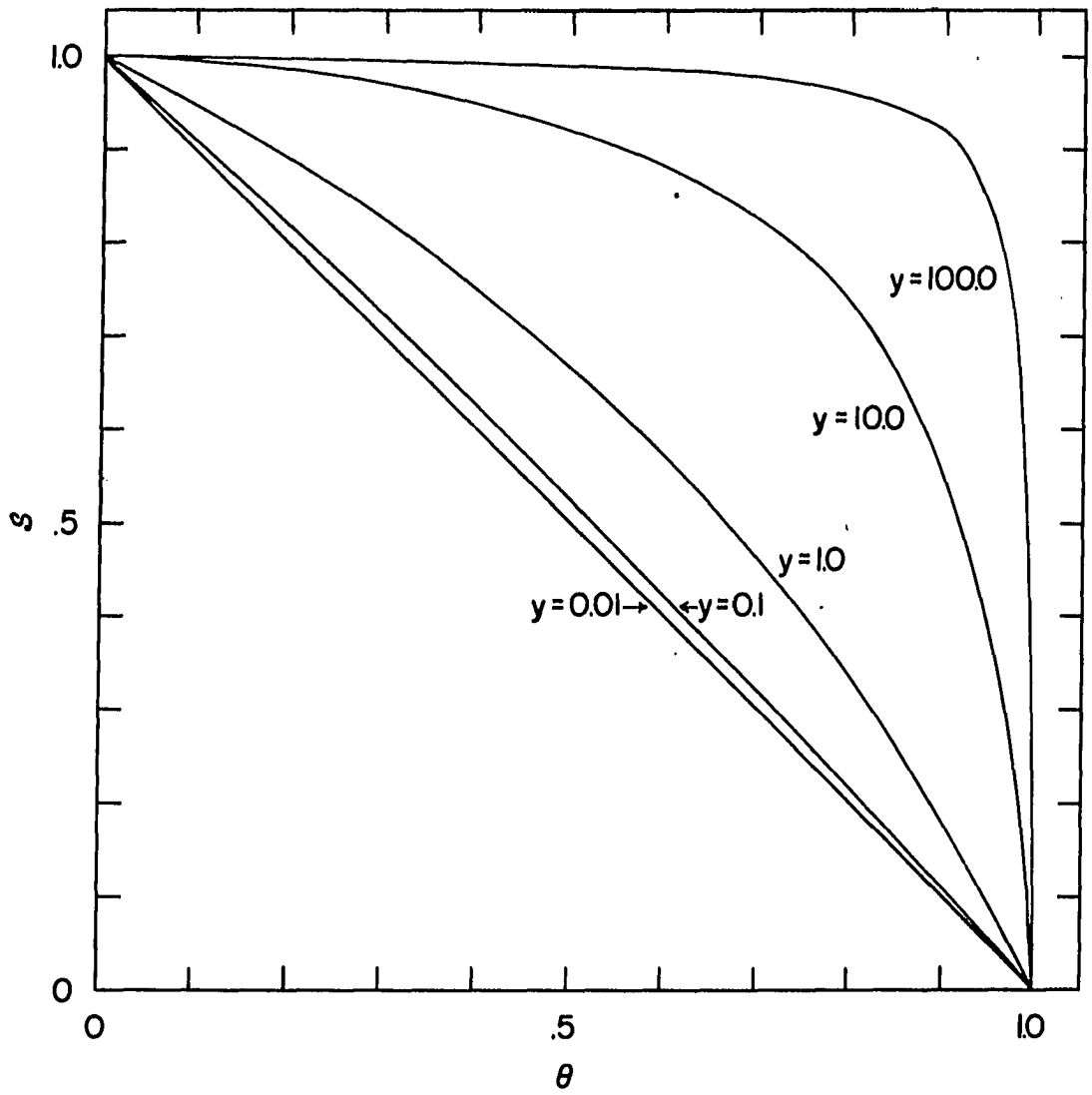

Figure 5.4. The sticking coefficient, S, for a two-step monomer adsorption mechanism, where there are no cooperative interactions between adsorbing molecules. Here, y is the ratio of the rate of desorption to the initial rate of chemisorption

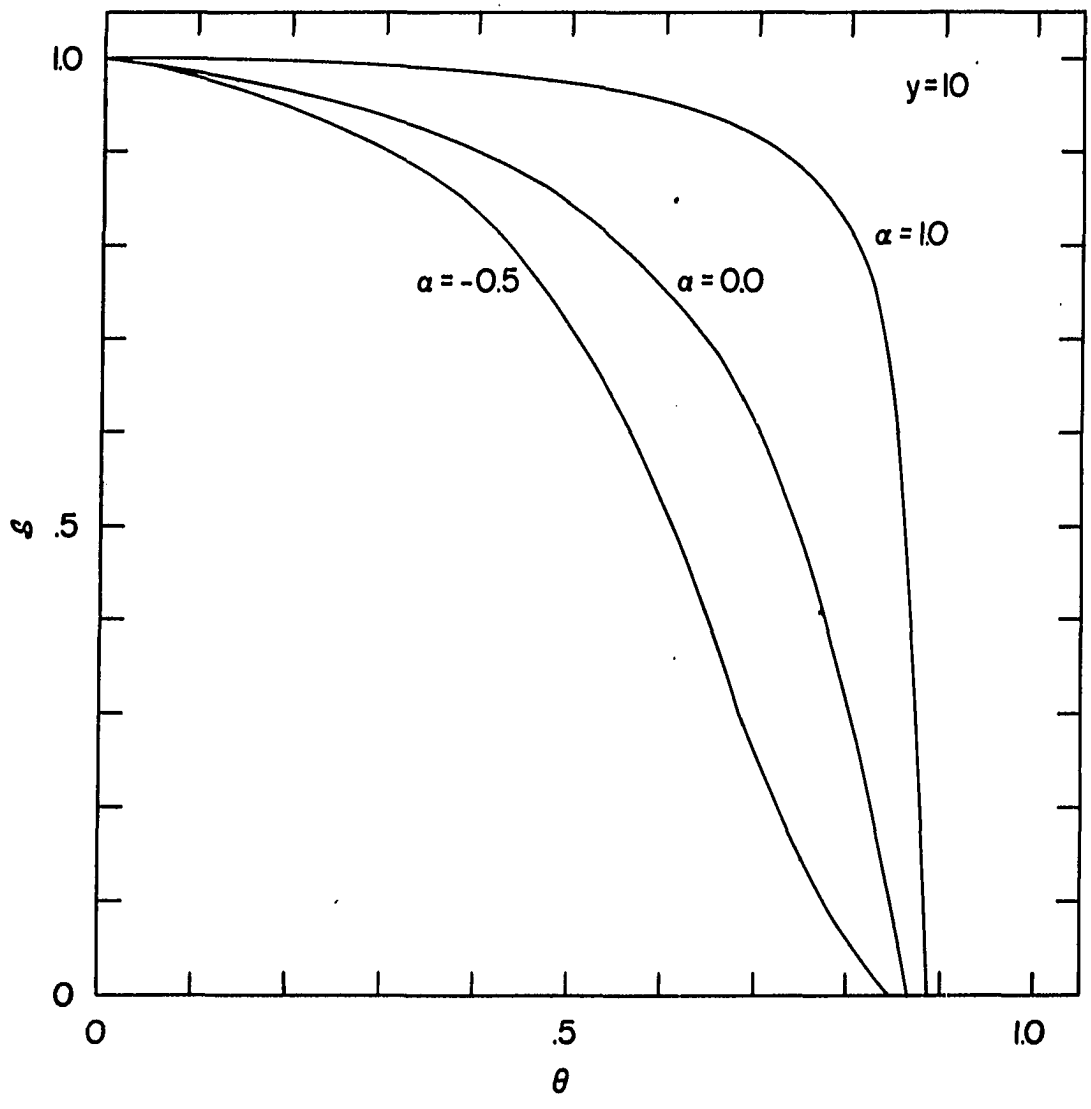

Figure 5.5. The sticking coefficient for a two-step dimer adsorption mechanism. In this figure, y=10

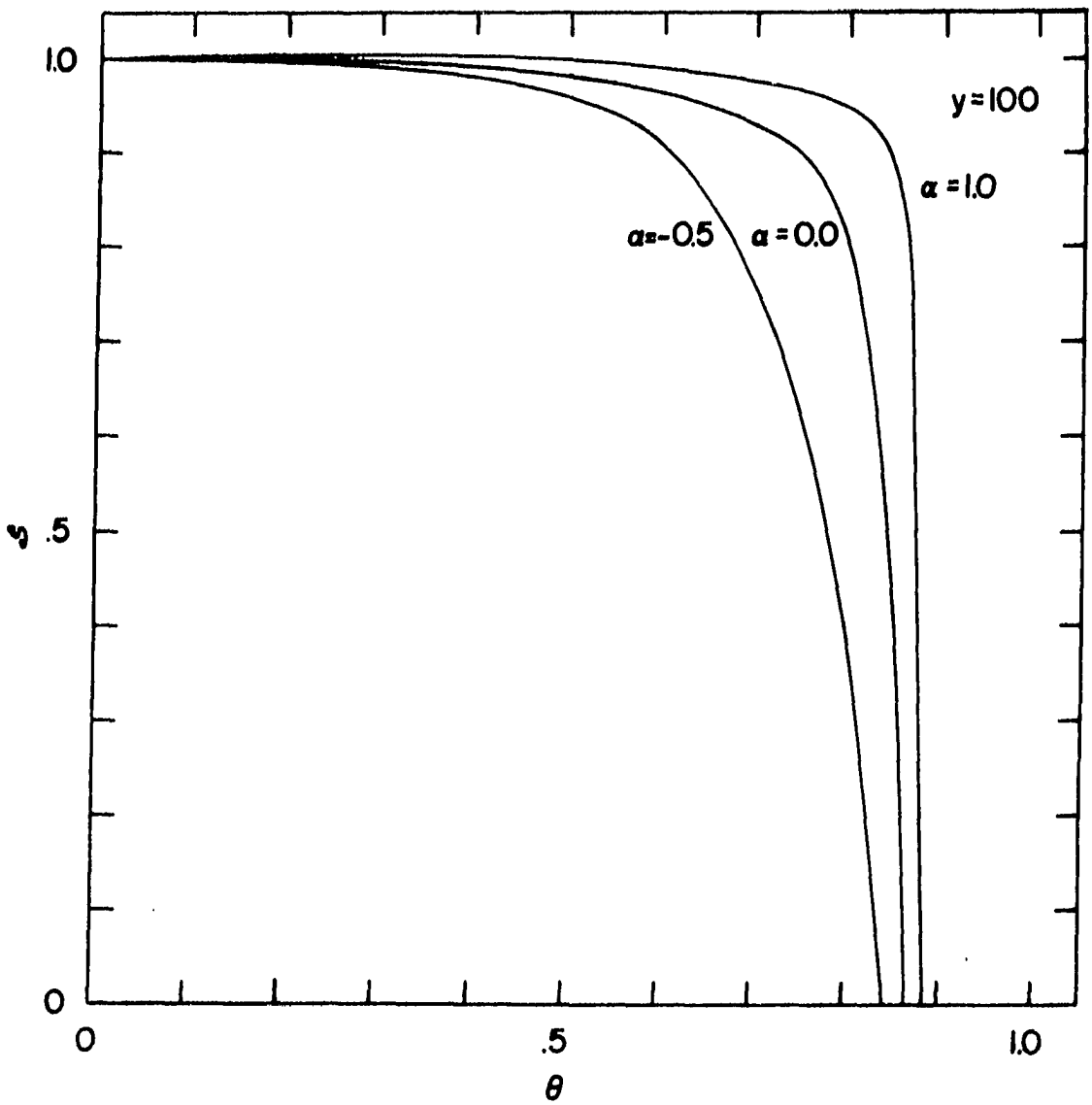

Figure 5.6. The sticking coefficient for a two-step dimer adsorption mechanism. Here, y=100

noncooperative case, characterize the sticking coefficient for molecules with attractive interactions.

In comparing the results of the above analysis with the experimental sticking coefficient curve for the adsorption of N_2 on W(100), we quickly conclude from the general shape of the curve that the adsorption proceeds through a mobile precursor state which has a lifetime that is long campared to the rate of chemisorption. We also conclude from the shape of the curve near saturation that adsorbed nitrogen molecules have a repulsive influence on the rate of chemisorption at neighboring surface vacancies. These conclusions are supported by the findings of other workers (53,54).

We note that our models reproduce the general features of the experimental curves, however certain of their structural features (e.g., the peculiar hump in the cyanogen curve) do not lie within the range of model predictions produced by parameter variations. First, it must be remembered that we are comparing the results of a one-dimensional model with data from a basically two-dimensional system. In some cases, most notably the adsorption onto the troughs of crystal faces with very open geometry (18) or preferential adsorption along terraces in a crystal face (48), the one-dimensional models are perhaps appropriate. However, in other systems this comparison could result in quantitative (but probably not qualitative) deviations.

Secondly, it is, of course, not possible to perform an experiment with theoretical precision. Errors due to surface heterogeneities and lack of cleanliness, inaccuracies in measurements, and several other factors contribute to the imprecision in experimental results.

Since noble gases do not chemisorb at ordinary temperatures, there is little experimental data to compare against our predictions for monatomic adsorption. However, at very low temperatures ($\sim$10°K) these gases physisorb with sufficiently long residence times (55) that the adsorption can be considered irreversible and can be described reasonably well by a sticking coefficient. Since the interactions associated with physisorption are weak, we would expect these systems to have small α values.

Sticking Coefficient Density Expansions on the Infinite Lattice

The density expansions of the distribution functions, given in Chapter 3 can be substituted into Eqn. 5.5 to obtain truncated expansion approximations of the form

$$S' = 1 + B\theta + C\theta^2 + D\theta^3 + \ldots \qquad (5.12)$$

for the sticking coefficient. These expansions, parametrized on α, are written below for monomers and dimers:

$$S'_{\text{monomer}} = 1 - (1-2\alpha)\theta-(2\alpha+\alpha^2)\theta^2+\tfrac{1}{3}(5\alpha^2+2\alpha^3-\alpha^4)\theta^3 + \tfrac{1}{12}(-4\alpha^2-24\alpha^3+5\alpha^4+18\alpha^5+\alpha^6)\theta^4 + \ldots , \quad (5.13)$$

and

$$S'_{\text{dimer}} = 1 - (3-2\alpha)(\tfrac{\theta}{2})+(1-3\alpha-\alpha^2)(\tfrac{\theta}{2})^2 + \tfrac{1}{3}(2-6\alpha+5\alpha^2+2\alpha^3-\alpha^4)(\tfrac{\theta}{2})^3 + \tfrac{1}{12}(8-24\alpha+30\alpha^2-24\alpha^3-3\alpha^4+18\alpha^5+\alpha^6)(\tfrac{\theta}{2})^4 + \ldots . \quad (5.14)$$

In Fig. 5.7, expansions of S'_{monomer} through quartic density terms (i.e., Eqn. 5.13), for α values of -0.8, -0.5, 1.0 and 5.0 are plotted. Comparison with Fig. 5.1 illustrates the valid range of these density expansions. As expected from the results of Chapter 3, the truncated expansion is best at low densities and for small values of α.

At low molecular densities the sticking coefficient varies linearly with the covering fraction, and hence by comparing the coefficient of the linear term in Eqn. 5.14 with the initial slope of the experimental curves, we can obtain an estimate of α. Furthermore, if we have experimental data as a function of temperature, we can estimate the activation energy. The value of α and its temperature dependence determined in this way is, at best, a crude estimate due to the lack of reliability of the experimental data at low densities.

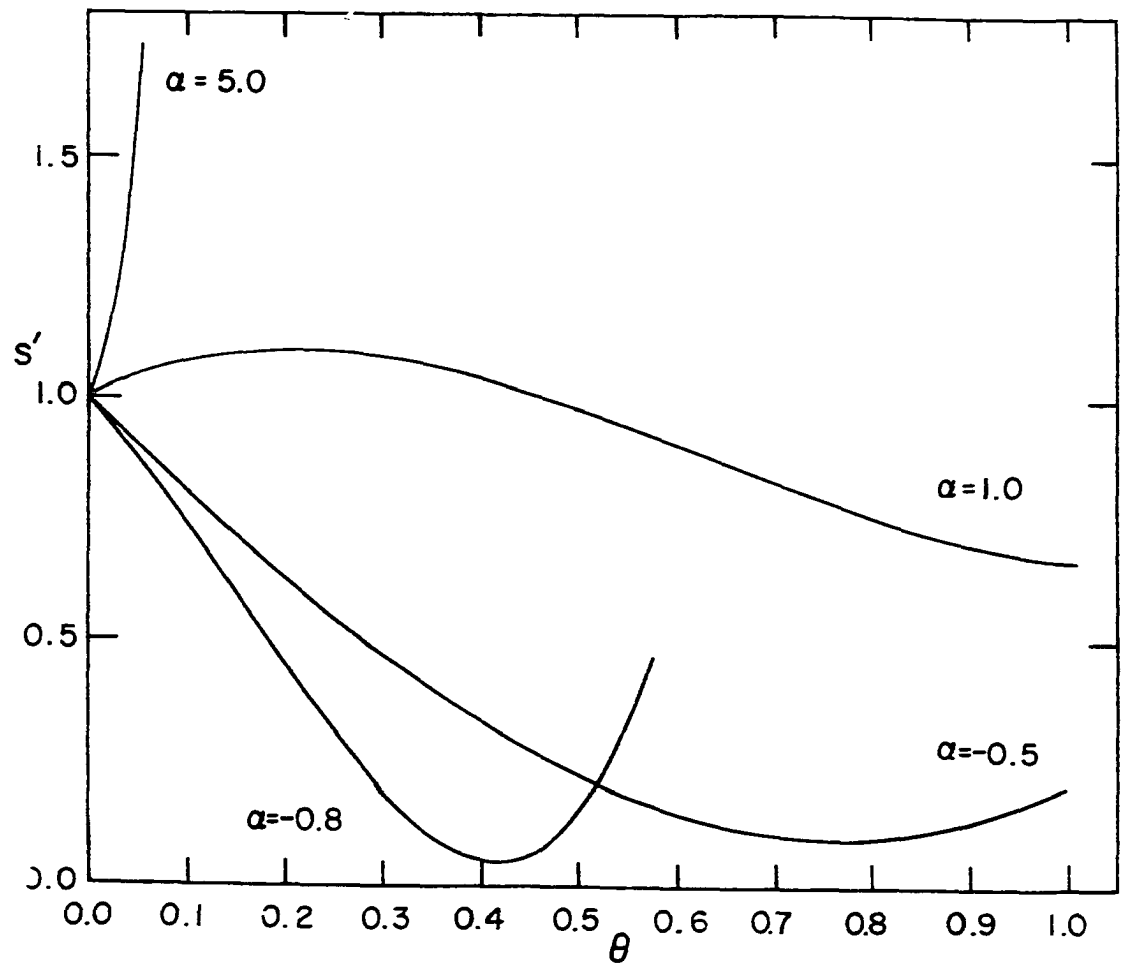

Figure 5.7. Four term density expansions of the sticking coefficient S' for the adsorption of a monomer with lst n.n. cooperative interactions

Of course, if desorption competes with chemisorption, we should use the sticking coefficient of Eqn. 5.10. By expanding S in the density, we find that

$$S = 1 + (\frac{1}{1+y})B\theta + \ldots , \qquad (5.15)$$

where B is the coefficient of the linear term in the density expansion of Eqn. 5.12.

As described in Chapter 3, density expansions of the probability distribution functions (and hence the sticking coefficient) can be obtained by the virial expansion method. Since this method can be applied to a lattice of arbitrary dimensionality, we can write an exact density expansion for a two-dimensional lattice of any desired geometry, and use the above procedure to determine α. Since adsorption is basically a two-dimensional phenomenon, this is presumably the appropriate way to determine α. However, the approximation in one-dimension obtained from Eqn. 5.14 is still of interest for comparative purposes. For the case where the atomic sites are arranged in a square lattice, the virial expansion method gives that (25) B in Eqn. 5.12 is given by

$$B = \frac{1}{4}(18\alpha-7). \qquad (5.16)$$

We now examine an experimental situation for which we make use of this result.

Engelhardt and Menzel (56) have studied the temperature dependence of the chemisorption of O_2 on Ag(110) (which is one of a very few studies of this type). The (110) face of Ag has a rectangular unit cell, and we assume that the active adsorption sites have the same symmetry. For simplicity, we approximate the rectangular lattice by a square lattice in order to utilize Eqn. 5.16. On substituting the interaction parameter $\alpha = \exp\{\frac{-(\phi_1-\phi_0)}{kT}\} - 1$ into Eqn. 5.16, we find that B is given by

$$B = \frac{1}{4}(-25+18\exp\{\frac{-(\phi_1-\phi_0)}{kT}\}). \qquad (5.17)$$

The activation energy difference $(\phi_1-\phi_0)$ (i.e., the difference in the activation energy to the transition of a site with and without the 2nd n.n. site being occupied) is assumed to be temperature independent, and hence the temperature dependence of B is determined by the factor of 1/T in the argument of the exponent. The activation energy difference is easily calculated from the slope of the experimental curves.

In Fig. 5.8, the temperature dependence of B is compared to the variation in initial slope of the experimental sticking coefficient curves. The value of the activation energy difference used in the model calculations is $(\phi_1-\phi_0) = 0.326$ kcal/mole, which is the activation energy

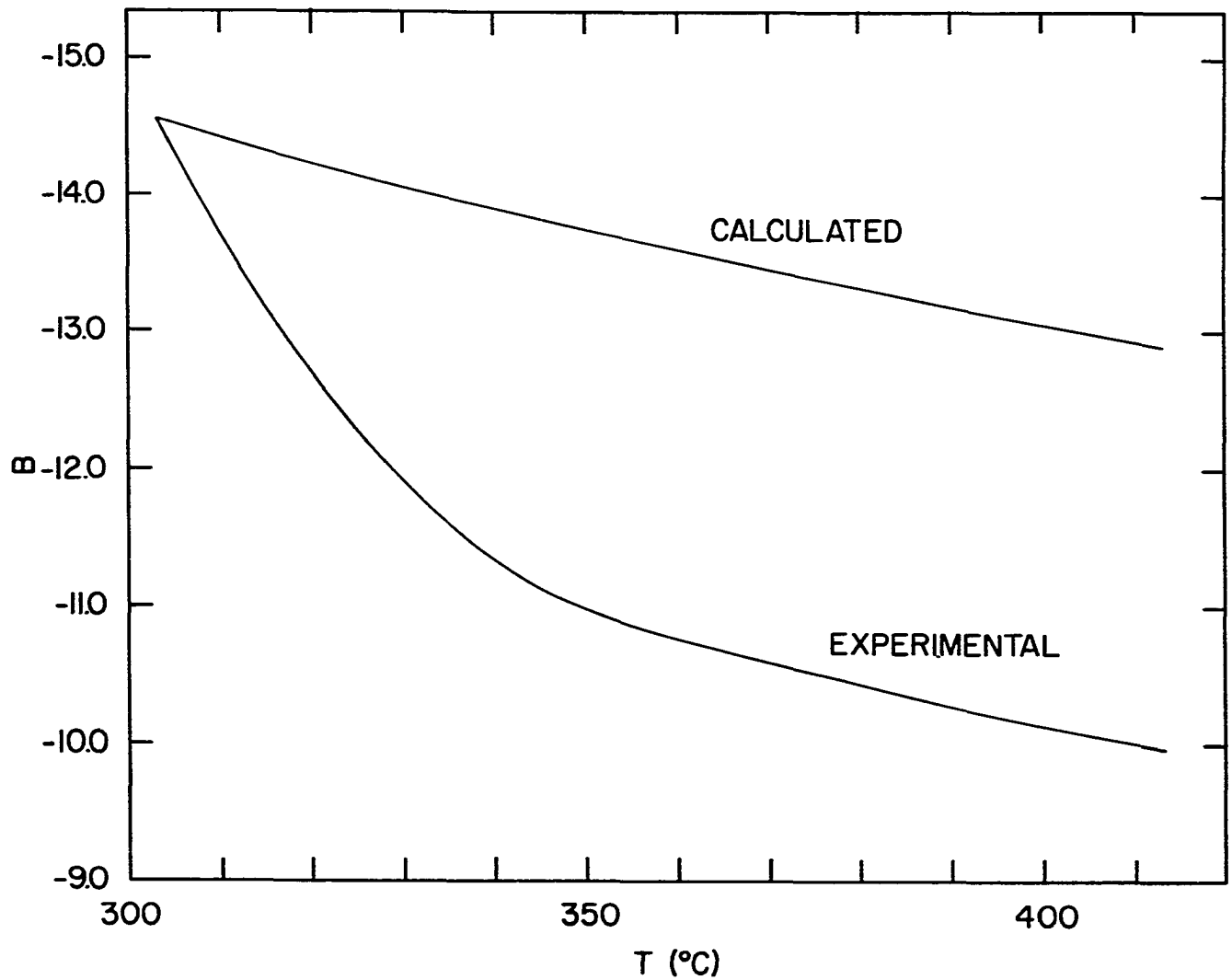

Figure 5.8. A comparison of the theoretical (S') and experimentally determined temperature dependence of the initial (low density) slopes of the sticking coefficient curves for O_2 on Ag(110) (56)

difference for which the theory and experiment agree at $T = 303°C$. It is seen in this figure that the general trends in the variation in experimental slopes with temperature are predicted by the model, but it falls short of accurately representing the temperature dependence. There are at least two possible explanations for the discrepancy. First, the activation energy difference could be temperature dependent. Such a dependence could possibly arise if the mechanism by which the interactions are transmitted through the lattice is temperature dependent. For example, the chemisorption of a molecule might affect the activation energy by altering the local electron density, where this density, itself, is temperature dependent. Second, the temperature variation could also appear if the rate of desorption competes with the rate of chemisorption. In such a case, we should use Eqn. 5.15 to describe the sticking coefficient, and the difference between experiment and theory in Fig. 5.8 can then be ascribed to the temperature dependence of the factor of $1/(1+y)$. Figure 5.9 shows the temperature variation in y for this latter case, assuming that the first case above does not contribute. If we can assume that this curve has some physical content (i.e., if the observed variation in y is not totally due to experimental error in the measurement in the low density sticking coefficient), then we note that the sharp change in the slope of y near $T = 350°C$ indicates a

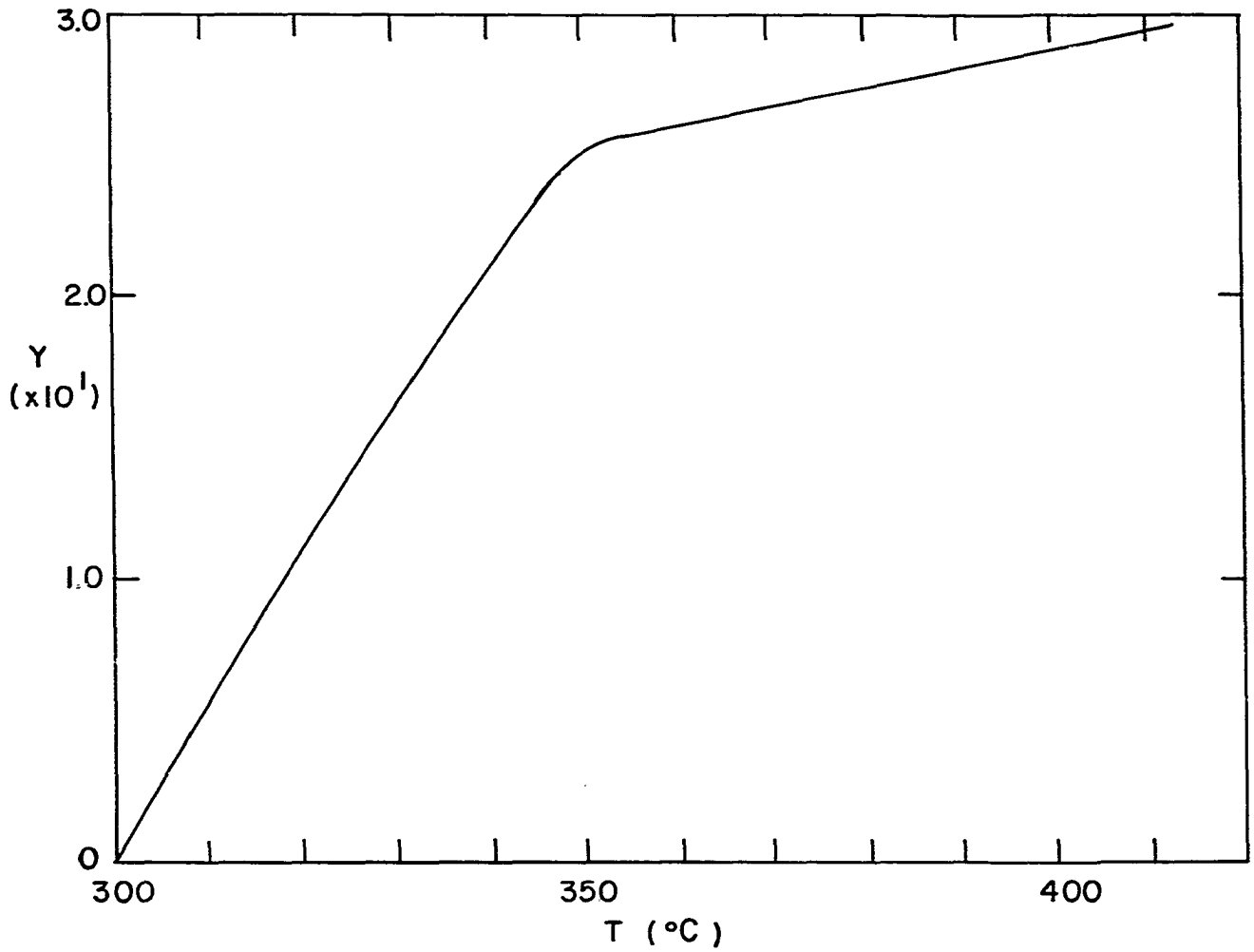

Figure 5.9. The temperature dependence of y as determined from Fig. 5.8

change in the difference between the activation energies for the chemisorption and desorption steps, and hence a change in the adsorption mechanism. Such a mechanistic change could possibly be attributed to a change in the active site for chemisorption or other changes in the chemisorbed state.

We now comment on the effects of the dimensionality of the model on B. From Eqns. 5.14 and 5.16, we see that these limiting slopes for dimers derived from the one- and two-dimensional models are $B_1 = \frac{1}{2}(-3+2\alpha)$ and $B_2 = \frac{1}{4}(-7+18\alpha)$. It is readily apparent that the dimensionality has a quantitative, but not qualitative effect. In the special case of $\alpha=0$ (the Langmuir model), the slopes are nearly the same, i.e., $B_1 = -3/2$ and $B_2 = -7/4$, while in the limit as $\alpha \to -1$ (the infinitely repulsive interaction), the slopes are $B_1 = -5/2$ and $B_2 = -25/4$. The difference in the two slopes can be directly attributed to the increased surface coordination number (i.e., the number of nearest neighbors) of a site on the two-dimensional lattice, as compared to the one-dimensional lattice. The adsorption of a dimer onto the square lattice blocks a larger number of nearest neighbor sites from occupation than on the linear lattice. This gives rise to the slightly larger negative slope of the non-cooperative case. Since the ratio of the number of 2nd n.n. sites on the two-dimensional lattice to that of the one-dimensional lattice is substantially larger than a similar

ratio for 1st n.n. sites, the effect of dimensionality on the α dependence is even more marked. The qualitative similarity of the form of the two initial slopes is due to the assumption of pairwise additivity of the activation energies.

Nucleation Effects on the Sticking Coefficient

It is possible to study the effects on the sticking coefficient of nucleating adsorption on the lattice. The simplest means of doing so is to randomly seed the infinite lattice with adsorbed molecules and determine the sticking coefficient based on this initial lattice state. We can accomplish this by changing the boundary conditions which the kinetic equations must satisfy; that is, we set $q_j=\mu$ at $t=0$, for all j, where $0<\mu<1$. It is then possible to truncate the kinetic hierarchy as in Chapters 2 and 3, and solve for the sticking coeffficient. For example, if we wish to randomly nucleate 0.1% of the sites, then we require that the boundary condition $q_j = 0.999$ at $t=0$, for all j, be satisfied. This is formally equivalent to allowing the adsorption process to begin with all cooperative interactions turned off, and then turning on the interactions when the required atomic density is reached. With this method, however, we are not allowed the freedom of independently varying the interactions of the nucleated sites (i.e., in this case, the influence of <u>all</u> adsorbed molecules

is governed by α). The results obtained in this comparatively simple manner are not qualitatively different from the results we will obtain when we independently vary the influence of the nucleating sites. Therefore, having duly discussed this method, we proceed to the more general case.

We can also model nucleation effects where the end sites are the nucleating sites. To this end, we can define the average sticking coefficient in an ensemble of lattices of finite length as

$$S' = N \sum_{n=0}^{\infty} r_{n+1} \sum_{j=0}^{\infty} \frac{dP^{(1)}_{\{j+1\},n}(0)}{dt} , \qquad (5.18)$$

where $dP^{(1)}_{\{j\},n}(0)/dt$ is the sticking coefficient of site j on a lattice of length n, r_n is the probability distribution of a lattice of length n in the ensemble, and N is the appropriate constant to normalize the sticking coefficient to one at t=0. The singlet vacancy distributions, $P^{(1)}_{\{j\},n}(0)$, required in Eqn. 5.18 are for the finite lattice with n sites. However, for computational simplicity, we assume that end effects are of sufficiently short range that a given site is at most influenced by the closest end site. This means we can use probabilities on the semi-infinite lattice is our calculations. Substituting the singlet vacancy distributions on the semi-infinite lattice (i.e., Eqns. 4.5, 4.33 and 4.34), which are not a function of n,

into Eqn. 5.18 allows us to write S' in the form

$$S' = N \sum_{j=0}^{\infty} \frac{dP_{j+1}^{(1)}(0)}{dt} \sum_{n=r}^{\infty} r_{n+1}, \tag{5.19}$$

which is the starting point of our analysis.

The similarity of this equation to the transforms of Chapter 4 is evident and can be exploited to directly utilize the transform functions in the solution of S'. To do this we first split S' into two infinite sums in the following manner:

$$S' = N \sum_{j=0}^{\infty} \frac{dP_{j+1}^{(1)}(0)}{dt} \sum_{m=0}^{\infty} \sum_{n=m}^{\infty} r_{n+1} \delta_{j,m} \tag{5.20}$$

where $\delta_{j,m}$ is the kroneker delta. From the theory of complex variables $\delta_{j,m}$ has the well-known integral form

$$\delta_{j,m} = \frac{1}{2\pi i} \int_C \frac{d\zeta}{\zeta} \zeta^{j-m}, \tag{5.21}$$

where C is a circular contour around the origin with radius $r<1$. Substituting this result into Eqn. 5.20, we obtain

$$S' = \frac{N}{2\pi i} \int_C \frac{d\zeta}{\zeta} \left\{ \sum_{j=0}^{\infty} \zeta^j \frac{dP_{j+1}^{(1)}(0)}{dt} \sum_{m=0}^{\infty} \zeta^{-m} \sum_{n=m}^{\infty} r_{n+1} \right\}. \tag{5.22}$$

Thus, the sticking coefficient can be written in the form

$$S' = \frac{N}{2\pi i} \int_C \frac{d\zeta}{\zeta} \frac{d\psi(\zeta, q_2)}{dt} \omega(\zeta, \lambda), \tag{5.23}$$

where

$$\psi(\zeta,q_2) = \sum_{j=0}^{\infty} \zeta^j \, P_{j+1}^{(1)}(0), \tag{5.24}$$

and

$$\omega(\zeta,\lambda) = \sum_{m=0}^{\infty} \zeta^j \sum_{n=m}^{\infty} r_{n+1}. \tag{5.25}$$

Here, $\omega(\zeta,\lambda)$ has been written as an explicit function of lattice length λ. In terms of the transforms defined in Chapter 4

$$\psi(\zeta,q_2) = Z(\zeta,q_2) + P_1^{(1)}(0). \tag{5.26}$$

To complete the derivation, we need only to specify the form of r_n, the ensemble probability distribution of lattice lengths, and obtain its transform, $\omega(\zeta,\lambda)$. In the absence of any a priori reason to expect that one lattice length is to be favored over another in the ensemble, we assume the lattice lengths are randomly distributed about some mean. Since the number of lattices in the ensemble is very large and the probability for any particular lattice length is small, the appropriate distribution of lattice lengths in the ensemble is the Poisson distribution

$$r_n = \frac{\lambda^n \, e^{-\lambda}}{n!} \tag{5.27}$$

where, again, λ is the average lattice length. Substituting this distribution into Eqn. 5.25, we obtain

$$\omega(\zeta,\lambda) = \sum_{m=0}^{\infty} \zeta^{-m} \sum_{n=m}^{\infty} e^{-\lambda} \frac{\lambda^{n+1}}{(n+1)!} . \qquad (5.28)$$

After interchanging summations and performing some simple algebra, we obtain

$$\omega(\zeta,\lambda) = \frac{\zeta}{1-\zeta} \{e^{\lambda/\zeta-\lambda} - 1\}, \qquad (5.29)$$

and hence Eqn. 5.23 can now be written as

$$S' = \frac{N}{2\pi i} \int_C \frac{d\zeta}{\zeta} \frac{d}{dt} \left(Z(\zeta,q_2) + P_1^{(1)}(0)\right) \frac{\zeta}{1-\zeta} e^{\lambda/\zeta-\lambda}. \qquad (5.30)$$

The term $-\zeta/1-\zeta$ of $\omega(\zeta,\lambda)$ does not contribute to this equation since it does not contain a pole inside the contour C. Further substitution of the explicit form for the derivatives of $Z(\zeta,q_2)$ and $P_1^{(1)}(0)$ from Eqns. 4.31 and 4.3 into Eqn. 5.30 yields the following expression for the sticking coefficient as a function of q_2:

$$S' = \frac{N}{2\pi i} \int_C \frac{d\zeta}{\zeta} \frac{\zeta}{(1-\zeta)} e^{\lambda/\zeta-\lambda} \Bigg[\rho_{11} \Bigg\{ \zeta q_2^{\rho_{11}} \int_1^{q_2} dq' e^{\gamma(q'-1)} \times q'^{(\rho_{01}+\eta_0-\rho_{11}-1)} \left((\rho_{01}-\rho_{11})+(1-2\rho_{01}+\rho_{11})q'\right) + q_2^{\rho_{11}} \int_1^{q_2} dq' \, e^{\gamma(q'-1)} q'^{(2\rho_{01}-\rho_{11}-1)}$$

$$\times \left((1+\zeta)(\rho_{01}-\rho_{11}) + \zeta(1-2\rho_{01}+\rho_{11})q'\right)e^{\gamma\zeta(q'-1)}$$

$$\times \left\{\gamma\zeta \int_1^{q'} dq''\, e^{-\gamma\zeta(q''-1)}q''^{\delta} + \frac{\zeta}{1-\zeta}\right\} + q_2^{\rho_{11}}\frac{\zeta}{1-\zeta}\Bigg\}$$

$$+ e^{\gamma(q_2-1)}q_2^{2\rho_{01}}\left((1+\zeta)(\rho_{01}-\rho_{11})\right.$$

$$\left. + \zeta(1-2\rho_{01}-\rho_{11})q_2\right)e^{\gamma\zeta(q_2-1)}\left\{\gamma\zeta \int_1^{q_2} dq'\, e^{-\gamma\zeta(q'-1)}\right.$$

$$\left.\times q'^{\delta} + \frac{\zeta}{1-\zeta}\right\} + \zeta\, q_2^{(\rho_{01}+\eta_0)}e^{\gamma(q_2-1)}\left((\rho_{01}-\rho_{11})\right.$$

$$\left. + (1-2\rho_{01}+\rho_{11})q_2\right) + (\eta_0-\eta_1)q_2^{(\rho_{01}+\eta_0)}e^{\gamma(q_2-1)}$$

$$+ \eta_1 q_2^{\eta_1}\left\{(\eta_0-\eta_1)\int_1^{q_2} dq'\, q'^{(\rho_{01}+\eta_0-\eta_1-1)}\right.$$

$$\left.\times e^{\gamma(q'-1)} + 1\right\}\Bigg]. \qquad (5.31)$$

Some of the complex integrals of this expression can be directly evaluated by residue theory; we evaluate the remaining complex integrals using a modified form of the method of steepest descents (57). The circumstances requiring the modification are sufficiently unusual that they merit a brief discussion.

In a typical application, the method of steepest descents is used to evaluate the asymptotic (large λ) behavior of complex integrals of the form

$$I = \int_C dz\ e^{\lambda f(z)}\ g(z), \tag{5.32}$$

The idea is to pick an appropriate contour passing through, z_0, the saddle point of f(z). If this is done, the major contribution to the integral comes from the part of the contour in the neighborhood of z_0. For large λ, the exponential function $e^{\lambda f(z)}$ is effectively a sharply peaked Gaussian along the contour near the saddle point and hence the integral can be approximated by

$$I \approx \frac{g(z_0)e^{\lambda f(z_0)}}{|\lambda f''(z_0)|^{1/2}} \int_{-\infty}^{\infty} dt\ e^{-t^2/2}. \tag{5.33}$$

In Eqn. 5.31, however, the complex integrals have the general form

$$I = \frac{e^{-\lambda}}{2\pi i} \int_C d\zeta\ \frac{e^{\lambda/\zeta}\ \zeta^j\ e^{\kappa\zeta}}{(1-\zeta)^{\ell}}\ , \tag{5.34}$$

for which the argument of the dominating exponential term, $f(\zeta) = 1/\zeta$, has no saddle point. It is therefore advantageous to write the entire integrand as the argument of an exponent to formally create a saddle point at which the steepest descent method can be applied. The integrand,

which we denote by $\exp[g(\lambda,\zeta)]$, then has the form

$$\exp[g(\lambda,\zeta)] = \exp\{\lambda/\zeta + j\ \ell n\ \zeta - \ell\ \ell n(1-\zeta) + \kappa\zeta\}. \tag{5.35}$$

Expanding the integrand in a Taylor series about the saddle point, $\zeta_0(\kappa)$, we obtain

$$I = \frac{e^{\lambda/\zeta_0(\kappa) - \lambda}\ \zeta_0(\kappa)^j\ e^{\kappa\zeta_0(\kappa)}}{(1 - \zeta_0(\kappa))^\ell\ 2\pi} \int_C d\zeta\ \exp\left\{\sum_{n=2}^{\infty} \frac{g^{(n)}(\lambda,\zeta_0(\kappa))}{n!} \left(\zeta-\zeta_0(\kappa)\right)^n\right\}, \tag{5.36}$$

where $g^{(n)}$ is the nth derivative of g with respect to ζ. For future use, we have explicitly indicated the κ dependence of $\zeta_0(\kappa)$. However, this integrand is not a Gaussian along the contour at the saddle point because all factors in the exponent are not scaled by λ. The integrand is sharply peaked at large λ, but it is always skewed from a Gaussian function. In other words, more terms of the Taylor expansion of the argument of the exponent must be retained to provide an accurate representation of the integral. To evaluate the integral retaining several terms of the Taylor series in the exponent is a problem comparable in difficulty to the evaluation of the original integral. For this reason, we approximate the integral in the following manner: The examination

of Eqn. 5.15 reveals that for large λ, the saddle point is basically determined by the terms λ/ζ and $\ell\ \ell n(1-\zeta)$ and hence there is only a weak dependence of $\zeta_0(\kappa)$ on κ. It is therefore convenient to examine the integral $I(\kappa=0)$, which from Eqn. 5.34, has the form

$$I(\kappa=0) = \frac{e^{-\lambda}}{2\pi i}\int_C d\zeta\ \frac{e^{\lambda/\zeta}\ \zeta^j}{(1-\zeta)^{\ell}}\ . \tag{5.37}$$

This integral can be exactly evaluated in closed form by residue theory to yield

$$I(\kappa=0)=(\lambda-j)^{\ell-1}. \tag{5.38}$$

Since the integrand of Eqn. 5.34 is sharply peaked at a point that is only weakly affected by $e^{\kappa\zeta}$, this factor is effectively constant on the portion of the contour near the saddle point. Thus, we can write

$$I \approx e^{\kappa\zeta_0(\kappa=0)}\ I(\kappa=0) = (\lambda-j)^{\ell}\ e^{\kappa\zeta_0(\kappa=0)}\ . \tag{5.39}$$

This result can be used to evaluate the complex integrals of Eqn. 5.31 that cannot be readily evaluated in closed form by residue theory. The real integrals of Eqn. 5.31 can be numerically integrated with a twenty point Gauss-Legendre integration scheme as used in previous calculations.

Figure 5.10 shows the results of the evaluation of Eqn. 5.31 as described above, where λ and η_0 have the values

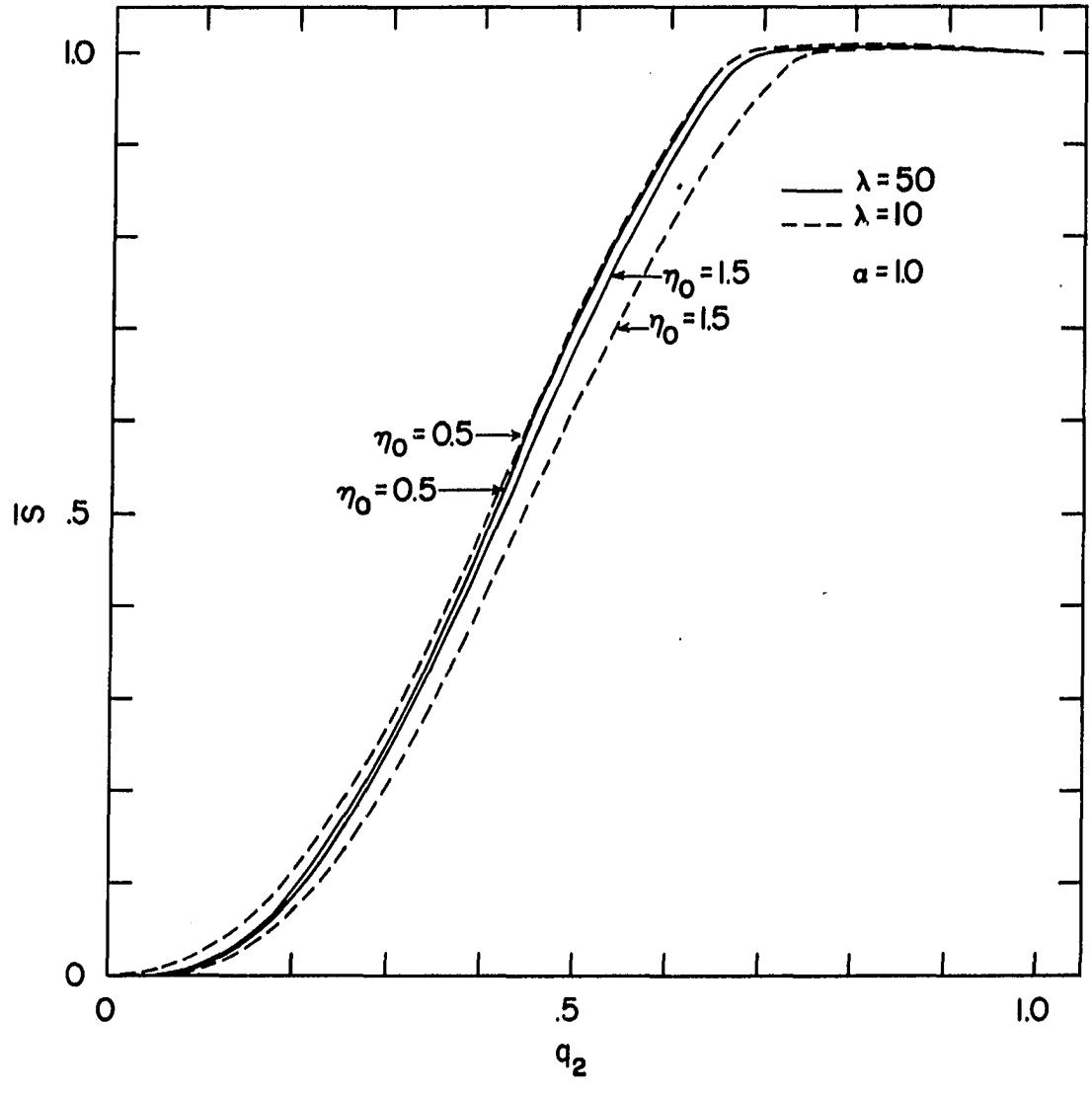

Figure 5.10. The influence of the lattice length and the transition probability of the end site of a finite lattice on the sticking coefficient

λ=10 and 50, and η_0=0.5 and 2.0. The value of α used in these calculations is α=1.0. In this figure $q_2 = e^{-\tau_{00}t}$ is the independent variable, and since q_2 is basically a time variable, this figure reflects the time evolution of the sticking coefficient. The function S' can also be easily obtained as a function of the average singlet vacancy distribution, $\bar{P}^{(1)}(0)$, (and hence the average covering fraction, $\bar{\theta}$, since $\bar{\theta} = 1 - \bar{P}^{(1)}(0)$) by numerically integrating the curves of this figure to obtain $\bar{P}^{(1)}(0)$ as a function of q_2. We note a marked dependence of the sticking coefficient on the lattice length, λ. This dependence is directly related to the fraction of sites of the lattice that are influenced by the transition rate η_0. For long lattices, the fraction of sites influenced by the end site is smaller than that for short lattices and hence the effect of η_0 on the sticking coefficient is less for the former. For example, if the range of influence of the end site for a particular value of η_0 and α is two sites, then for a fifty site lattice 4/50 or 8% of the sites are influenced by the value of η_0. This compares to the fact that 4/10 or 40% of a ten site lattice would be influenced under the same circumstances. As shown in Chapter 4, the range of the influence of the end site is primarily determined by the value of α and the magnitude of the influence is due to η_0.

CHAPTER 6. OTHER APPLICATIONS

The objective of this Chapter is to bring together and briefly discuss a number of examples illustrating the range of possible applications of our models to various problems in chemistry and physics. Some of the suggested applications are extensions of the work reviewed in Chapter 1. However, many more are original to the best of the author's knowledge, and, to an extent, some are speculative. Possible generalizations and extensions of the models are also discussed.

Surface Chemistry Applications

Our models can be applied to a number of different problems in surface chemistry. One problem of current importance is to study the activity of hydrodesulfurization catalysts in order to gain a deeper understanding of how they work and how their performance can be improved. The hydrodesulfurization process typically involves using a metal oxide (58) (or metal sulfide (58)) surface to catalytically remove sulfur from heterocyclic organic compounds, and is of particular importance to the petroleum industry. The catalytic activity of these surfaces is thought to depend on the distribution of anionic vacancies in the surface oxide layer as illustrated in Fig. 6.1. The vacancies allow the sulfur heterocycle to adsorb on or near the surface layer of metal atoms which then act as a source or sink of electrons

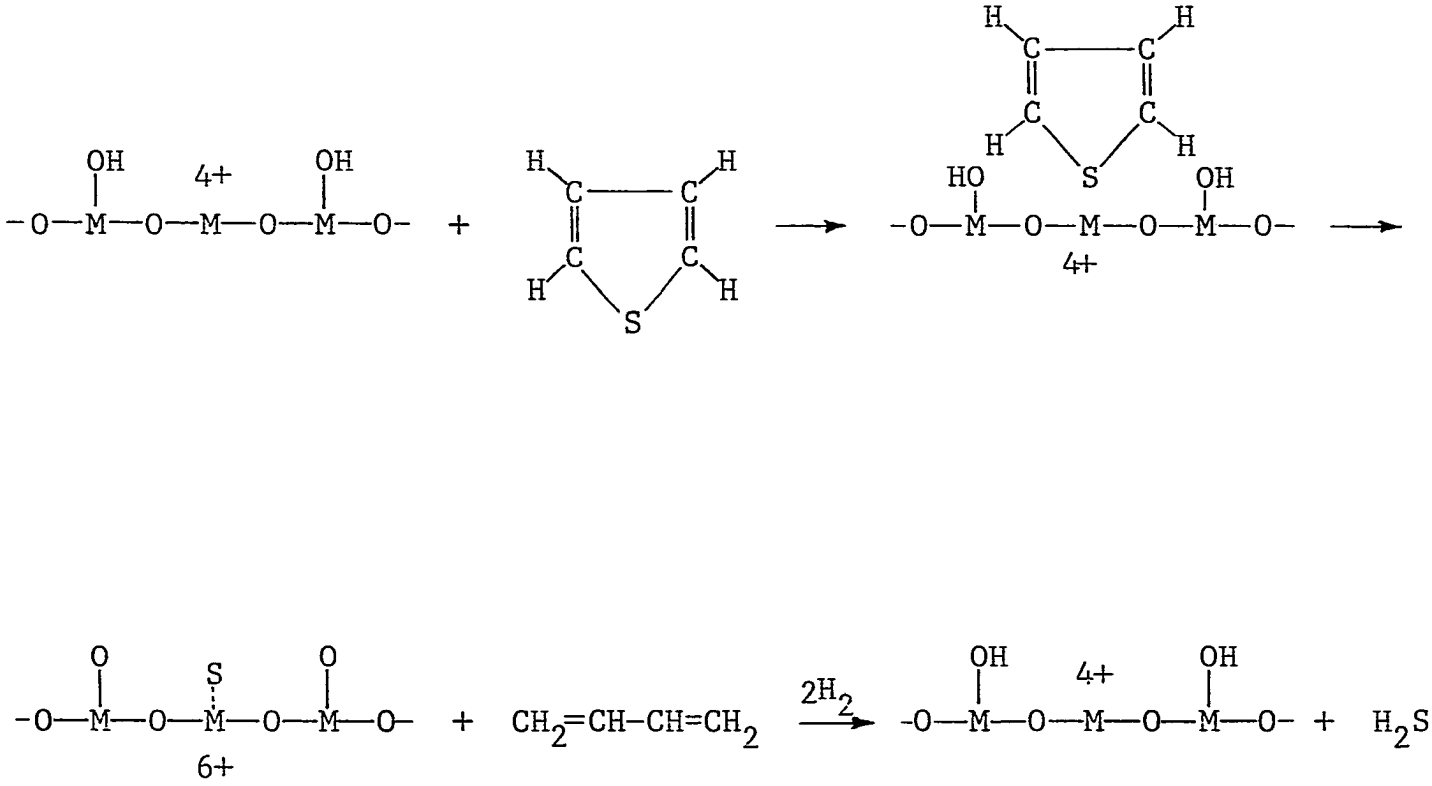

Figure 6.1. A proposed mechanism for the catalytic hydrodesulfurization of thiophene on a metal oxide surface (58). The charge on the metal atom refers to its oxidation state

during the catalytic processes. For the specific details of the mechanism the reader is directed to the review article by Amberg (58).

Under normal laboratory conditions, the metal oxide surfaces are strongly hydroxylated and are composed primarily of metal hydroxide species. To create the necessary vacancies (i.e., to activate the catalyst) the surface is heated to give the following dehydroxylation reaction, which is here depicted in one dimension:

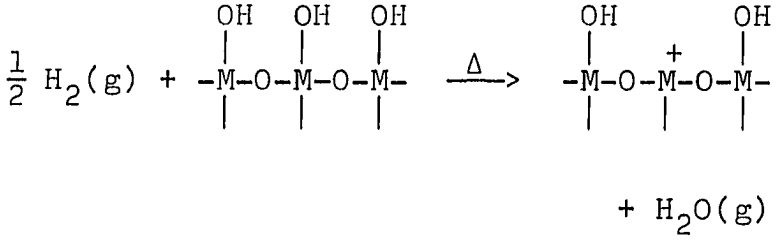

$$+ H_2O(g) + e^- . \qquad (6.1)$$

The resulting anionic vacancy flanked by hydroxyl groups form the postulated active site configuration of Fib. 6.1. Presumably, this surface could alternately be prepared by the rehydroxylation of a dehydroxylated metal oxide surface.

We are interested in studying the manner in which the method of preparation of the surface affects the distribution of active site configurations, and hence, the catalytic activity of the surface. The mechanism of the hydroxylation and dehydroxylation of a metal atom on a metal oxide surface is known to involve the reaction (i.e., the formation or decomposition) of one water molecule at a single metal site (59). We can therefore define two different types of

monomer (i.e., r=0) events to describe these reactions. The first event is defined to be an adsorption event which represents the hydroxylation of a metal site. In this case, the probability of the active site configuration of Fig. 6.1 is $P^{(3)}(101)$. The second event is defined to be a desorption event which corresponds to the dehydroxylation of a single metal site. In terms of desorption events, the probability of the active site configuration is $P^{(3)}(010)$. The distribution of adsorption events evidently describes a surface that was prepared by rehydroxylation, while the distribution of desorption events describes a surface that was prepared by dehydroxylation. It may be recalled from Chapter 3 that these two distribution functions are not calculated from the same hierarchy of equations. The $P^{(3)}(101)$ distribution can be written in terms of distributions of consecutive vacant sites, and thus it is calculated using Eqns. 3.7, 3.11, and 3.14, while $P^{(3)}(010)$ is expressed in terms of a distribution of nonconsecutive sites and hence requires the larger hierarchy that also includes Eqns. 3.28, 3.29 and 3.30. We therefore expect that the distribution of active site configurations will depend to some extent on the method of surface preparation.

In addition, we find that the cooperative influence of a desorption event on the rate of dehydroxylation of a neighboring hydroxylated site is not the same as the influence of

an adsorption event on the hydroxylation of a neighboring vacant site. By the principle of microscopic reversibility, we know (7) that the activation energy for the transition of a site and that of the reverse transition is related to the potential energy of the initial and final states of the lattice site by

$$E_{act}(0\rightarrow 1,x) - E_{act}(1\rightarrow 0,x) = U(1,x)-U(0,x), \qquad (6.2)$$

where $E_{act}(y\rightarrow z,x)$ is the activation energy for site transition from condition y to condition z with a 1st n.n. site in condition x. Also, U(y,x) is the potential energy of the lattice site in condition y with 1st n.n. site in condition x. It directly follows from this result that

$$[E_{act}(0\rightarrow 1,0)-E_{act}(0\rightarrow 1,1)] - [E_{act}(1\rightarrow 0,0) - E_{act}(1\rightarrow 0,1)] = \Delta U(0)-\Delta U(1), \qquad (6.3)$$

where $\Delta U(x) = U(1,x)-U(0,x)$. For simplicity, we can now assume that the change in the energy of a site due to its occupation is unaffected by the condition of neighboring sites, and Eqn. 6.3 reduces to

$$[E_{act}(0\rightarrow 1,0)-E_{act}(0\rightarrow 1,1)] = [E_{act}(1\rightarrow 0,0) - E_{act}(1\rightarrow 0,1)] \qquad (6.4)$$

To compare the cooperative influence of the adsorption and desorption events on the activation energy to the occurrence of the appropriate event on a neighboring site, we rewrite

Eqn. 6.4 in the form

$$[E_{act}(0\rightarrow 1,0)-E_{act}(0\rightarrow 1,1)] = -[E_{act}(\bar{0}\rightarrow\bar{1},\bar{0}) - E_{act}(\bar{0}\rightarrow\bar{1},\bar{1})], \qquad (6.5)$$

where $\bar{1}$ and $\bar{0}$ denote the condition of the site in terms of the occurrence (or lack thereof) of a desorption event. From Eqn. 6.5 it is immediately apparent that the influence of a desorption event on the activation energy for the dehydroxylation of a neighboring site is equal in magnitude, but opposite in sign to the influence of an adsorption event on the activation energy for the hydroxylation of a neighboring site. Since any entropic effects on the rate of transition are included in the pre-exponential factor A and are divided out when we solve the kinetic equations as a function of θ (i.e., τ_{ij} becomes ρ_{ij}), the change in activation energy determines the change in transition rate for the appropriate event. The different influence of the two types of events on the neighboring sites can therefore be reflected in the values of α chosen for each type of event.

Figure 6.2 illustrates the $P^{(3)}(101)$ and $P^{(3)}(010)$ as a function of the density of surface hydroxyl groups for the case where $(\phi_1-\phi_0)_{adsor} = -0.4193$ kcal/mole. It is evident from these plots that the probability of the desorption event configuration is greater for a given value of θ than of the corresponding adsorption event configuration. In

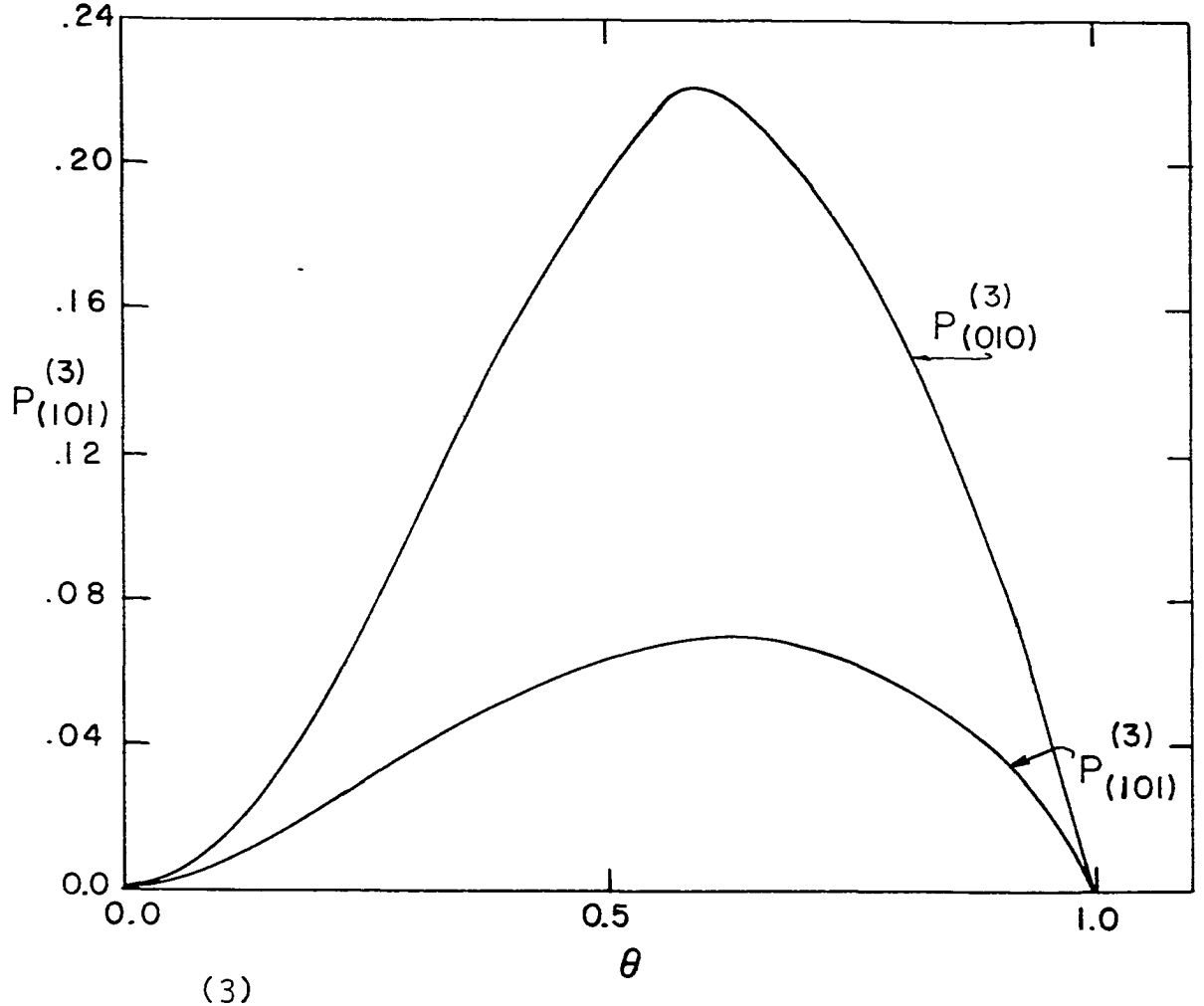

Figure 6.2. The $P^{(3)}_{(101)}$ distribution of monomers resulting from the deposition of molecules onto an empty lattice ($P^{(3)}_{(101)}$) and from stripping molecules from a completely occupied surface ($P^{(3)}_{(010)}$)

other words, for this value of $(\phi_1-\phi_0)$, the dehydroxylation of a fully hydroxylated surface gives a higher density of active site configurations than does the rehydroxylation of a dehydroxylated surface and hence a higher catalytic activity. This is to be expected because adsorption events will tend to cluster in this case leaving a lower density of anionic vacancies flanked by two hydroxyl species. The desorption events on the other hand tend to be more diffuse and hence giving rise of a higher density of active site configurations. For positive values of $(\phi_1-\phi_0)_{adsor}$, we expect that the adsorption events will give a more favorable distribution of active sites and this is borne out by calculations. We can also note from these curves the covering fraction at which the highest catalytic activity occurs. Such information is of potential importance for determining the best way to carry out the activation process. Another interesting feature illustrated in the figure is the nonreversibility of the distributions during a cyclic adsorption-desorption process. Our model curves predict a hysteresis loop in the event distributions when the adsorption and desorption processes are performed under similar experimental conditions. Our models can also be used to compare the distributions arising from adsorption and desorption under different ambient conditions; however, differences in the distributions noted in this case do not constitute a hysteresis effect.

In the case of the cyclic adsorption-desorption of dimers, the physical difference in the boundary conditions satisfied by the distributions can also affect the distribution of events. As we recall, dimer events saturate the lattice at an event density of $\eta<\frac{1}{2}$ or $\theta<1$. The desorption step immediately following the initial adsorption step therefore does not start from a fully occupied lattice, but rather from a lattice with isolated vacancies. It is easily seen that the surface distribution at a given covering fraction will change with each succeeding cycle because of the change in the boundary conditions. This change continues until some steady-state configuration of sites is reached.

Experimentally, hysteresis loops in cyclic adsorption-desorption processes are noted in the study of the hydration of γ-alumina by Fuller and Agron (60), and of thoria by Gammage et al. (61). Other systems are discussed by Adamson (55).

Our models can also be applied to other surface chemistry and heterogeneous catalysis problems. For example, Peri and Hensley (36) and Fuller et al. (1) have reported theoretical studies of the surface structure or surface composition of silica gel. The problem of determining the surface composition of silica gel is somewhat similar to that discussed above in that ambient conditions produce a silica surface dominated by hydroxyl groups. On heating, the

hydroxyl groups on two nearest neighbor silicon atoms condense, liberating H_2O, and leaving an oxygen atom bridging two silicon atoms. This is illustrated in the following reaction:

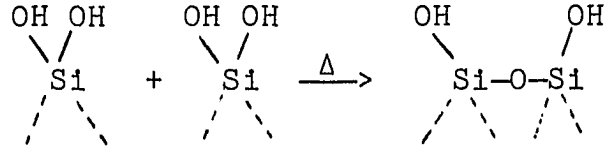

(6.6)

It is clear that this is the two-dimensional analogue to the Flory model. If the event here is defined to be the reaction of two neighboring hydroxide groups, we can apply the dimer (or r=1) cooperative model to determine the kinetic distribution of bridging oxygen atoms and unreacted hydroxide groups. These results can then be compared to the Monte Carlo calculations and random model results of Peri and Hensley, and Fuller et al., discussed in Chapter 1.

Another application to a catalysis problem is the calculation of the product distribution arising from the Fischer-Tropsch synthesis. In the Fischer-Tropsch process, adsorbed carbon monoxide and hydrogen react to form hydrocarbons of various chain lengths. One proposed mechanism (55) for this process is illustrated in Fig. 6.3, and can be briefly described as follows. Adsorbed CO molecules react with hydrogen reducing the CO to an adsorbed methanolic intermediate. Two of these intermediates can then react to form a chemisorbed ethanol species, the carbon chain length increases with each succeeding reaction with an intermediate

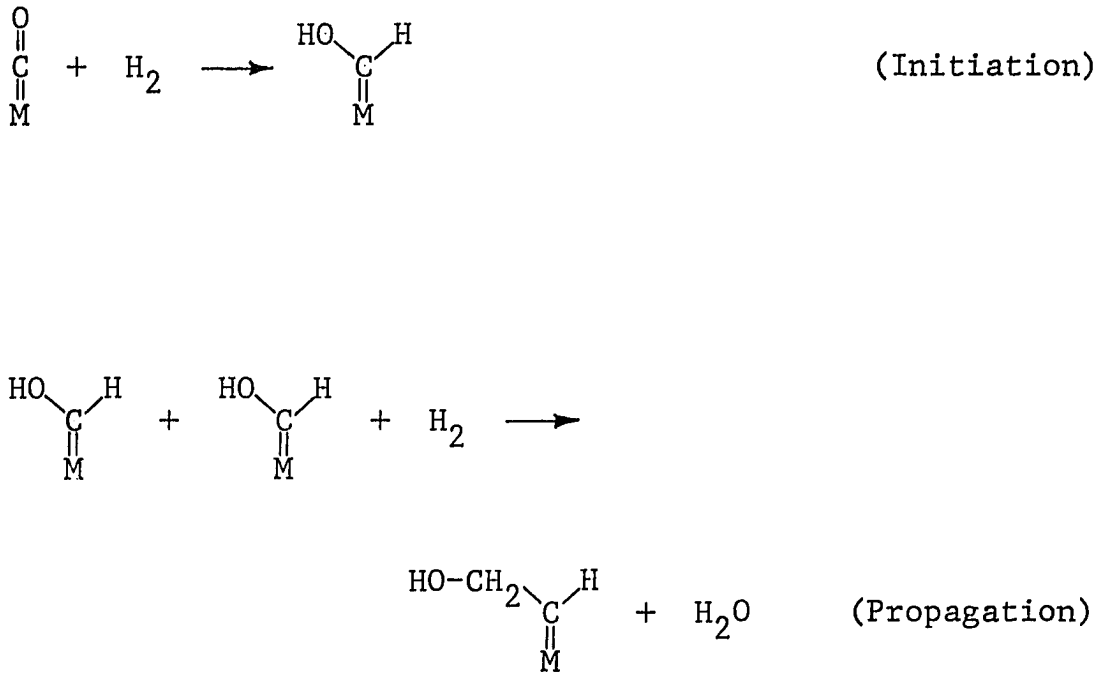

Figure 6.3. A proposed Fischer-Tropsch Mechanism (55)

species. The chain can be terminated through reaction with a hydrogen molecule. Variations of this basic mechanism, in general, give rise to a mixture of acids, alcohols, and other hydrocarbons of various carbon chain lengths as reaction products, depending on the conditions of the reaction and the choice of catalytic surfaces. For example, it has been shown (62) that on supported group 8 metals the Fischer-Tropsch process yields hydrocarbons ranging from almost pure methane on Pd to paraffinic waxes on Ru. The event for the simple mechanism discussed above is the formation of a carbon-carbon bond in the chain. The distribution of a sequence of adjacent events then determines the distribution of product molecules. For example, an $f^{(5)}_{(01110)}$ event distribution gives the probability of producing a molecule containing four carbon atoms. Our models can, of course, be used to obtain such distributions.

Of continuing interest in surface chemistry is the effect of promoters and poisons on the rate of chemisorption or catalytic activity of a surface. In a very general sense, promoters and poisons are chemical species on the surface, or those physical features of the surface, which act to accelerate or retard the rate of reaction. Promoters are generally associated with lattice dislocations, point defects, and other surface defects (49) that accelerate surface reactions by providing preferential locations for

nucleation reactions. Poisons, on the other hand, are often associated with molecules that occupy an active site or otherwise serve to remove an active site from use. The effects of promoters and poisons on a surface distribution of events can be qualitatively described by our semi-infinite or finite lattice models; the independent end site transition rate is utilized to mimic the effect of the promoter or poison. Since our models are for one-dimensional lattices, the only type of defect we can describe is a point defect. On the two-dimensional surface, however, there can be a number of one-dimensional defects, such as terraces, kinks and grain or phase boundaries, in addition to the point defects. A quantitative description of the effect of these higher dimensional defects, of course, requires a two-dimensional model. Adsorption directly along the one-dimensional defects (e.g., terraces) perhaps could be directly described by our models.

Examples of systems where the distribution of events is known to be effected by a promoting element are found in a variety of experiments. In a LEED study of the high index (i.e., stepped) crystal faces of Pt, Baron et al. (48) report that kinks and terraces in the platinum surface have a marked effect on the activity of the surface toward the chemisorption of various hydrocarbons. Their results indicate that the terraces promote surface reaction by

providing favored sites for the adsorption and dehydrogenation of hydrocarbons. A high concentration of kinks in the terraces promotes the rapid decomposition of the hydrocarbons. Hall and Rasé (63) report a strong dependence of the catalytic activity of LiF crystals in the dehydrogenation of ethanol on the density of lattice dislocations. Point defects in the lattice of metal oxides with the scheelite structure are purported to play a direct role in the mechanisms of olefin oxidation in the kinetic studies reported by Sleight and Lynn (64).

Nucleated surface reactions do not, however, always require a surface defect for promotion. Orent and Hansen (65) describe a highly cooperative surface structural rearrangement which occurs during the chemisorption of O_2 and NO on Ru($10\bar{1}0$). These authors report that at high temperatures an adsorbing oxygen (or NO) molecule can interact with the lattice to effect a change in the position of several Ru atoms. The probability that this rearrangement occurs at a given surface cell is very small; however, once nucleated, the rearrangement is thought to proceed rapidly in a highly ordered manner.

Applications to Other Lattice Systems

Polymer systems also form a fertile area of application of cooperative, irreversible, kinetic models. Furthermore,

since such systems often can be adequately represented as being one-dimensional, they are particularly well-suited for study using our models. In fact, much of the development of one-dimensional models has been done in connection with polymer chemistry, and applications of these models to polymer systems are numerous in the literature. A fairly comprehensive review of these applications is included in the first chapter; several applications suggested in this section are extensions of these works. The kinetic analysis of polypeptide denaturation reported by McQuarrie et al. (33) can be extended to include the effects of the finite molecular length on the polymer structure with the models developed on the finite or semi-infinite lattice. The polypeptide chain is composed of monomer units with the following form:

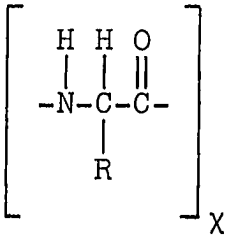

(6.7)

and takes on the structure of an α helix with the formation of a hydrogen bond between an amine hydrogen on each monomer unit and the acidic oxygen of the third following monomer unit on the chain. The event for this model is the formation of the hydrogen bond, and the distribution of events determines the conformational structure of the polymer. The

saturated lattice, in this case, represents a perfect α helix. In a related problem, the titration of polymer acids or polypeptides result in a distribution of ions on the polymer chain which affects the helical nature of the polymer molecule. Defining the event for this system to be the removal of an acidic proton from a monomer unit, we can calculate the distribution of charged (and hence highly solvated) groups on the molecule which can then be related to the helical structure of the molecule. Finally, one possible interdisciplinary application of our models is the study of the adsorption of polymers onto pseudo-linear surfaces. The adsorption of such a molecule is an event with a very long range blocking potential. Hence, an analysis in the spirit of that of Chapter 2, in the section concerning the infinite line, is appropriate.

Three-dimensional lattice systems offer some interesting applications of cooperative kinetic models. For example (66), perfect crystals of several sodium and calcium salts, most notably $CaCO_3$, $CaSO_4$, Na_2CO_3 and Na_2SO_4, are stable for long periods of time. However, if the crystals are scratched, they immediately begin to decompose along the scratch and continue to react only along the interface between the two solid phases. Chemical systems exhibiting this behavior are termed topochemical. These systems are strongly cooperative, as witnessed by the progression of the

reaction along the line of the decomposed phase. They rely on a promoter (here, the scratch) to nucleate the reaction, and hence, are clearly amenable to analysis by three-dimensional versions of our models on the finite or semi-infinite lattice. The one-dimensional analogue where the nucleating feature is a point defect on the lattice can be treated as discussed in the last section and should give qualitative information about the process. Other chemical problems that can be considered to be topochemical and well-suited to analysis by our models include the stability of explosives (55), the corrosion of metal surfaces, and the sublimation of crystalline solids.

In addition to the topochemical applications noted above, higher dimensional generalizations of our models can be used to calculate distributions arising from other irreversible processes in a three-dimensional lattice system. As a particular example, calcite, the naturally occurring hexagonal form of $CaCO_3$, undergoes molecular decomposition according to the reaction

$$CaCO_3(s) \xrightarrow{\Delta} CaO(s) + CO_2(g), \qquad (6.8)$$

and gives rise to a distribution of CaO throughout the calcite crystals. The cooperative effect of a decomposed molecule on the decomposition of a neighboring site is an extremely interesting question and should be amenable to

treatment along the lines we have developed for one-dimensional systems. In the somewhat similar problem of damage of a crystal by x-ray radiation, it should be possible to investigate the distribution of damaged molecules. The investigation of cooperative solid-solid phase transitions in a lattice and lattice melting might also be performed using generalizations of our models and methods.

Jackson and Montroll (38) have studied the recombination of trapped nitrogen radicals in solid nitrogen. These authors present model calculations for one-, two-, and three-dimensional systems in which nitrogen radicals condense from a gas to form a crystalline solid. They are then allowed to randomly recombine with one nearest neighbor radical to form a nitrogen molecule. The average number of unreacted radical species is the quantity of interest. As discussed in Chapter 1, the calculations of Jackson and Montroll are not based on kinetics and hence, are not completely appropriate to the problem. However, by defining an event for this system to be the recombination of two nitrogen radicals, this system could also be modeled along the lines we have developed to obtain the distribution of nitrogen molecules resulting from the irreversible kinetic process. The similarity of this problem to those considered by Flory and Peri and Hensley is evident.

In a related problem, we can consider a one-, two-, or three-dimensional solid matrix composed of unsaturated hydrocarbons in which a very small number of radicals have been embedded. In this case, the radicals are assumed to be so sparsely distributed that the reaction of two of the radicals is unlikely. Instead, the radicals react with neighboring hydrocarbon molecules to create hydrocarbon radicals, which in turn react with other hydrocarbons, thus giving rise to addition polymerization. The polymerization continues until chain termination results from the reaction of the radical ends of two chains (or by reaction with the vessel walls). There are two types of lattice problems associated with this process, which are possible candidates for analysis by methods of the type which we have discussed. The first involves determining and controlling the distribution of radical precursors in the matrix preparation process. This distribution is clearly an important determinant of the nature of the final polymer product. The second problem is concerned with how the polymerization bonding evolves from a given distribution of radicals. This is somewhat similar to the Fischer-Tropsch problem discussed in the previous section.

Model Refinements

In the preceding sections we have discussed a wide range of possible applications for the models developed earlier in this work and extensions of these models. We now wish to examine in some detail the limits of applicability of our models and to discuss the various possible refinements required to treat the problems we have considered. It was seen in the previous chapter that the sticking coefficient as calculated from a one-dimensional model was in good qualitative agreement with experimental results, but the two-dimensional version of this model somewhat improved the quantitative agreement. This is, of course, expected since surfaces are two-dimensional. We think that this is a typical example of the type of qualitative information which is gained by using a one-dimensional model to treat a problem of higher dimensionality. For quantitative considerations, we need kinetic equations for lattices of higher dimensionality. These kinetic equations have been developed and are similar to those in one-dimension in that they also form an infinite hierarchy of coupled differential equations (25). As previously mentioned, these hierarchies cannot be truncated exactly and hence, exact, closed form solutions cannot be obtained. Solutions in various degrees of approximation can be obtained for arbitrary interaction range and various lattice geometries through methods similar

to that described by Vette et al. (12) in their investigation of two-dimensional models for non-cooperative events. The virial expansion formalism (25) discussed in Chapters 1, 3 and 5 provides an alternative, exact solution to the higher dimensional models in the form of an infinite expansion.

There are features of our models, other than dimensionality, which at present limit the physical systems which can be quantitatively studied. One is that we have only one type of event site, another is that we have only one type of event. In a sense, these two restrictions are related in that for a perfect lattice we need only consider the entire unit cell (and the various possible types of sites contained therein) as a single site on which many different types of events can occur (7). This point of view has obvious theoretical advantages, but as a practical matter, it may be more convenient to consider that there are both different types of events and different types of sites. A reversible model is a specific case where it is useful to explicitly consider two different events in the form of an event and the reverse of that event. More generally, the lattice may not be perfect, in which case one must consider that there is a distribution of sites on which the events of interest can occur. This distribution could itself be formed from an earlier irreversible process. Examples of this are the radical polymerization of hydrocarbons discussed in the

previous section, and the cyclic hydration-dehydration of various surfaces as discussed in the first section of this chapter. Finally, an important generalization is when an event occurs at more than one site. Of course, this is exactly the case for the space-filling lattice discussed in Chapter 2. However, our starting point for that discussion was an event lattice on which an event was described as a transition of a single site. It is not always possible to define such an event lattice. For example, reversible, dissociative dimer adsorption can give rise to atomic distributions which cannot be described by distributions of events occurring at a single site. This is illustrated in Fig. 6.4. Kinetic equations for all these situations can be derived using the techniques and processes we have developed in this thesis. As might be expected, the equations increase rapidly in complexity as the models become more general.

Some of the generalizations mentioned above have already been considered. For example, Cohen and Reiss (10) have considered the effect of a distribution of active and inactive sites on the distribution of non-cooperative events for a one-dimensional lattice. As previously discussed, Glauber (2) has utilized a master equation approach to describe the reversible kinetics of events on a homogeneous (i.e., only one type of site), one-dimensional lattice. Hoffman (7) uses a similar master equation approach to

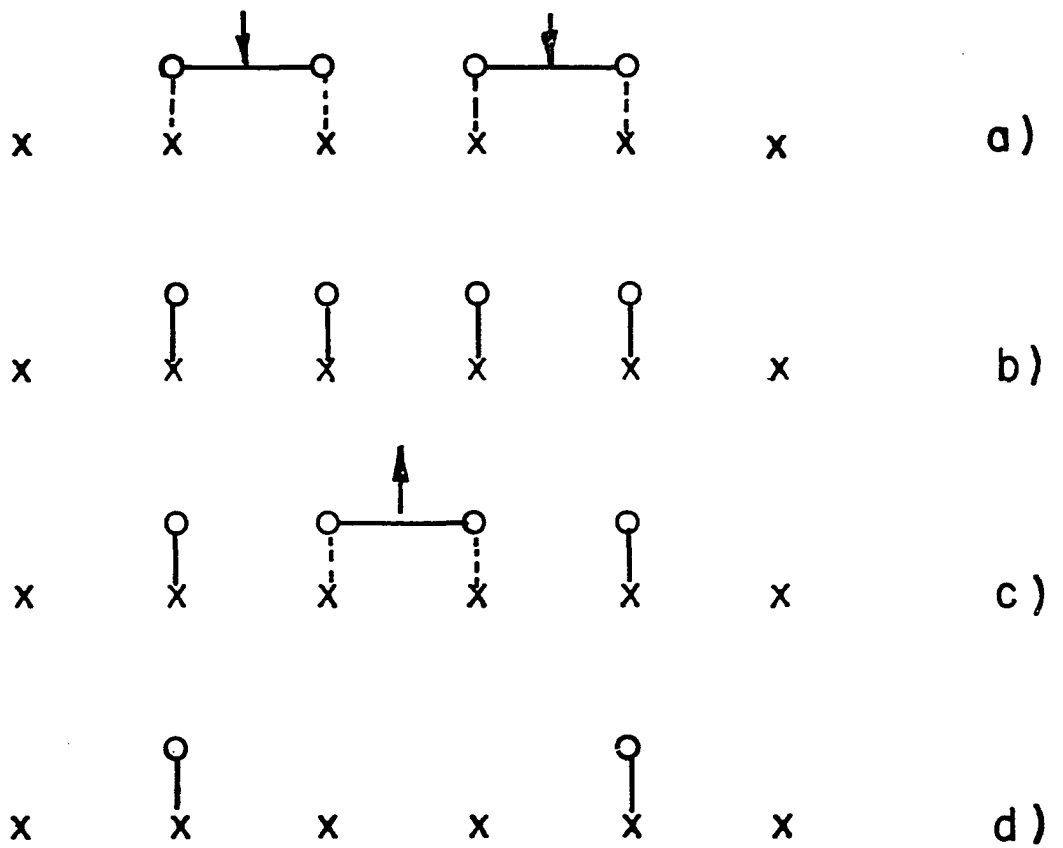

Figure 6.4. A schematic illustration of the reversible adsorption of a dimer which depicts a space-filling lattice distribution for which no event lattice can be devised

describe reversible kinetics on a lattice of general dimensionality and composition.

Further generalizations of kinetic lattice models and their applications to problems of the type we have discussed promise to offer intriguing topics for further research.

CHAPTER 7. THE ACTIVATED CHEMISORPTION OF METHANE ON W(110): AN EXPERIMENTAL STUDY

Introduction

In this final chapter, we describe an experimental investigation of the vibrational state dependence of the rate of chemisorption (i.e., the sticking coefficient) of normal methane, CH_4, on the hexagonal (110) face of crystalline tungsten. This study was undertaken to compliment our statistical investigation of the molecular sticking coefficient, as reported in Chapter 5, and to gain further insight into the mechanism of chemisorption of polyatomic molecules. We note at the outset that the results of our study proved to be inconclusive because of various technical problems. These problems, and their possible solutions, are discussed in a later section of this chapter.

The chemisorption of diatomic molecules on transition metal surfaces has been studied extensively and is known to occur via molecular dissociation and the adsorption of the atomic species on the surface (55). On a clean surface this process generally occurs with a large sticking coefficient and it is therefore thought that no significant activation barrier exists to inhibit dissociative adsorption. On the other hand, the detailed chemisorption mechanism of polyatomic molecules has not been as well characterized because

of its complexity. Most investigators, however, recognize that saturated hydrocarbons chemisorb slowly with a significant activation barrier. For example, the chemisorption of methane on rhodium has an activation energy of ∿7 kcal/mole (67). The molecules are presumably activated by the population (thermal or otherwise) of their various internal energy levels. It is of present interest to determine which of these internal degrees of freedom are important to the activation process.

Only a few studies have been reported in which the detailed chemisorption mechanisms of simple, saturated hydrocarbons have been investigated. Stewart and Ehrlich (67) report a study of activated chemisorption of methane on rhodium in which the energy levels of normal methane and the various deuterated isotopes of methane were thermally populated over the temperature range of $300°K \leq T_{Gas} \leq 710°K$ and allowed to chemisorb on the rhodium surface which was held at 245°K. Essentially no chemisorption of any of the methane isotopes was observed until the gas temperature was in the range $600°K \leq T_{Gas} \leq 710°K$, at which time the rates of chemisorption of all species were increased. In this temperature range, the rate of chemisorption of CH_4 was ∿10 times that of CD_4 and ∿3 times that of CH_2D_2. This kinetic isotope effect suggests that translational and rotational energy levels are not primarily responsible for promoting the

activated process since the difference in translational and rotational energy levels between the isotopic species could not account for the large rate differences. Electronic energy levels were also excluded on the basis that the lowest excited electronic state of CH_4 lies $\sim$150 kcal/mole above the ground state, which is much higher than the measured activation energy of $\sim$7 kcal/mole. Thus, the thermal population of excited electronic levels at 600°K is negligible. The remaining viable excitation mode, molecular vibrations, was therefore determined to promote the activated adsorption process. This is a reasonable deduction on the basis of the energetics of the situation (the ν_2 vibrational mode of CH_4 at 2180 cm^{-1} lies 6.24 kcal/mole above the ground vibrational state and the activation energy for the process was determined to be $\sim$7 kcal/mole), and the fact that molecular dissociation usually involves excited vibrational states. To explain the large kinetic isotope effect in the vibrational activation, Stewart and Ehrlich invoke Slater's unimolecular reaction model and propose that the ν_4 beinding mode is the critical vibration which leads to dissociation. This analysis, however, met with only marginal success.

In a related study, H. F. Winters (68) studied the activated chemisorption of methane on a tungsten surface by heating the tungsten surface to temperatures in the range of $600°K \leq T_{Surface} \leq 2600°K$. With this technique, he noted an

increase in the rate of activated chemisorption similar to that of Stewart and Ehrlich, and a similar, but more marked kinetic isotope effect at the higher temperatures. In a later article (69), Winters explains his results, including the large kinetic isotope effect, in terms of a quantum mechanical tunneling model for the dissociation of C-H or C-D bond in which three adjustable parameters are utilized. The model calculations for the ν_1 and ν_2 vibrational modes agree well with experimental results.

It is convincingly shown in the papers discussed above that vibrational modes are responsible for the activation of the chemisorption process; however, there is no evidence presented to support which of the modes are most effective in promoting the process. It is seen from Table 7.1 that in the thermal excitation of the vibrational energy levels, all modes are significantly populated and it would therefore be difficult to distinguish the contributions of the individual modes in promoting the activated chemisorption.

Table 7.1. The thermal population of n=1 vibration levels in CH_4

T, °K	ν_1	ν_2	ν_3	ν_4
700	1.89×10^{-3}	6.48×10^{-2}	4.57×10^{-3}	1.51×10^{-2}
1100	8.44×10^{-3}	1.03×10^{-1}	2.21×10^{-2}	2.05×10^{-1}
1500	1.04×10^{-2}	7.83×10^{-2}	2.82×10^{-2}	1.44×10^{-1}

The goal of the experiment we describe in this chapter is to selectively excite individual infrared active vibrational levels of normal methane, CH_4, and monitor the rate of chemisorption on a tungsten (110) surface for each of the levels. In this manner, we can hope to determine the relative effectiveness of each vibrational mode in promoting activated chemisorption.

Experimental Methods

Preliminary considerations

The experimental technique we utilize is conceptually simple. In an ultra-high vacuum system we physisorb approximately one monolayer of methane onto an atomically clean tungsten surface. These molecules are vibrationally excited by infrared radiation of frequency appropriate to the vibrational mode under study and allowed to chemisorb. The physisorbed methane is flashed off and the amount of chemisorbed methane is determined by Auger analysis.

Preliminary to the experiment, several details must be carefully considered. Methane is a rotational spherical top with a very nearly spherical electronic distribution. Chemically, it is a rather inert gas which has a normal boiling point of 111.7°K. In order to physisorb the required amount of methane on the surface, we have to significantly cool the tungsten crystal. At liquid nitrogen temperatures,

the saturation vapor pressure of methane, P_0, is $\sim$15 torr. In a typical gas-solid adsorption situation, monolayer coverage is attained when $P/P_0 > 0.05$. We therefore estimate a dosing pressure of $\sim$0.5 torr will result in a significant surface coverage where the crystal is held at $\sim$77°K.

The lifetime, τ, of the vibrationally excited molecule on the surface and the rate of excitation of the molecules determine the concentration of excited molecules on the surface. We assume, because the methane is only weakly bound to the surface, that the coupling of the vibrational states of the molecule with the various surface and bulk excitations of the solid (e.g., phonons) is negligible and that the lifetimes of the excited states can be approximated by their gas phase radiative lifetimes. The radiative lifetimes of the IR active ν_3 (3020 cm^{-1}) and ν_4 (1306 cm^{-1}) modes have been reported (70) as 0.037 seconds and 0.39 seconds, respectively. We can estimate the transition rates into these states as a function of the radiation field intensity by solving the optical kinetic equation (71)

$$\frac{dN_A}{dt} = (N - 4/3\ N_A)\ \frac{c^3 I(\nu)}{24\pi h\nu^3 \tau} - \frac{N_A}{\tau}\ , \qquad (7.1)$$

where N_A and N are the number of molecules in state A and the total number of molecules, respectively, and $I(\nu)$ is the intensity of the radiation field as a function of frequency. In Eqn. 7.1 the degeneracy of state A is taken to be 3

because both the ν_3 and ν_4 modes are triply degenerate. The infrared source we utilize in this experiment is a Nernst glower. To obtain $I(\nu)$ we therefore assume our radiation source is a blackbody at a temperature of $\sim$1200°K and write Eqn. 7.1 in the form

$$\frac{df_A}{dt} = 0.22(1 - 4/3\ f_A)(\exp\{h\nu/kT\}-1)^{-1}\tau^{-1} - f_A\tau^{-1}, \qquad (7.2)$$

where $f_A = N_A/N$. This result can easily be solved to give the fraction of molecules in the ν_3 and ν_4 modes; namely

$$f_{\nu_3} = 0.01\ (1 - e^{-27t}), \qquad (7.3)$$

and

$$f_{\nu_4} = 0.1\ (1 - e^{-3t}). \qquad (7.4)$$

It should be remembered that these results are based on gas phase lifetimes and transition frequencies. We ignore any symmetry or energetic changes in the molecule brought about by adsorption. The results of Eqns. 7.3 and 7.4 must therefore be regarded as estimates. Because of the relatively small fractions of excited state molecules shown above, we expect that it will be necessary to irradiate the physisorbed molecules for as long as practically possible. At partial pressures of gaseous contaminants in the 10^{-8} to 10^{-10} torr range (the contaminants are primarily CO and H_2 from the background gases in the vacuum system) a monolayer

of contaminants could form in as little as 100 seconds at 10^{-8} torr, thus limiting the duration of the experiment to somewhat less than five minutes.

Apparatus

The experimental system we used is schematically depicted in Fig. 7.1. The ultra-high vacuum system is a commercial unit from Varian consisting of an ion-pumped, stainless steel bell jar equipped with an electron gun and cylindrical mirror analyzer (CMA) for Auger analysis, UTI quadrupole mass spectrometer (not shown), and a nude Bayard Alpert gauge. Pressures of 10^{-10} torr were regularly attainable in the bell jar after bakeout. The mass spectrometer was used to determine the composition of the background atmosphere of the vacuum system.

The tungsten (110) crystal used in our work has been used in previous experiments at this laboratory and is described in detail elsewhere (72). Prior to its use in this experiment, the crystal was mechanically polished, and before each experiment run, the residual surface carbon was removed by repeatedly reacting the crystal with oxygen and heating until Auger analysis indicated a negligible amount of surface carbon. This crystal was mounted in the vacuum system on a rotary manipulator which was equipped with a resistive element for heating the crystal to $\sim$1300°K and

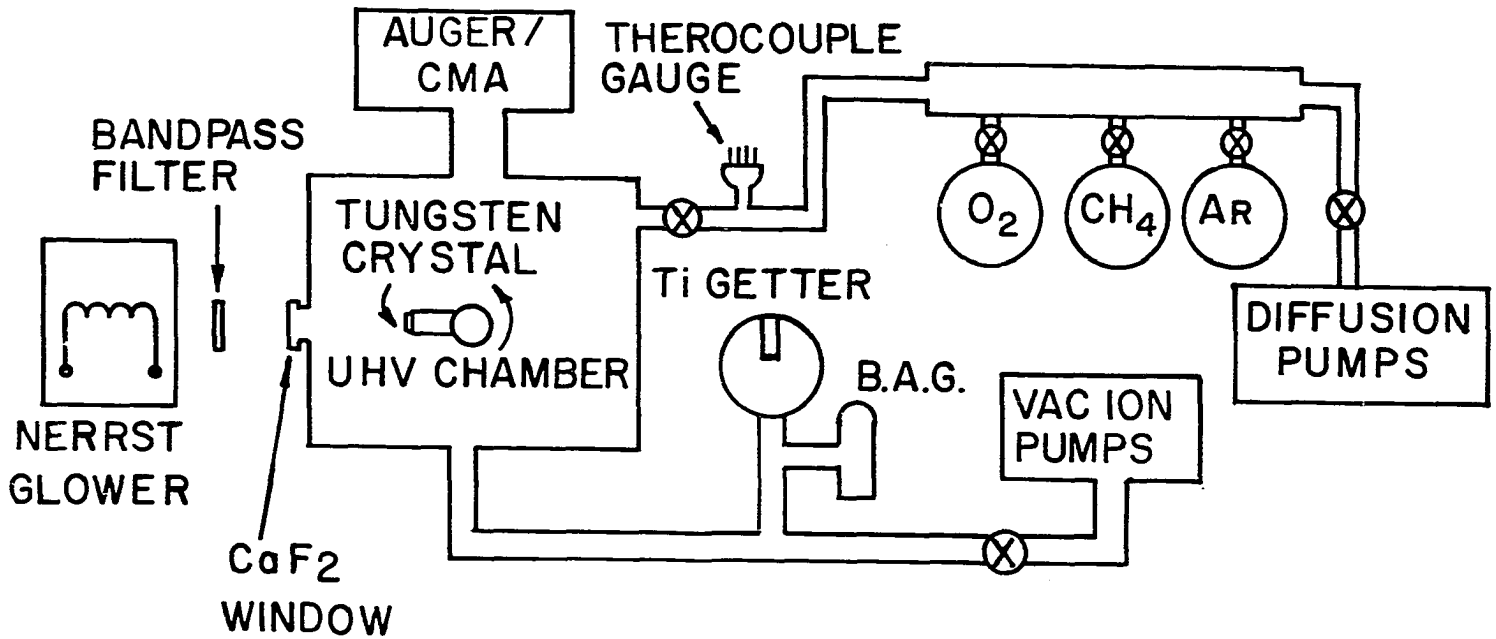

Figure 7.1. A schematic of the system used in the investigation of the activated chemisorption of CH_4 on W(110)

liquid nitrogen cooling coils that allowed the crystal to be cooled to ∿130°K. A W-Re 5%, W-Re 26% thermocouple was spot welded to the edge of the crystal face to monitor surface temperatures. The methane gas (Linde research grade, 99.99% purity) was admitted into the bell jar through an auxillary vacuum system and a leak valve to minimize the atmospheric contamination of the gas. As previously mentioned, the infrared radiation fo this experiment was provided by a Nernst glower and admitted into the system via a CaF_2 window. The appropriate ν_3 and ν_4 transition frequencies were obtained by filtering the glower radiation with bandpass filters with 100 cm^{-1} bandwidth centered near the gas phase transition frequency.

Procedure

The procedure followed in a typical experimental run can be summarized as follows:

1) The surface was cleaned as described above.
2) The crystal was cooled to ∿130°K. This operation typically took 30 to 45 minutes.
3) A "blank" Auger spectrum of the cooled crystal was taken to determine the condition of the surface prior to the physisorption step.
4) The methane was dosed into the bell jar at pressures on the order of 10^{-3} torr and the resulting physisorbed layer was irradiated

for three to five minutes at the desired frequency.

5) After irradiation, the methane gas was pumped out of the system, the physisorbed methane was flashed off by heating the crystal to ∿300°K for 30 seconds, and the increase in surface carbon due to the chemisorption of methane was determined by Auger analysis.

Results and Discussion

As mentioned at the outset of this chapter, we were not able to obtain any conclusions from this experiment because of technical problems in the experimental procedure. The primary problem was determined to be the contamination of the surface from background levels of CO and H_2 before the methane was physisorbed. The blank Auger spectra (step 3 above) showed in all cases that carbon had accumulated on the surface, presumably from chemisorbed CO, during the cool down period in amounts that were roughly equivalent to that contained in the physisorbed layer. The amount of chemisorbed H_2, of course, could not be determined by Auger analysis; however, the H_2:CO ratio in the background gases was shown to be approximately 5:1, and we must therefore assume that a proportional amount of H_2 was also chemisorbed. Under such surface conditions the probability that a

vibrationally excited methane molecule will find a vacant surface site on which to chemisorb is small. In addition, it was found that because of inadequacies of instrumental design the crystal could only be cooled to ∿130°K, well above the desired temperature of 77°K. The dosing pressure of 10^{-3} torr was also lower than the desired pressure of 0.5 torr noted earlier. As a result, less methane was physisorbed than expected, thereby further reducing the probability that a significant amount of methane could chemisorb.

We attempted to resolve the surface contamination problem by lowering the system pressure into the 10^{-11} torr range with more frequent and longer bakeouts, cryogenic pumping, and adsorption onto a freshly deposited Ti film, all without measurable success. Dosing pressures were raised to offset the higher crystal temperatures during physisorption; however, because of the levels of surface contamination no increase in the amount of carbon was noted after irradiation.

Several modifications of the existing apparatus can be made to minimize the problems noted above. For example, it is known that strictly ion-pumped systems have a high background level of hydrogen, whereas systems pumped by diffusion pumps do not have this problem. The use of a diffusion pump in conjunction with the ion-pumps of our system might help reduce hydrogen levels. Unfortunately, CO is much more

difficult to remove than hydrogen, although the amount of CO in the system might be reduced with a Ni getter. Another important modification is to increase the contact of the cooling coils with the manipulator to reduce cool down time, and hence, lower the level of surface contamination.

In conclusion, we feel that the method described above is a viable manner to study the participation of an individual vibrational mode in the activated chemisorption of methane when the cited technical problems can be overcome. It should be noted in closing that the lack of conclusive results from this experiment has no bearing on any of the theoretical material presented in earlier chapters.

LITERATURE CITED

1. E. L. Fuller, S. Ebey and V. R. R. Uppuluri, "Statistical modelling of Adsorption Processes on Catalyst Surfaces: Preliminary Report", ORNL-5231, Oak Ridge National Laboratory, Oak Ridge, Tennessee (1976).

2. R. J. Glauber, J. Math. Phys. 4, 294 (1967).

3. D. J. Isbister and D. A. McQuarrie, J. Chem. Phys. 60, 1937 (1974).

4. I. Langmuir, J. Amer. Chem. Soc. 40, 1361 (1918).

5. P. J. Flory, J. Amer. Chem. Soc. 61, 1518 (1939).

6. I. Oppenheim, K. E. Shuler and G. H. Weiss, Stochastic Processes in Chemical Physics: The Master Equation (MIT Press, Cambridge, Mass., 1977).

7. D. K. Hoffman, Department of Chemistry, Iowa State University (to be published).

8. J. O. Hirschfelder, C. F. Curtiss and R. B. Bird, Molecular Theory of Gases and Liquids (John Wiley and Sons, Inc., New York, N.Y., 1967) chapter 7.

9. R. B. McQuistan and D. Lichtman, J. Math Phys. 9, 1680 (1968).

10. E. R. Cohen and H. Reiss, J. Chem. Phys. 38, 680 (1963).

11. E. S. Page, J. Roy. Stat. Soc. B21, 364 (1959).

12. K. J. Vette, T. W. Orent, D. K. Hoffman and R. S. Hansen, J. Chem. Phys. 60, 4854 (1974).

13. T. L. Hill, Introduction to Statistical Thermodynamics (Addison-Wesley, Inc., Reading, Mass., 1960).

14. B. Widom, J. Chem. Phys. 44, 3888 (1966).

15. A. Rényi, Magyar Tudományos Akad. Mat. Kutató Int. Közleményi 3, 109 (1958), also in Selected Transl. Math. Stat. Prob. 4, 205 (1963).

16. B. Widom, J. Chem. Phys. 58, 4043 (1973).

17. E. A. Boucher, J. Chem. Phys. 59, 3848 (1973).

18. J. K. Mackenzie, J. Chem. Phys. 37, 723 (1962).

19. C. Domb, Proc. Camb. Phil. Soc. 43, 329 (1947).

20. P. E. Ney, Ann. Math. Stat. 33, 702 (1962).

21. G. Schwarz, Ber. Bunsenges. Physik. Chem. 75, 40 (1971).

22. E. A. Boucher, Chem. Phys. Letters 17, 221 (1972).

23. E. A. Boucher, J. Chem. Soc.; Faraday Trans. II 69, 1839 (1973).

24. J. J. Gonzalez, P. C. Hemmer and J. S. Hoye, Chem. Phys. 3, 228 (1974).

25. D. K. Hoffman, J. Chem. Phys. 65, 95 (1976).

26. N. Gō, J. Phys. Soc. Jap. 22, 413 (1967).

27. R. Kikuchi, Ann. Phys. 10, 127 (1960).

28. H. W. Huang, Phys. Rev. B 11, 1144 (1975).

29. T. H. K. Barron and E. A. Boucher, Trans. Far. Soc. 69, 3301 (1969).

30. T. Alfrey, Jr. and W. G. Lloyd, J. Chem. Phys. 38, 318 (1963).

31. C. B. Arends, J. Chem. Phys. 38, 322 (1963).

32. J. B. Keller, J. Chem. Phys. 37, 2584 (1962).

33. D. A. McQuarrie, J. P. McTague and H. Reiss, Biopolymers 3, 657 (1963).

34. B. H. Zimm and J. K. Bragg, J. Chem. Phys. 31, 526 (1959).

35. N. Gō, J. Phys. Soc. Jap. 22, 416 (1967).

36. J. B. Peri and A. L. Hensley, Jr., J. Phys. Chem. 72, 2926 (1968).

37. J. B. Peri, J. Phys. Chem. 69, 220 (1965).

38. J. L. Jackson and E. W. Montroll, J. Chem. Phys. 28, 1101 (1958).

39. J. K. Roberts and A. R. Miller, Proc. Camb. Phil. Soc. 35, 293 (1939).

40. D. Lichtman and R. B. McQuistan, J. Math Phys. 8, 2441 (1967).

41. M. Abramowitz and I. A. Stegun, editors, Handbook of Mathematical Functions (Dover Publications, Inc., New York, 1970).

42. W. E. Boyce and R. C. DiPrima, Elementary Differential Equations and Boundary Value Problems (J. Wiley and Sons, New York, 1969), p. 50.

43. C. W. Gear, Numerical Initial Value Problems in Ordinary Differential Equations (Prentice-Hall, Inc., Englewood Cliffs, N.J., 1971).

44. A. C. Hindmarsh, "GEAR: Ordinary Differential Equation System Solver", UCID-30001 Rev. 3 Computer Documentation, Lawrence Livermore Laboratory, Livermore, CA, (1970).

45. H. Padé, Ann. Ec. Norm. Sup. 9, 1 (1892).

46. G. A. Baker, Jr., Essentials of Pade Approximants (Academic Press, New York, 1975).

47. R. V. Churchill, J. W. Brown and R. F. Verhey, Complex Variables and Applications (McGraw-Hill, New York, 1974).

48. K. Baron, D. W. Blakely and G. A. Somorjai, Surface Science 41, 45 (1974).

49. A. Clarke, The Theory of Adsorption and Catalysts (Academic Press, New York, 1970).

50. P. G. Hall and D. A. King, Surface Science 36, 810 (1973).

51. M. E. Bridge, R. A. Marbrow and R. M. Lambert, Surface Science 57, 415 (1976).

52. J. Oudar, Physics and Chemistry of Surfaces (Blackie and Sons, Ltd., Glasgow, 1975), p. 55.

53. D. A. King and M. G. Wells, Surface Science 29, 454 (1972).

54. D. L. Adams, Surface Science 42, 12 (1974).

55. A. W. Adamson, Physical Chemistry of Surfaces (Wiley Interscience, New York, 1967).

56. H. A. Engelhardt and D. Menzel, Surface Science 57, 591 (1976).

57. G. Arfken, Mathematical Methods for Physicists (Academic Press, New York, 1970).

58. C. H. Amberg, J. Less-Common Metals 36, 339 (1974).

59. R. S. Hansen, Ames Laboratory, DOE (Private communication).

60. E. L. Fuller and P. A. Agron, "Surface Properties in Reactions of Cobalt-Molybdate Hydrotreating Catalysts: A Preliminary Report", ORNL-5168, Oak Ridge National Laboratory, Oak Ridge, Tennessee (1976).

61. R. B. Gammage, E. L. Fuller and H. E. Holms, J. Phys. Chem. 74, 4276 (1970).

62. M. A. Vannice, J. Catalysis 37, 449 (1975).

63. J. W. Hall and H. F. Rasé, Nature 199, 585 (1963).

64. A. W. Sleight and W. J. Linn, Ann. New York Acad. Sci. 272, 22 (1976).

65. T. W. Orent and R. S. Hansen, Surface Science 67, 325 (1977).

66. I. Langmuir, J. Amer. Chem. Soc. 38, 2221 (1916).

67. C. N. Stewart and G. Ehrlich, J. Chem. Phys. 62, 4672 (1975).

68. H. F. Winters, J. Chem. Phys. 62, 2454 (1975).

69. H. F. Winters, J. Chem. Phys. 64, 3495 (1976).

70. J. T. Yardley and C. B. Moore, J. Chem. Phys. 49, 1111 (1968).

71. J. I. Steinfeld, Molecules and Radiation (Harper and Row, New York, 1974), p. 29.

72. D. Summers, Ph.D. thesis, Iowa State University, 1974.

ACKNOWLEDGEMENTS

I would like to thank Dr. D. K. Hoffman, my major professor, for his patient support and guidance throughout my graduate career. His influence is apparent throughout this work. I would also like to gratefully acknowledge Dr. R. S. Hansen for his generous support of the experimental work described herein. Special thanks are due to Dave Evans and David Burgess, comrades in arms, for their tolerance and their inspiration. Finally, I want to express my deepest thanks to my wife, Codie, for her patience and understanding through the long, lean years of graduate study.